Spectral Efficiency Evaluation of Downlink Cell-Free Massive MIMO Using Hybrid Precoder

Mekuanint Melaku Tiruneh

A Thesis Submitted to

The Department of Electronics and Communication Engineering

School of Electrical Engineering and Computing

Presented in Partial Fulfillment of the Requirement for the Degree of Master's in Electronics and Communication Engineering

Office of Post Graduate Studies

Adama Science and Technology University

July 2023

Adama, Ethiopia

Spectral Efficiency Evaluation of Downlink Cell-Free Massive MIMO Using Hybrid Precoder

Mekuanint Melaku Tiruneh

Major Advisor:- Dr. Ram Sewak Singh (PhD)

Co-Advisor:- Mr. Garoma Gerbi (MSc)

A Thesis Submitted to

The Department of Electronics and Communication Engineering

School of Electrical Engineering and Computing

Presented in Partial Fulfillment of the Requirement for the Degree of Master's in Electronics and Communication Engineering

Office of Post Graduate Studies

Adama Science and Technology University

July 2023

Adama, Ethiopia

APPROVAL PAGE of M.SC. THESIS

We, the advisors of the thesis entitled "**Spectral Efficiency Evaluation of Downlink Cell-Free Massive MIMO Using Hybrid Precoder**" and developed by **Mekuanint Melaku Tiruneh**, hereby certify that the recommendation and suggestions made by the board of examiners are appropriately incorporated into the final version of the thesis.

Dr. Ram Sewak Singh	_____	_____
Major Advisor	Signature	Date
Mr. Garoma Gerbi	_____	_____
Co-Advisor	Signature	Date

We, the undersigned members of the board of Examiners of the thesis by **Mekuanint Melaku Tiruneh** have read and evaluated the thesis entitled "**Spectral Efficiency Evaluation of Downlink Cell-Free Massive MIMO Using Hybrid Precoder**" and examined the candidate during open defense. This is, therefore, to certify that the thesis is accepted for partial fulfillment of the requirement of the degree of Master of Science in Electronics and Communication engineering.

_____	_____	_____
Chairperson	Signature	Date
_____	_____	_____
Internal Examiner	Signature	Date
_____	_____	_____
External Examiner	Signature	Date

Finally, approval and acceptance of the thesis is contingent upon submission of its final copy to the Office of Postgraduate Studies (OPGS) through the Department Graduate Council (DGC) and School Graduate Committee (SGC).

_____	_____	_____
Department Head	Signature	Date
_____	_____	_____
School Dean	Signature	Date
_____	_____	_____
Office of Postgraduate Studies, Dean	Signature	Date

DECLARATION

I hereby declare that this Master Thesis entitled "**Spectral Efficiency Evaluation of Downlink Cell-Free Massive MIMO Using Hybrid Precoder"** is my own work and has not been submitted to any university for the award of any academic degree, diploma or certificate. The references used in this thesis are duly recognized by proper citations.

Mekuanint Melaku Tiruneh	_____	_____
Name of Student	Signature	Date

RECOMMENDATION

We, the advisors of this thesis, hereby certify that we have read the revised version of the thesis entitled "**Spectral Efficiency Evaluation of Downlink Cell-Free Massive MIMO Using Hybrid Precoder**" prepared under our guidance by **Mekuanint Melaku Tiruneh** submitted in partial fulfillment of the requirements for the degree of Mater's of Science in Electronics and Communication Engineering. Therefore, we recommend the submission of revised version of the thesis to the department following the applicable procedures.

_____	_____	_____
Major Advisor	Signature	Date
_____	_____	_____
Co-advisor	Signature	Date

ACKNOWLEDGEMENT

I begin by expressing my gratitude and thanks to the Almighty God for his blessings and mercy, which have eenabled me to successfully complete this thesis. I would like to extend my heartfelt appreciation to my advisor, Dr. Ram Sewak Singh (PhD), for his unwavering support, encouragement, and valuable time. His guidance and freedom allowed me to explore this thesis deeply and work in my own way. Without his assistance, it would not have been possible to achieve the ultimate goal of this thesis. He was always available whenever I needed his help.

I also want to acknowledge my co-advisor, Mr. Garoma Gerbi (MSc), for his continuous support throughout my M.Sc. research. His patience, motivation, and enthusiasm were invaluable in guiding me through the research and writing of this thesis.

Additionally, I would like to express my gratitude to Adama Science and Technology University (ASTU) and the School of Electrical Engineering and Computing (SoEEC), particularly the program of electronics and communication engineering, for providing an excellent educational and research environment. I am thankful to all the students in the Communication Engineering division who shared their knowledge with me.

Lastly, I am grateful to my family for their unwavering support, allowing me to pursue my dreams and making me feel empowered to do whatever I wanted without feeling pressured.

TABLE OF CONTENT

LIST OF TABLES

LIST OF FIGURES

ACRONYMS

5G	Fifth Generation
6G	Sixth Generation
APs	Access Points
BS	Base Station
CB	Conjugate Beamforming
CCI	Co-channel Interference
CDF	Comulative Distribution Function
CF	Convergence Factor
C-MIMO	Collocated Multiple Input Multiple Output
CoMP	Coordinated Multi-Point
CPU	Central Processing Unit
CRAN	Cloud Radio Access Network
CSI	Channel State Information
CZF	Centralized Zero Forcing
DAS	Distributed Antenna System
D-LMIMO	Distributed Large-Scale MIMO
D-MIMO	Distributed MIMO
DCC	Dynamic Cooperative Clustering
DUCC	Dynamic User-centric Clustering
ECB	Enhanced Conjugate Beamforming
EM	Electromagnetic
eMRT	extended Maximum Ratio Transmission
eZF	extended Zero Forcing
EW-MMSE	Element wise Minimum Mean Square Error
FADs	Fish Aggregate Devices
FDD	Frequency Division Duplex
fpZF	full pilot Zero Forcing
Hz	Hertz
ICI	Inter-cell Interference
JCD	Joint Centralized and Distributed
JMRZF	Joint Maximum Ratio and Zero Forcing

LMMSE	Local Minimum Mean Square Error
LMR	Local Maximum Ratio
LPMMSE	Local Partial Minimum Mean Square Error
MIMO	Multiple Input Multiple Output
MMSE	Minimum Mean Square Error
MMSE-SIC	MMSE Successive Interference Cancellation
MPA	Marine Predator Algorithm
MR	Maximum Ratio
MRT	Maximum Ratio Transmission
MU-MIMO	Multi-user MIMO
PC	Power Control
PMMSE	Partial Minimum Mean Square Error
PRZF	Partial Regularized Zero Forcing
RF	Radio Frequency
RPs	Radio Ports
SJZF	Scalable Joint Zero Forcing
SE	Spectral Efficiency
SNR	Signal to Noise Ratio
TDD	Time Division Duplex
TPC	Transmit Preprocessing
UCC	User-centric Clustering
UEs	User Equipments
ZF	Zero Forcing

ABSTRACT

The rapid advancement of communication technologies is connecting the world faster than ever before. However, this has resulted in a scarcity of frequency spectrum as the available communication bandwidth is limited. To maximize data transmission rates while using a fixed bandwidth, a mechanism is needed to improve spectral efficiency. Distributed massive multiple input multiple output (MIMO) systems involve deploying a large number of transmitting antennas around user equipment (UEs) to achieve this goal. However, in cellular massive MIMO, signal interference around cell edges can present a problem. To address interference issues around cell edges in cellular massive MIMO, cell-free massive MIMO was introduced, which incorporates both massive MIMO and distributed MIMO principles. Cell-free massive MIMO is advantageous as it places users closer to access points (APs), enabling higher spectral efficiency. While cell-free massive MIMO improves spectral efficiency, signal processing techniques such as precoding are needed to maximize it further. Precoding is a transmitter signal processing method that maximizes the received signal for specific receivers while minimizing interference for all other receivers. This thesis work proposes a better-performing precoding algorithm for cell-free massive MIMO based on partial regularized zero-forcing (PRZF) and the marine predator algorithm (MPA). Compared to the PRZF precoder, the proposed algorithm has resulted in an average spectral efficiency improvement of 11.8% for 20 users and 13.65% for 100 users within the coverage area, assuming that the network is equipped with 1500 APs, each having a single antenna. Additionally, it has improved the sum spectral efficiency by 13.6% for 60 users within the coverage area, given that the network is equipped with 1500 APs, each having a single antenna. Furthermore, the computational complexity of the proposed method is relatively comparable to that of existing precoders.

Keywords: *Cell-free massive MIMO, Marine Predator Algorithm, Partial Regularized Zero Forcing, Spectral Efficiency, Precoding, Computational Complexity*

CHAPTER ONE

1. INTRODUCTION

1.1 Background of the Study

Since 2019, fifth-generation (5G) wireless communication systems have been set up all over the world to attain high levels of connectivity, extreme reliability, and minimal latency. Massive multiple-input multiple-output (MIMO) (Marzetta, 2010), one of the 5G enabling technologies, can achieve high spectral efficiency (SE), link reliability , and energy efficiency by centrally deploying a large number of base station (BS) antennas and providing extremely high beamforming and spatial multiplexing gain. Wireless communication networks must deliver improved coverage and consistent performance for users over a wide coverage area to keep up with the exponential growth for higher data speeds and traffic volume, which 5G cannot do (Xiaohu et al., 2021).

A comprehensive wireless network ought to offer consistently excellent service over a specified area. Massive MIMO has garnered a lot of interest as a candidate for fifth-generation physical layer thechnology in this regard. A promising 5G wirless access method is massive MIMO, which enables a base station with numerous antennas to serve numerous users concurrently in the same time-frequency resource while requiring minimal signal processing (H. Yang & Marzetta, 2014). At the base stations, enormous antenna arrays can be built up either collocated or scattered. Low backhaul requirements are a benefit of collocated massive MIMO designs when all service antennas are positioned in a small space. In contrast, the service antennas in distributed massive MIMO systems are dispersed over a wide area. Distributed networks can provide a substantially higher probability of coverage than collocated massive MIMO (Zhou et al., 2003) because of their improved ability to leverage diversity against shadow fading, but at the expense of greater backhaul needs.

Distributed antenna systems (DAS), which give macro-diversity and cover dead spots in MIMO systems, have been proposed to enhance the performance of cell-edge users (Choi & Andrews, 2007). Better coverage is offered, and power overhead of the system is decreased. Additionally, it was suggested to use coordinated multi-point (CoMP) and Network MIMO to increase cooperation between nearby access points (APs) and reduce inter-cell interference (J. Zhang et al., 2009). To limit data exchange, they separate the APs into clusters of disjointed cooperation. Inter-cell interference, however, can’t be eliminated inside

the cellular architecture, interfering clusters a crucial issue. This is because, when the cellular paradigm is taken into account, inter-cell interference can't be eliminated.

A distributed massive MIMO network that serves a significantly lower number of autonomous users dispersed over a big region using a large number of serving antennas known as APs (Ngo et al., 2015). Time-division duplex (TDD) operation allows all APs to serve all users in the same time-frequency resource while cooperating phase-coherently through a backhaul network. Cells and borders don't exist. We refer to this system as "Cell-Free Massive MIMO" as a result.

The central processing unit (CPU), often known as an edge-cloud processor or cloud radio access network (CRAN) data center, is to be built up and connected to significant proportion of scattered single-antenna access point (APs). The CPU controls the system in a Network MIMO mode without cell borders to serve the UEs jointly through coherent joint transmission and reception. Cell-free massive MIMO differs from traditional Network MIMO in that it operates in a mode where there are many more APs than UEs (Kumar & Chandana, 2021). The incorporation of imperfect channel state information (CSI), as compared to perfect CSI, which was usually assumed in the past, in the performance analysis was a significant analytical innovation.

It is anticipated that cell-free massive MIMO will benefit fully from these two systems because it incorporates the distributed MIMO and massive MIMO principles. Additionally, cell-free massive MIMO can provide a high probability of coverage, because the users are now close to the APs.

1.2 Motivation of the Study

The need for high spectral efficiency in wireless communication systems has increased rapidly due to the growing demand for high-speed data transmission in various applications. In recent years, cell-free massive MIMO has emerged as a promising technology to improve spectral efficiency by exploiting large numbers of distributed antennas. However, the performance of cell-free massive MIMO depends on various factors such as channel estimation, pilot contamination, and user clustering. Therefore, there is a need for further research in spectral efficiency analysis of cell-free massive MIMO to develop efficient algorithms and techniques that can address these challenges. This research can lead to

significant improvements in wireless communication systems and pave the way for the deployment of cell-free massive MIMO technology in practical applications.

1.3 Statement of the Problem

Despite having strong data rates at the cell center, contemporary cellular networks have significant data rate changes at the cell edges and at the cell center. Given the tremendous data needs that are only going to increase, these inconsistent data rates make cellular services less effective. In addition, more and more wireless applications, such as autonomous vehicles, navigation, and autonomous traffic systems, are emerging recently, necessitating the provision of a consistent data transfer speed across the entire coverage area, ensuring a uniform quality of service for each users. There have been attempts to achieve this goal by decreasing the cell coverage area and increasing the number of APs per area unit.

The number of APs enhances the network's capacity, but this tendency progressively reverses and may even lower it when inter-cell interference rises. Therefore, increasing network density is not the way to ensure that wireless networks can continue to meet demand in the long run. Wireless network operations require a paradigm shift from conventional "cellular" networks to "cell-free" networks. By efficiently reducing interference and enhancing system throughput, this paves the door for the collaborative functioning of all APs to cooperatively serve the UEs in a given space. Cell-free massive MIMO is regarded as a highly promising technology for next-generation mobile networks (beyond 5G and 6G) to attain this objective.

Cell-free massive MIMO faces major challenges in scalability, computational complexity, and interference management. As the number of users and APs increase, the system becomes harder to scale, and processing the complex signal algorithms in real-time becomes more difficult. The distributed nature of the system also leads to interference, which can degrade the quality of service. To address these challenges, researchers have to explore new signal processing and interference management techniques, such as efficient precoding algorithms. Despite these obstacles, ongoing research aims to develop practical solutions for the deployment of cell-free massive MIMO systems in the future.

1.4 Objective

1.4.1 General Objective

The general objective of this research is to analyze the downlink spectral efficiency of a cell-free massive MIMO communication system using different precoding techniques over fading channels.

1.4.2 Specific Objectives

- To analyze the effect of the number of antennas per each AP on the spectral efficiency of a cell-free massive MIMO system.
- To compare the downlink spectral efficiency between centralized and distributed cell-free massive MIMO.
- To mitigate the interference of APs in cell-free massive MIMO systems and enhance spectral efficiency.
- To analyze the spectral efficiency parameter of a cell-free massive MIMO system over fading propagation environment.
- To compare precoding techniques based on spectral efficiency and computational complexity performance parameter.

1.5 Significance of the Study

This research work is expected to be helpful to aware and assesses the merit and drawbacks of different precoding techniques whether each candidate precoder enables the cell-free massive MIMO to maximize its spectral efficiency or not and also whether it is effective or not. Moreover, this work gives direction to researchers to do more researches that can facilitate the implementation of cell-free massive MIMO communication technology.

1.6 Expected Outcome of the Study

We expect to get an improved spectral efficiency with a given bandwidth using a combination of existing precoding techniques and nature-inspired metaheuristic optimization algorithms. By using less complex precoding techniques combined with metaheuristic algorithm, we expect to get a competitive result with those powerful and high-complexity precoding techniques.

1.7 Scope of the Study

The main scope of this work is to study the future cell-free massive MIMO communication system and deep understanding of downlink data transmission. Due to the scarcity of communication bandwidth, every communication system should use its assigned bandwidth efficiently. To use the given frequency spectrum effectively, we need to implement different signal processing techniques. Precoding involves error reduction and increment of the data rate in the downlink transmission from different APs to a specific UE. Spectral efficiency analysis is one of the core areas for future communion systems. In this thesis work, we propose to work on the spectral efficiency analysis of cell-free massive MIMO systems in downlink data transmission using different precoding techniques compared with the proposed precoder.

1.8 Organization of the thesis

The remaining part of this thesis is organized as follows: **Chapter Two** provides an introduction to the topic, including an explanation of the working principles of cellular and cell-free massive MIMO, as well as an overview of related research on downlink precoding schemes in cell-free massive MIMO. **Chapter Three** outlines the methods used in this thesis, including the system model and mathematical models of different precoding schemes, both in distributed and centralized operations. **Chapter Four** presents the simulation results and a comprehensive discussion of the findings. Finally, the conclusion and recommendations for future research are presented in the last section of the thesis.

CHAPTER TWO

2. LITERATURE REVIEW

2.1 Introduction

Beginning with the early ideas created in the 1950s and 1960s and continuing through to the first commercial deployment in 1979 (Kinoshita et al., 2018), the structure of cellular networks has been essential in allowing mobile communications. Making effective use of the scarce frequency spectrum by allowing numerous concurrent communications within the network's coverage area was the driving force behind the growth of cellular networks. The coverage area was segmented into predetermined geographic areas, referred to as cells, where a fixed AP manages the service to regulate interference between transmissions. To reduce inter-cell interference, a predefined frequency plan was initially used to ensure that adjacent cells used distinct frequency resources. Increasing the number of APs per area unit has allowed business cellular networks to become denser over time. Instead of fixed-beam antennas, each AP should have steerable multi-antenna panels to reduce crosstalk between nearby cells and preserve the benefits of the current frequency plans. Different types of AP hardware are utilized based on the implementation scenario, which could be indoor or outdoor, the frequency band used, the coverage area, and the distance between the AP and the nearest user location. The resulting microcells, picocells, and femtocells are a few different names for the ensuing cellular network components. When speaking of such networks, we will generally refer to them as small cells (Alzubaidi et al., 2022a). Regarding the amount of data that can be transmitted in a specific region per second, using smaller and smaller cells has proven to be an effective technique for expanding the capacity of networks. In theory, the network capacity is expected to rise in proportion to the total number of active APs and users. However, this trend gradually shifts as inter-cell interference increases, leading to a decrease in network capacity (Deepa et al., 2023). Further network densification can eventually result in a network's capability decreasing rather than improving. This is especially true in the ultra-dense network era, where there are extra APs than there are concurrently active users. In a situation where there are so many APs, even having a small number of antennas would not be sufficient to eliminate interference (Wang et al., 2023). A cell-free network indicates an effort to go beyond the limitations mentioned above.

2.2 Cellular Networks

A cellular network is a kind of wireless communication system that uses radio waves to transmit speech and data over great distances. By segmenting the network into smaller regions known as cells, the network is created to provide service over an extensive geographical area. The base station in each cell acts as the center of contact for devices within the cell. The base station consists of a transceiver, antennas, and other equipment that enables wireless communication between devices and the network. The efficient use of available radio frequencies is made possible by the use of cells in cellular networks. To prevent interference with nearby cells, each cell employs a unique set of frequencies. Cellular networks can support numerous concurrent users while offering high-quality voice and data services thanks to the frequency reuse technique. The standard cellular network architecture in Figure 2.1 shows that each user in the network is served by a single AP having either a single antenna or multiple antenna. Each AP serves a UE which is located in the same cell.

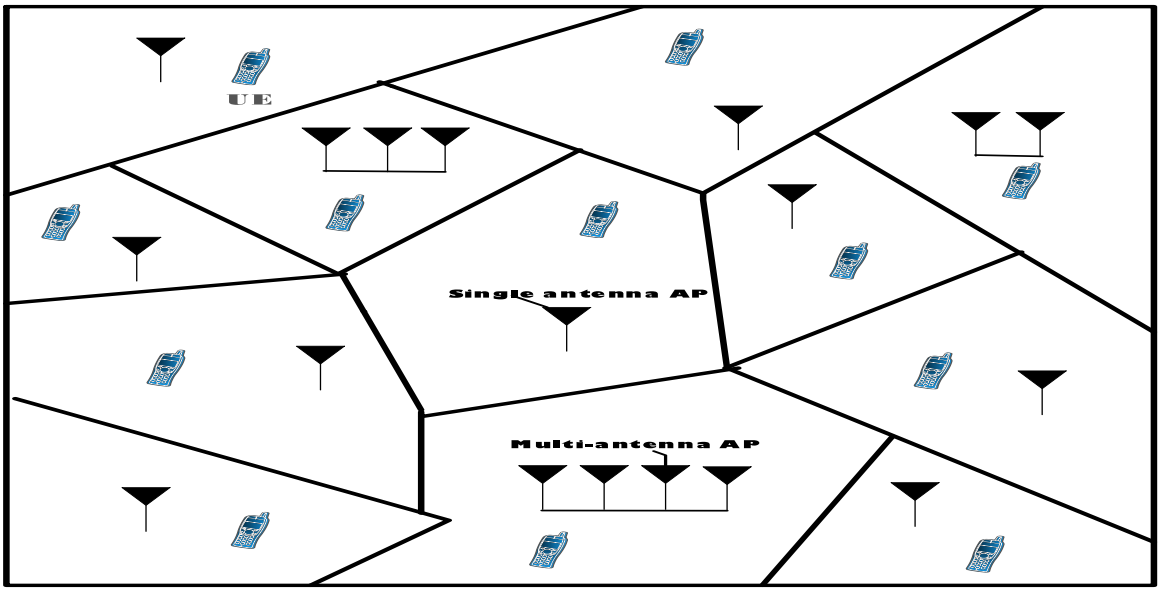

Figure 2.1: A standard cellular network in which each user is only linked to a singlr AP (Interdonato et al., 2019).

By transmitting and receiving radio signals to and from a nearby base station, mobile devices, such as smartphones and tablets, interact with the cellular network. The mobile device instantly switches to the base station with the strongest signal as the user moves through the network, enabling uninterrupted communication even when in motion. The most

important aspect of cellular networks that guarantees continuous connectivity for users is the handoff procedure.

2.3 Massive MIMO

MIMO technology boosts a wireless communication system's capacity by employing numerous antennas located at both the transmitting and receiving ends. The fundamental concept behind MIMO is to use spatial diversity to boost the wireless channel's capacity. The transmitter and receiver ends of conventional wireless communication devices use a single antenna. The bandwidth available in such systems determines the data rate, and the signal-to-noise ratio determines the system capacity. By using several antennas at both the transmitting and receiving ends, MIMO technology gets around these restrictions. Utilizing several antennas at the transmitti end, MIMO technology transmits multiple data streams simultaneously. Multiple antennas are used at the receiver end to extract these data streams and merge them to increase the received signal quality. Spatial diversity is made possible by the use of multiple antennas at both ends of a communication link, which increases the quality of the signal that is received (Jia et al., 2022).

With the help of multiple antennas at the transmitter and receiver side, the wireless communication technology known as multi-user MIMO (MU-MIMO) enables multiple users to communicate with a base station simultaneously. By enabling multiple users to share the same channel, MU-MIMO technology is intended to increase the capacity as well as the efficiency of wireless networks. MU-MIMO works by dividing the channel into several sub-channels, each of which is assigned to a separate user. The base station transmits data to numerous users simultaneously on various sub-channels using several antennas. The base station can also simultaneously receive data from multiple users on various sub-channels by using multiple antennas (Marzetta, 2010). Because MU-MIMO enables simultaneous communication between multiple users, it decreases user wait times and boosts total network capacity.

The capacity, as well as efficiency of wireless networks, are increased by the use of massive MIMO, a wireless communication technique that employs a large number of antennas at both the transmitter and the receiver. Massive MIMO improves the network's total capacity by enabling the base station to serve a large number of users simultaneously. By employing a significant number of antennas to send data over greater distances, Massive MIMO

additionally has the potential to broaden the service area of wireless networks (Larsson et al., 2014). A generalized massive MIMO idea is depicted in Figure 2.2, in which many transmitting antennas are used to serve many user equipment that is relatively few compared to the transmitting antenna.

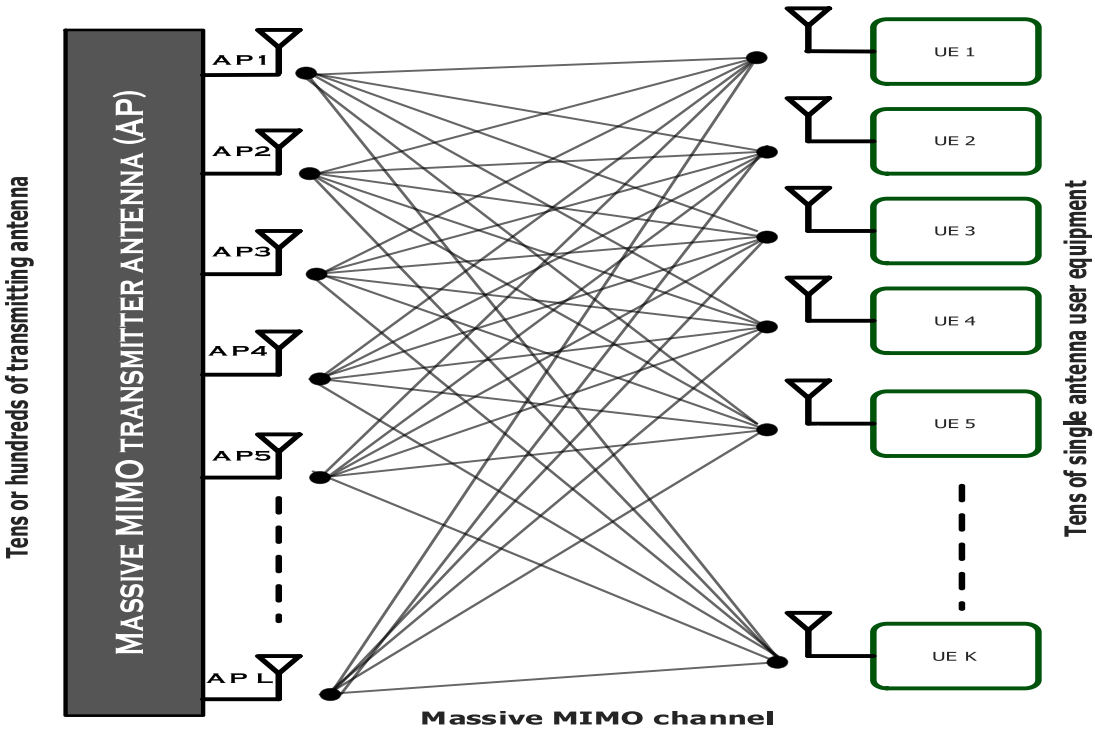

Figure 2.2: Massive MIMO architecture (Albreem et al., 2019).

2.4 Network Densification

The process of installing a lot of small cells within a cellular network is known as network densification. Low-power base stations known as small cells are usually placed in indoor and outdoor spaces like streets, airports, and shopping centers. Improved network coverage, increased network bandwidth, and improved user experience are the main goals of network densification. Each user can now be served by a small cell close because of the implantation of small cells, which lowers the number of users that can be supported by a single macro cell (Akyildiz et al., 2020). Network densification makes it possible to distribute traffic more evenly, which eases network congestion and improves total network performance. But as more BSs are added, the investment demanded will increase significantly, requiring improvements in hardware simplification and cost minimization. However, significant performance degradation issues have also been brought on by inter-cell interference (ICI) and inadequate signal quality at boundaries of cells (Alzubaidi et al., 2022b). To address

users located in close proximity to the cell boundaries, improved interference suppression approaches, such as coordinated beamforming (Li et al., 2015), network MIMO (J. Zhang et al., 2009), DASs (Castanheira & Gameiro, 2010), and CoMP (Solaija et al., 2021), have been proposed. These techniques involve increasing collaboration among APs that are located close to each other, thereby reducing ICI. Even though these techniques may improve system efficiency and provide macro- and micro-diversity gain, arranging the APs into cooperative clusters resulted in interference between the clusters (Irram et al., 2020). The standard network-centric configuration of CoMP is shown in Figure 2.3, where the APs create disjoint clusters that function as cells by communicating with the UEs located inside their joint coverage area.

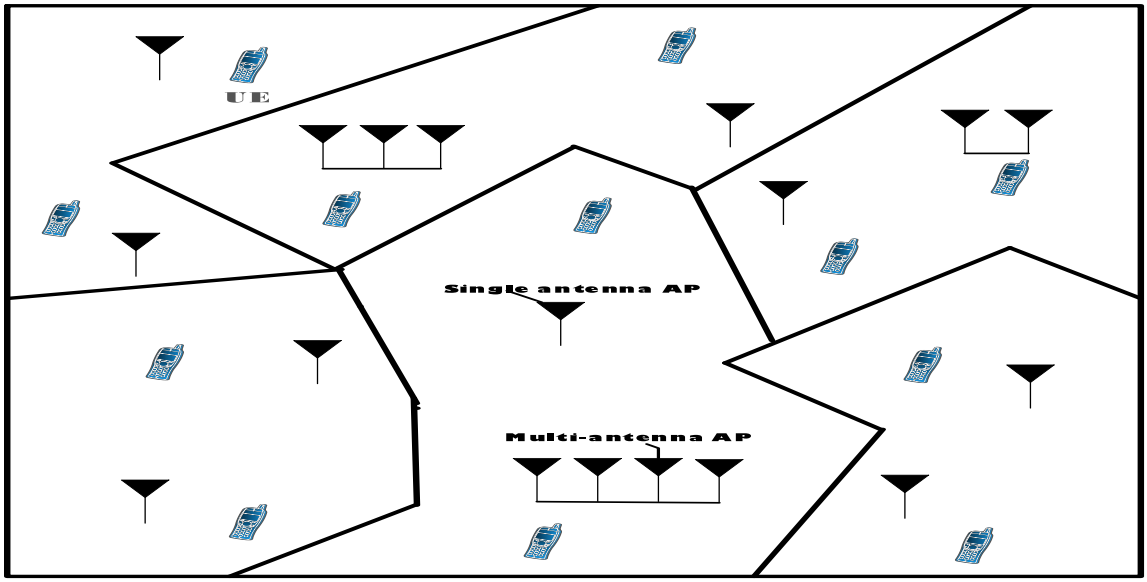

Figure 2.3: A conventional implementation of CoMP network architecture (Interdonato et al., 2019).

2.5 Cell-Free Massive MIMO

Based on spectral and energy efficiency, 5G cellular technology outperforms earlier generations significantly. However, users near the cell's center receive the greatest advantage from the significant performance increase. The performance of users around the cell edge is still severely limited by the inherent issues with cellular technology, such as ICI. Cell-free massive MIMO systems are anticipated to have significant roles in enhancing the performance at cell edges in 5G and future wireless systems. (Jin et al., 2021).

A useful implementation of the generally distributed massive MIMO idea has been suggested by (Ngo et al., 2017), (Nayebi et al., 2017) as a cell-free massive MIMO system infrastructure. With the use of TDD operation, numerous antennas located at different geographical locations can work together via a fronthaul network and a CPU to deliver service to a smaller number of UEs using the same time-frequency resource to obtain information. Cell-free massive MIMO technology differs from the network MIMO concept in that the concept of cellular or cell boundaries are diminished, and all antennas serve the users simultaneously, giving rise to the name of the technology. More specifically, by utilizing local CSI and carrying out joint transmission, all the UEs are served by multiple distributed APs using either one or multiple antennas at the same time. The APs receive data from the UEs in the uplink and feed it back to the CPU via fronthaul links. The CPU provides the APs with downlink data and coefficients for power control. Only channel statistics are used at the CPU in cell-free massive MIMO to effectively implement joint detection. To provide wireless coverage in indoor or hotspot environments, such as shopping centers, smart factories, train stations, small towns, stadiums, hospitals, subways, community centers, or college campuses, the cell-free massive MIMO technique is an excellent solution (J. Zhang et al., 2019). Figure 2.4 shows cell-free massive MIMO architecture having multiple users in a network.

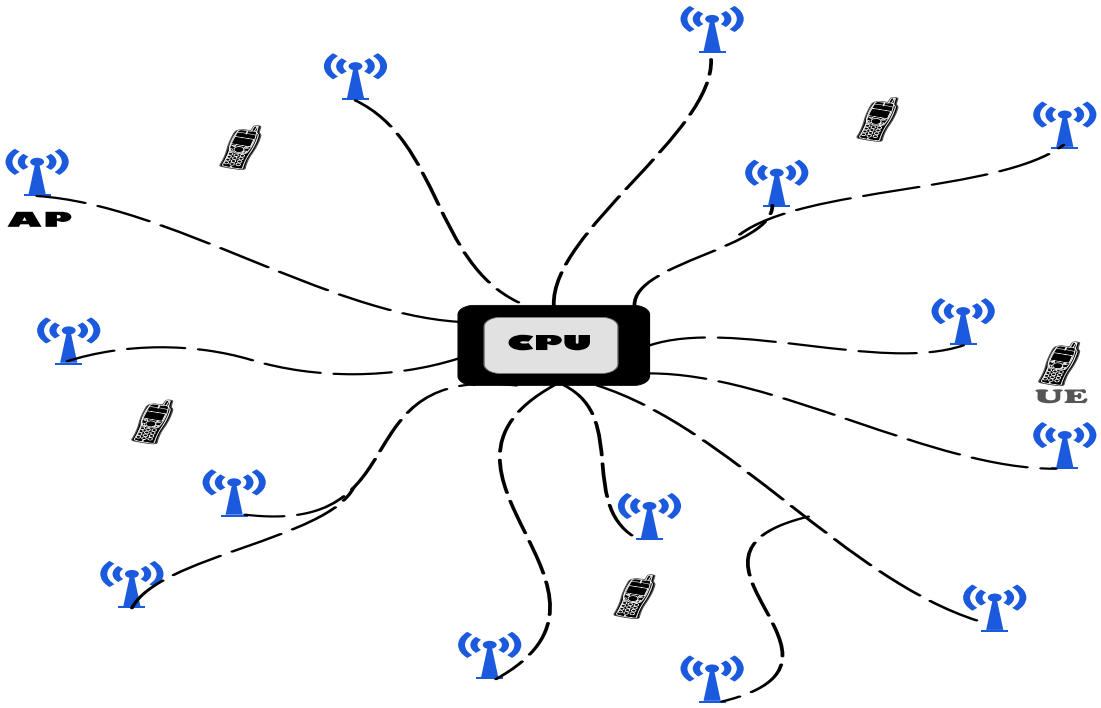

Figure 2.4: Multiuser cell-free massive MIMO system (Tan et al., 2022), (Wiame et al., 2023), (Alammari et al., 2022).

Once more, the basic idea behind cell-free massive MIMO systems is to take full advantage of network MIMO solutions by offering significantly a much larger number of antennas than the number of UEs, which enables us to use transmit signal preprocessing to remove interference at the UEs. Scalable solutions can be supported by taking advantage of the major characteristics of massive MIMO. Using the law of large numbers enables the averaging out of noise, fading, and inter-user interference. One of the benefitsof cell-free massive MIMO networks is their ability to provide better service than traditional uncoordinated small cells. This includes high data rates across the entire coverage area, consistent quality of service, exceptionally high reliability, and the prevention of cell interference due to the absence of cell boundaries (H. He et al., 2021). Additionally, cell-free massive MIMO can offer effective macro diversity for picking the most suitable APs from among many nearby APs (Alonzo et al., 2019).

2.5.1 User-Centric Cell-Free Massive MIMO

The conventional implementation of cell-free massive MIMO considers that every AP has connectivity to a single CPU. As more APs are connected to the network, the number of fronthaul connections accordingly grows. Additionally, the overall fronthaul capacity demand rises as each AP serves all customers. Due to these constraints, the traditional configuration is challenging and not particularly possible given the high number of APs that are to be placed in a cell-free system.

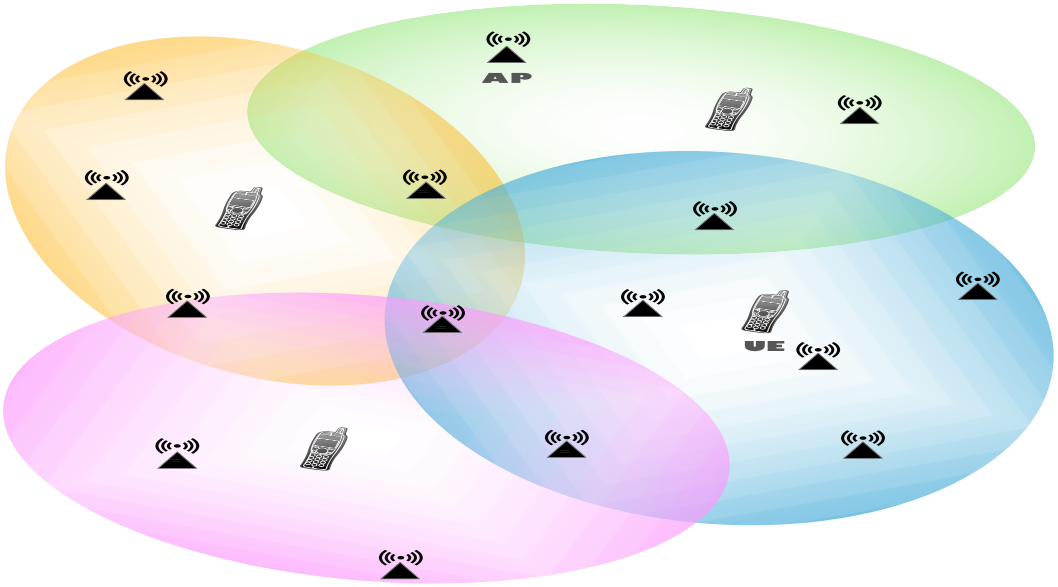

Figure 2.5: User-centric cell-free network architecture (Yao et al., 2022).

The creation of so-called user-centric clusters is used to solve the scalability issue (Buzzi & D'Andrea, 2017), (Datta et al., 2022). Every user should choose the APs that offer optimal performance, according to the plan. This means that only a small number of neighboring APs, as shown in Figure 2.1, serve all users jointly. This makes sense because the user's performance isn't much impacted by APs located distance from them. Using a user-centric approach to serve a smaller number of users through each AP results in fronthaul savings since less data needs to be transferred over the fronthaul lines. Multiple interlinked CPUs may be used to achieve true scalability of cell-free network. Disjoint AP clusters are created since each CPU is given a certain amount of APs. Furthermore, APs managed by various CPUs may make up a user-centric cluster. In this scenario, in order for the user to receive collaborative processing and transmission/reception, the CPUs need to establish communication with each other via the backhaul link (Mendoza et al., 2020).

2.6 Dynamic User-Centric Clustering

User-centric Clustering (UCC) of APs uses the de-cellular approach and the network serving UE concept to group APs based on user needs. The ultra-dense network allows for the intelligent recognition of the user's wireless communication environment and the flexible organization of the necessary User-centric APs clustering to serve the user, giving the UE the impression that they are always in the middle of a wide area of coverage. In a complex wireless environment, UCC can track UE behavior and provide UEs with user-centric services including on-demand service and movement tracking. Every registered UE (Hu et al., 2017) is provided with a dynamic UCC (DUCC) that has a specific UCC_ID and follows the user whether it is in mobile or static condition. For each user, a customized DUCC built on the ultra-dense network is developed to deliver improved services. In the control plane, numerous APs with small coverage are combined via DUCC technology, which modifies the standard cell design concept. This creates a fictitious huge cell. In UCC, the UE roams in the attached AP as though it were stationary in a single big cell (Z. Zhang et al., 2018), (S. He et al., 2020). DUCC is a perfect fit in cell-free massive MIMO networks to reduce scalability problems and computational complexity (Bjornson & Sanguinetti, 2019). In addition to that the DUCC technology increases the system performance as indicated in (Björnson & Sanguinetti, 2020).

2.7 Spectral Efficiency

The spectral efficiency of a communication channel with bandwidth B Hz is defined by the band-limited communication signal sent over the channel, consisting of 2B real-valued equal-spaced samples per second, as per the Nyquist-Shannon sampling theorem. However, when considering the complex-baseband representation of the signal, the more natural amount is B complex-valued samples per second. These B samples provide the degrees of freedom for creating the communication signal, and the spectral efficiency is the amount of information per complex-valued sample that can be transmitted successfully. Therefore, SE is a deterministic quantity that can be expressed in bits per complex-valued sample. Since there are B samples per second, SE can be expressed in bit/s/Hz, which is a unit of SE that can be compared. The SE can be viewed as the average bit rate per Hz across the realizations for fading channels that change over time. Throughout this thesis, we refer to the SE of a channel between a UE and an AP as the "SE of the UE" for convenience. The information rate [bit/s], which is obtained by multiplying the SE by the bandwidth B, is a comparable statistic (Björnson et al., 2017).

2.8 Precoding

Precoding is a method used to preprocess the transmit signal of a radio frequency system in order to enhance system performance and increase spectral efficiency. By utilizing CSI at the transmitter, precoding is able to implement the superposition of multiple beams, each containing separate data streams, for spatial multiplexing. It is supposed that the transmitter has knowledge of the CSI. A typical precoding process begins with channel sounding, where a coded message, also known as a sounding packet or a pilot signal, is transmitted to the receiver. Each user responds to the transmitter with their unique CSI, which is then used to set the precoding matrix for the subsequent data transfer. Precoding is typically used to describe a software application of communication theory, whereas beamforming is more commonly used to describe a hardware implementation involving the system's antennas. Furthermore, while beamforming can be used on both transmitters and receivers, precoding usually refers to the transmitter side. (Kuo et al., 2008).

2.9 Metaheuristic Algorithms

The term "metaheuristic" originates from the Greek verb "heuriskein," which signifies the act of finding or discovering, combined with the word "meta," denoting something higher or more advanced. Real-world applications typically involve complex factors, parameters, and

constraints that influence the behavior of the system. As a result, a distinct approach is required to optimize resource utilization in any field as compared to basic scientific thinking (Koziel & Yang, 2011). Due to the complexity of the problem, searching for every possible solution or combination of solutions is not practical. Therefore, it becomes necessary to identify suitable solutions that are effective and can be found within a reasonable timeframe. Metaheuristic approaches offer a potential solution for a variety of applications and problems due to their ability to deal with uncertainty and irregular structures in an intuitive and sophisticated manner.

Numerous classical heuristic optimization methods employ local search procedures, iteratively improving upon the existing solution to reach a better outcome. Typically, these searches terminate once a local optimum is attained. Despite commonly using randomization and reboot techniques to improve solutions and achieve more optimal values, they often turn out to be ineffective. In contrast, metaheuristic methods typically integrate various heuristic approaches, resulting in superior solutions compared to those obtained through local search alone (Onwubolu & Babu, 2004).

The core elements of any metaheuristic algorithm encompass exploitation and exploration. Exploration involves searching the entire solution space and generating diverse solutions, while exploitation focuses on seeking the best solutions within specific regions using knowledge gained from selected solutions. It emphasizes local search within those regions and the selection of the most promising candidate solutions. Randomization plays a crucial role in exploration by preventing the algorithm from becoming trapped in local optima. The exploration phase enables the algorithm to efficiently navigate the solution space (Talatahari, 2013). In other words, the algorithm explores the search area to identify the best solution, searches the vicinity of this solution, and simultaneously continues exploration to uncover even better solutions.

In contrast, these methods are often referred to as algorithms that draw inspiration from a range of natural features and unique abilities exhibited by living organisms, physical and chemical phenomena observed in substances, genetic/evolutionary processes, natural systems and phenomena. For instance, the taboo search algorithm simulates human memory, the ant colony algorithm replicates the foraging behavior of ants, and the genetic algorithm mimics the true genetic structure. Just like in nature, these methods also exhibit diverse characteristics and distinctions.

As an example, swarm intelligence-based methods, including cuckoo search, firefly algorithm, and particle swarm optimization, embody the collective intelligence exhibited by living organisms when acting collectively, particularly in finding food. These metaheuristic algorithms are popular due to their simplicity, ease of implementation, and effectiveness in solving various complex and often nonlinear problems (X.-S. Yang et al., 2013), (Rezaei & Rezaei, 2022). Another example involves methods that utilize memory. Techniques such as genetic algorithm, ant colony optimization, harmony search, and tabu search leverage memory to store solutions, allowing the obtained solutions during the search process to be utilized in subsequent iterations (H. Zhang & Sun, 2002), (Katoch et al., 2021).

2.9.1 Marine predator algorithm

As described in (Faramarzi et al., 2020), (Al-Betar et al., 2023) marine predator algorithm (MPA) optimization method consists of three phases that aim to balance exploration and exploitation in the search for optimal solutions. The first phase, shown as Phase 1 in Figure 2.6, is focused on exploration. The prey individuals move in Brownian motion, which allows them to explore their neighborhoods separately and find abundant food areas. The fitness of each prey individual is evaluated, and if it is better than the previous position, it is replaced. This phase helps the individuals to explore the search domain and identify promising regions.

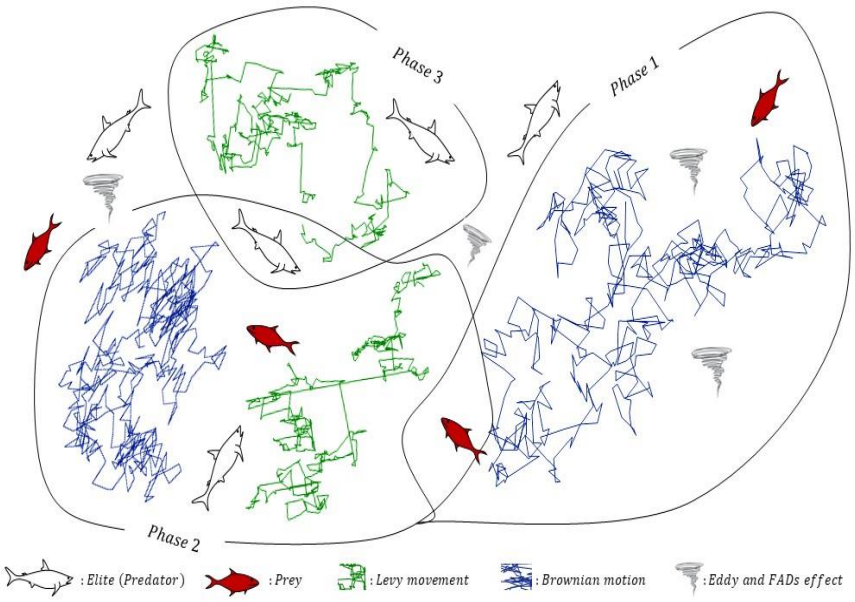

Figure 2.6: The three optimization phases of MPA (Faramarzi et al., 2020)

During the second phase, which is illustrated as Phase 2 in Figure 2.6, both predator and prey individuals search for food. The population is divided into two halves, with half devoted to exploration and the other half to exploitation. The predator individuals use Brownian motion to search for their prey, while the prey individuals switch to the Lévy approach. The Lévy strategy enables the prey to efficiently search its nearby surroundings and take long jumps when food cannot be found. The Brownian motion used by the predator individuals helps them to explore the domain and locate the prey individuals. The FADs effect, combined with the long steps of the Lévy approach, helps the method to avoid getting stuck in local optima and enhances its performance.

During the third phase, depicted as Phase 3 in Figure 2.6, the optimization process requires high exploitation capability. The predator individuals change their behavior from Brownian to Lévy strategy to efficiently search a specific neighborhood. An adaptive convergence factor (CF) is utilized in this phase to limit the predators' search areas within a particular neighborhood for exploitation. This adaptive CF also prevents search effort from being wasted on non-promising regions of the domain. The aim of this phase is to exploit the promising regions discovered in the previous phases and find optimal solutions.

Overall, the three phases of the optimization method aim to balance exploration and exploitation and prevent the method from getting stuck in local optima. Brownian motion and Lévy strategy are used to explore and exploit the search domain, respectively, while the FADs effect and adaptive CF help to enhance the performance of the technique by avoiding stagnation and wasting search effort. The method is a promising approach for solving optimization problems in various domains, such as engineering, finance, and computer science.

2.10 Fading Channels

Wireless communication systems use radio waves or other forms of electromagnetic radiation to transmit data between devices without the need for physical cables. In a typical wireless communication system, such as a smartphone or Wi-Fi network, there is a transmitter that sends signals to a receiver. However, the path between the transmitter and receiver is not always smooth, and the transmitted signal can encounter various types of attenuation, which can weaken or distort the signal. Some common types of attenuation include path loss, which is the reduction in signal strength due to the distance between the transmitter and receiver, and multipath attenuation, which is the distortion of the signal due

to reflections, refractions, and other effects caused by obstacles in the environment. The amount of signal attenuation that occurs depends on various factors, such as the time at which the signal is transmitted, the frequency of the signal, and the position of the transmitter and receiver. For example, a signal transmitted at a higher frequency will experience more attenuation than a signal transmitted at a lower frequency, and a signal transmitted over a longer distance will experience more path loss than a signal transmitted over a shorter distance. The channel between the transmitter and receiver can be either time-varying or fixed, depending on whether the devices are stationary or in motion relative to each other. For example, in a stationary Wi-Fi network, the channel between the router and the connected devices is usually fixed, while in a mobile communication system, such as a cellular network, the channel between the base station and the mobile device is time-varying due to the movement of the mobile device (Viswanathan & Weldon, 2014), (Pandi & Nargund, 2018).

In wireless communication, the term "fading" pertains to the fluctuation in the strength of the received signal caused by alterations in the transmission medium or paths. Fading can occur in both fixed and mobile scenarios and is influenced by various factors such as atmospheric conditions (e.g. rainfall, lightning) and obstacles in the environment. In a fixed scenario, fading is typically caused by atmospheric effects that are constant or slowly varying over time. In a mobile scenario, however, fading is more complex and is caused by obstacles over the path that are constantly changing with respect to time, such as buildings, trees, and vehicles. These obstacles can cause reflections, diffraction, and other transmission effects that can significantly impact the quality and reliability of the transmitted signal. As a result, wireless communication systems employ various techniques to overcome the effects of fading, such as diversity techniques and equalization (Kaluuba et al., 2006).

There are two main types of fading: slow fading and fast fading. Slow fading occurs when the signal experiences large-scale attenuation due to the distance between the transmitter and receiver. This type of fading is typically constant or slowly varying over time and is often caused by atmospheric effects, such as absorption and scattering of the signal by objects in the environment. Fast fading, on the other hand, occurs when the signal experiences rapid fluctuations in signal strength. This type of fading is typically caused by small-scale variations in the transmission medium, such as reflections, refractions, and diffractions of the signal by objects in the environment (Vadda et al., 2016). Fast fading can be further classified into two types: Rayleigh fading and Rician fading.

Rayleigh fading is a suitable model to consider in urban area networks because it accurately represents the stochastic nature of wireless channels in such environments. In urban areas, the wireless propagation environment is characterized by multiple obstacles and reflections, which can cause the received signal to fluctuate randomly over time. Rayleigh fading is a fading model that captures this stochastic behavior, making it a useful tool for analyzing the performance of wireless communication systems in urban areas. Moreover, Rayleigh fading is particularly suitable for modeling small-scale fading, which is characterized by rapid variations in the received signal due to changes in the relative phases and magnitudes of the different propagation paths. Small-scale fading is a common phenomenon in urban areas, where the signal can be obstructed by buildings and other obstacles. Rayleigh fading accurately captures the statistical properties of small-scale fading, making it a useful tool for analyzing the performance of wireless communication systems in urban areas (Garg et al., 2013).

Rician fading is another statistical model that is often used to describe the effects of multipath propagation in rural or suburban environments. In Rician fading, the received signal contains a dominant line-of-sight component and multiple scattered components. The amplitude of the scattered components is modeled as a random process that follows a Rice distribution, which is a combination of a deterministic component and a random component (kaur et al., 2017), (Pathak & Katiyar, 2016).

2.11 Related Work

In this section, some related literature is reviewed on the spectral efficiency performance of massive MIMO system technologies which are directly related to the objective of this study. Since both cellular and cell-free communication systems support massive MIMO, the merits, and limitations of the reviewed literature based on spectral efficiency using different precoding algorithms are discussed.

The study by (Interdonato et al., 2021) states that, in a cell-free massive MIMO network, channel gain fluctuations between users and access points are significant due to the system's distributed topology. These variations cause data decoding approaches that consider the channel as deterministic to perform poorly. To address this issue, a precoding scheme can be developed to equalize the effective channel gain perceived by users. However, conjugate beamforming (CB) is not effective in hardening the channel for users. To improve channel hardening, the study proposes the enhanced normalized CB (ECB) variant of CB, where the

precoding vector is composed of the channel estimate's conjugate, normalized by its squared norm. A downlink spectral efficiency that can be attained is calculated for this method, taking into account factors such as channel estimation errors, pilot reuse, and lack of CSI for users. The calculation assumes independent Rayleigh fading channels. Moreover, the approach suggests an optimal max-min fairness power distribution based on large-scale fading characteristics. The usage of ECB in this method considerably improves channel hardening, enabling users to decode data with high reliability based on statistical CSI. As the effective channel provided is nearly deterministic, the acquisition of CSI at the user's end is unlikely to result in a significant improvement in performance.

The study conducted by (Interdonato et al., 2020) focuses on the cell-free Massive MIMO architecture, which is a promising network design for 5G and beyond. This architecture delivers high spectral efficiency and ubiquitous coverage by utilizing signal processing at multiple APs, as well as spatial user multiplexing and macro-diversity gain. The study proposes two precoding techniques in distributed implementation, known as local partial zero-forcing (PZF) and local protective partial zero-forcing (PPZF), which further enhance spectral efficiency by balancing interference cancelation and desired signal boosting. These schemes require only a few antennas for access points and do not entail additional front-hauling overhead. The study derives the achievable spectral efficiency for both schemes, accounting for independent Rayleigh fading channels, channel estimation errors, and pilot contamination. According to the research, PZF and PPZF have better performance than MRT and zero-forcing. They are also able to achieve similar results to regularized zero-forcing (RZF), which is considered a benchmark in the downlink. Furthermore, the formulas developed in this study can be utilized to design effective long-term power control plans, which are also applicable to RZF, for which a closed-form formula for spectral efficiency is not available.

This study (Kim et al., 2022) discusses the design of precoding for cell-free massive MIMO systems with scalability. The proposed precoding scheme, called joint centralized and distributed (JCD) precoding, aims to balance the trade-off between centralization overhead and spectral efficiency. In this scheme, only some APs collaborate to implement centralized precoding through a CPU, while the remaining APs carry out distributed precoding using local CSI to decrease front-haul signaling overhead and computational complexity. The JCD precoding scheme utilizes partial minimum mean square error (PMMSE) and local PMMSE (LPMMSE) for centralized and distributed precoding, respectively. It also involves simple

AP selection and heuristic power allocation based on the large-scale parameter. System-level simulation results demonstrate that the proposed JCD precoding scheme outperforms existing local precoding methods, such as LPMMSE and maximum ratio (MR), even when only a small number of APs are centralized.

According to (Du et al., 2021), cell-free massive MIMO systems are a promising design for future wireless networks. These networks deploy numerous distributed APs that serve a smaller number of users over the same time-frequency resources, providing better service while maintaining high spectral efficiency, straightforward linear precoding methods and max-min power control. They propose a novel joint MR and ZF (JMRZF) precoding technique in which certain APs combine to carry-out centralized ZF, while others use simple MRT. The JMRZF precoding scheme proposed in this study provides a flexible balance between front-haul signaling overhead and spectral efficiency, and they also introduce a corresponding AP subset selection technique that relies on large-scale fading coefficients. A closed-form expression that can be used to determine the spectral efficiency that can be achievabled by the proposed technique, which encompasses both fully centralized ZF and fully distributed MRT cases was derived. Using this formula, they formulate and solve max-min power control with second-order cone and first-order methods. The results from numerical simulations indicate that the JMRZF technique can perform better than local precoding techniques significantly, even when only a small subset of APs are cooperated to perform ZF, and the proposed scheme can be implemented even when each AP has a limited number of antennas.

This article (Björnson & Sanguinetti, 2020) discusses the potential benefits of cell-free massive MIMO networks and presents a new framework for such systems that is scalable and practical. In cell-free operation, multiple wireless APs cooperate to serve UEs, rather than constructing autonomous cells. The proposed framework exploits the DCC concept from the Network MIMO literature and provides a new algorithm for cluster formation, joint pilot assignment, and initial access that is scalable. Additionally, the conventional precoding, combining, and channel estimation techniques are adapted to be scalable. The article proves a new duality between uplink and downlink transmissions and uses it to heuristically design precoding vectors based on combining vectors. The proposed scalable precoding and combining methods perform better than conventional MR processing and are comparable to the best unscalable alternatives. Overall, this framework aims to leverage the advantages of cell-free operation in a practical and scalable manner, with low computational complexity

and fronthaul requirements, even in large networks with many users. This new framework has the potential to address the interference problems that commonly occur in current cellular networks and enable efficient and scalable communication in large-scale wireless networks.

This study (Qiao et al., 2022) states that cell-free massive MIMO systems have the potential to be a key technology for beyond-5G and 6G, offering high power and spectral efficiency. However, the choice of precoding technique can result in a great impact on the system's spectral efficiency in the downlink transmission. While MRT is a commonly used precoding technique in cell-free massive MIMO networks, it can't effectively minimize interference. Centralized ZF (CZF) is a precoding technique with higher interference elimination capabilities, however, it cannot be easily scaled due to the significant computational demands and limited front-haul capacity.To address this challenge and achieve high spectral efficiency while also suppressing interference and supporting system scalability, the authors propose a new joint precoding technique called Scalable Joint ZF Precoding (SJZF). SJZF leverages customized ZF precoding techniques that are specifically designed to address varying levels of inter-AP interference, resulting in a significant increase in spectral efficiency while remaining computationally feasible. The study was able to establish a mathematical formula that expresses the spectral efficiency that can be achieved under independent Rayleigh fading channels and pilot contamination. In addition, this work proposed two innovative methods to enhance the system's spectral efficiency. The first method is a unique approach to assigning pilots randomly, while the second method is a power optimization algorithm based on the principle of max-min fairness. Based on numerical results, SJZF was found to be superior to other conventional precoding schemes in terms of spectral efficiency while maintaining reasonable computational complexity. Specifically, SJZF approached the performance of CZF.

This paper (Bjornson & Sanguinetti, 2020) analyzes the potential of cell-free massive MIMO technology in addressing the increasing demand for high-speed and high-capacity wireless networks. Multiple distributed APs in the network use joint coherent signal processing to communicate with all users, according to this technology. The study provides a comprehensive analysis of four different implementations of this technology, with a focus on uplink spectral efficiencies, linear processing, and spatially correlated fading. This study provides evidence that global or local minimum mean-square error (MMSE) combining is more effective approach than maximum-ratio combining, which is commonly recommended in other literature. The results show that this approach significantly outperforms

conventional cellular massive MIMO and small cell networks. The study also shows that a centralized deployment using optimal MMSE combining can decrease the amount of fronthaul signaling required when compared to the standard distributed implementation. As a result, this becomes the preferred way of operating cell-free massive MIMO systems. The paper also examines non-linear decoding, which is shown to bring only minimal improvements.

This article (Interdonato et al., 2018) focuses on the use of cell-free massive MIMO technology for high spectral efficiency in communication systems. However, the performance and scalability of the system are limited by interference and fronthauling traffic. To address this, the full-pilot ZF (fpZF) precoding technique is introduced to suppress both intra- and inter-cell interference having no CSI sharing between APs. The research introduces a new analytical method for determining the downlink spectral efficiency in a cell-free massive MIMO network that employs multi-antenna access points and fpZF precoding. The model accounts for imperfections in CSI and pilot contamination, and includes a max-min fairness approach to optimize downlink power. The findings demonstrate that fpZF precoding delivers superior performance compared to MRT, without maximizing the fronthauling overhead, as long as the network is adequately distributed.

The study (Qiu et al., 2019) explored the downlink spectral efficiency of cell-free massive MIMO in response to the growing need for faster and more efficient communication in 5G networks. The study examined various precoding and power control techniques over spatially correlated Rayleigh fading channels. The findings indicated that cell-free massive MIMO outperformed cellular massive MIMO based on downlink performance. The study also proposed an ad-hoc enabled cell-free massive MIMO architecture to further enhance its performance. Based on the simulation results the proposed architecture increased the 5% outage rate from 1.04 bit/s/Hz to 2.82 bit/s/Hz. Moreover, the ad-hoc enabled cell-free massive MIMO network demonstrated significantly higher spectral efficiency compared to cellular massive MIMO.

Table 2.1: Summary of some related literature

Year of publication	Title of the research	Theoretical model	Proposed method(s)	Finding(s)	Research gap
2022	Joint Precoding Scheme with Enhanced Spectral Efficiency for Cell-Free Massive MIMO Downlink	Scalable Joint Zero-Forcing Precoding applies different zero-forcing precoding schemes based on the degree of inter-AP interference	Scalable Joint Zero-Forcing Precoding	Scalability and downlink spectral efficiency increased.	Even though the downlink spectral efficiency increased, it is not compared with MMSE which is a powerful precoding technique
2021	Enhanced Normalized Conjugate Beamforming for Cell-Free Massive	In enhanced normalized Conjugate Beamforming (ECB), the precoding vector consists of the conjugate of the channel estimate normalized by its squared norm.	enhanced normalized Conjugate Beamforming	ECB greatly improves channel hardening, allowing users to reliably decode data based only on statistical CSI.	Do Not consider User-centric clustering and it is not scalable Considers only Statistical CSI

2021	Cell-Free Massive MIMO: Joint Maximum-Ratio and Zero-Forcing Precoder With Power Control	The JMRZF precoding scheme employs a hybrid approach where certain APs are used for centralized ZF, while others use MRT for transmitting signals.	Joint maximum-ratio and zero-forcing (JMRZF) precoding scheme	The JMRZF scheme can outperform local precoding schemes with few APs and antennas.	The proposed precoding scheme is compared with only local precoders, it doesn't compared with central precoding schemes
2020	Local Partial Zero-Forcing Precoding for Cell-Free Massive MIMO	Local Partial Zero-Forcing and Local Protective Partial Zero-Forcing try to balance interference cancelation and desired signal boosting, without additional front-hauling overhead	Local Partial Zero-Forcing (PZF) and Local Protective Partial Zero-Forcing (PPZF)	The proposed algorithms, PZF and PPZF can outperform maximum ratio transmission and zero-forcing based on spectral efficiency	The precoding techniques are limited only to local operations, the centralized operations are not addressed

2020	Scalable Cell-Free Massive MIMO Systems	Existing unscalable precoding schemes are re designed to consider part of users in the network area	Adapt the standard precoding methods to become scalable.	The proposed scalable precoders outperformed conventional MR processing and also performs closely to the best unscalable alternatives	The proposed precoders do not outperform the existing best unscalable alternatives

The contribution of this thesis is the development of a new precoding scheme for cell-free massive MIMO that can outperform existing precoding algorithms. By addressing the gaps and main challenges of cell-free massive MIMO, like scalability, computational complexity, and interference management, the new algorithm can improve system performance and reduce interference. Overall, this thesis aims to make a significant contribution to the field of wireless communication by proposing a new and improved precoding technique for cell-free massive MIMO.

CHAPTER THREE

3. MATERIAL AND METHODOLOGY

3.1 Introduction

In this thesis work, secondary sources of information about precoding techniques for downlink cell-free massive MIMO systems, such as previous researchers' works, various Institute of Electrical and Electronics Engineers (IEEE) articles, and journals, were reviewed. In downlink cell-free massive MIMO systems, researchers used their own proposed methodologies to come up with high-performance and low-complexity precoding techniques. Considering a literature review, problem statement, and the limitations of existing precoding methods, this work's approach is presented below.

3.2 Material

Software like MATLAB and ConceptDraw DIAGRAM are used in this thesis. Engineers and scientists can study, design, and invent technologies that will impact the world using the programming tool known as MATLAB. MATLAB R2022b software was used to create all of the simulation findings in chapter four of this thesis. ConceptDraw DIAGRAM is a drawing software that provides professional drawing tools, pre-made templates, an extensive object library, and various printing and file export options. All of the diagrams except the simulation results in chapter four were created using various objects from various libraries that are part of this software, such as Basic shapes, block diagrams, cloud computing diagrams, computer networks, computers and communications, network security diagrams, and telecommunication network diagrams.

3.3 Methodology

3.3.1 System design

- Analyzing the mathematical model of different precoding algorithms to calculate the spectral efficiency.
- Developing the hybrid precoding algorithm based on PRZF and MPA for downlink cell-free massive MIMO systems.

3.3.2 Simulation method

- Perform simulations of average spectral efficiency versus UEs to evaluate how the proposed precoding method performs in comparison to other existing algorithms.
- Perform a performance comparison of the proposed precoding method with other algorithms based on sum spectral efficiency versus UEs simulation.
- Perform simulations of CDF versus spectral efficiency per UE to compare the performance of the proposed scheme with other schemes.
- Perform a computational complexity comparison of the proposed precoder with existing precoding schemes in terms of the real number of multiplications versus the number of users' simulations.

3.3.3 Downlink mathematical system model of precoding algorithms for cell-free massive MIMO

3.3.3.1 System model

We take into account a cell-free massive MIMO system with L APs, each having N number of antennas, strategically positioned across the coverage region (see Figure 3.1). The total number of AP antennas in the network is represented by M = NL. The K single-antenna UEs are served collectively by the APs. To be more specific, each user is in communication with a subset of the APs that are chosen in accordance with the UE's requirements. The fronthaul links that connect the APs to the CPUs enable the AP cooperation.

We'll use $\mathbf{x}_l \in \mathbb{C}^N$ to represent the signal transmitted from AP *l* in the downlink transmission. The receiver noise is denoted by $n_k \sim \mathcal{N}_{\mathbb{C}}\left(0, \sigma_{\mathrm{dl}}^2\right)$, where it conforms to a normal distribution with a mean of 0 and a variance σ_{dl}^2. To represent the downlink channel, we use the Hermitian transpose of $\mathbf{h}_{kl}^{\mathrm{H}}$. Although in practice, only a transpose is needed and not any complex conjugate, we include the conjugation for simplicity in notation without affecting performance.

Subsequently, based on (Björnson & Sanguinetti, 2020) the signal received by user k can be formulated as

$$y_k^{\mathrm{dl}} = \sum_{l=1}^{L} \mathbf{h}_{kl}^{\mathrm{H}} \mathbf{x}_l + n_k \qquad (3.1)$$

$\varsigma_i \in \mathbb{C}^N$ is defined as the separate unit-power information signal intended for user i, hence $\mathbb{E}\{|\varsigma_i|^2\} = 1$. The transmitted signal by AP l is a constructed combination of the precoded signals that are designated for each of the supported UEs. In other words, this can be expressed as (Bjornson & Sanguinetti, 2019), (Björnson & Sanguinetti, 2020)

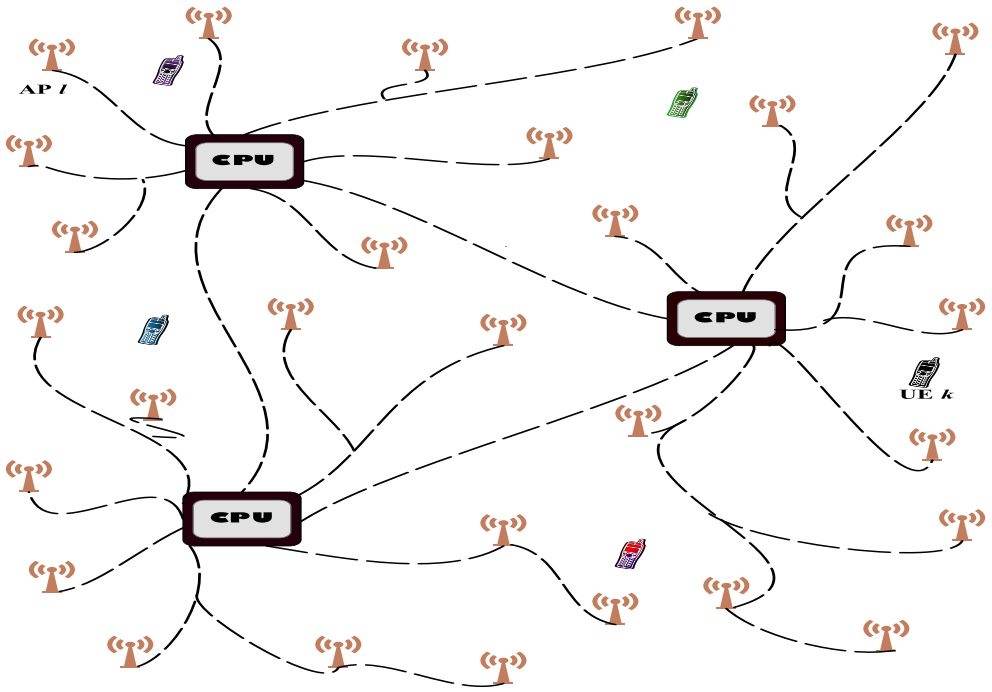

Figure 3.1: Scalable cell-free massive MIMO system model (Elhoushy et al., 2022).

$$\mathbf{x}_l = \sum_{i=1}^{K} \mathbf{c}_{il}\mathbf{P}_{il}\varsigma_i \tag{3. 2}$$

where the transmit precoding vector assigned to UE i by AP l is indicated by the symbol $\mathbf{P}_{il} \in \mathbb{C}^N$. This vector's effects on the transmission are significant in two ways: The spatial directionality is determined by the direction $\mathbf{P}_{il}/\|\mathbf{P}_{il}\|$, and the average transmit power is determined by the average squared norm $\mathbb{E}\{\|\mathbf{P}_{il}\|^2\}$. The efficient precoding vector can be described as

$$\mathbf{c}_{il}\mathbf{P}_{il} = \begin{cases} \mathbf{P}_{il} & l \in \mathcal{M}_i \\ \mathbf{0}_N & l \notin \mathcal{M}_i \end{cases} \tag{3. 3}$$

Given that $\mathbf{c}_{il} = \mathbf{0}_{N\times N}$, $\mathbf{c}_{il}\mathbf{P}_{il} = \mathbf{0}_N$ is implied and $\mathcal{M}_i$ refers to APs found in the cluster. It follows that each AP simply has to choose the precoding vectors for the UEs under its support.

Replacing the transmitted signal in equation (3.2) into equation (3.1) results in the downlink signal received at user k.

$$\begin{aligned} y_k^{\mathrm{dl}} &= \sum_{l=1}^{L} \mathbf{h}_{kl}^{\mathrm{H}} \left(\sum_{i=1}^{K} \mathbf{c}_{il} \mathbf{P}_{il} \varsigma_i \right) + n_k \\ &= \sum_{l=1}^{L} \mathbf{h}_{kl}^{\mathrm{H}} \mathbf{c}_{kl} \mathbf{P}_{kl} \varsigma_k + \sum_{\substack{i=1 \\ i \neq k}}^{K} \sum_{l=1}^{L} \mathbf{h}_{kl}^{\mathrm{H}} \mathbf{c}_{il} \mathbf{P}_{il} \varsigma_i + n_k \end{aligned} \tag{3. 4}$$

In equation (3. 4), the desired signal is the first term, followed by interference from users and noise.

3.3.3.2 Downlink centralized implementation

The most cutting-edge downlink version of cell-free massive MIMO technology is a completely centralized system, wherein the APs function solely as remote radio heads or relays that transmit signals generated by the CPU and transmitted through the fronthaul links. Think back to equation (3. 4) the downlink signal that UE k has received is

$$y_k^{\mathrm{dl}} = \sum_{l=1}^{L} \mathbf{h}_{kl}^{\mathrm{H}} \mathbf{x}_l + n_k = \sum_{l=1}^{L} \mathbf{h}_{kl}^{\mathrm{H}} \left(\sum_{i=1}^{K} \mathbf{c}_{il} \mathbf{P}_{il} \varsigma_i \right) + n_k \tag{3. 5}$$

where $n_k \sim \mathcal{N}_{\mathbb{C}}\left(0, \sigma_{\mathrm{dl}}^2\right)$ is noise from the receiver and

$$\mathbf{x}_l = \sum_{i=1}^{K} \mathbf{c}_{il} \mathbf{P}_{il} \varsigma_i \tag{3. 6}$$

is the transmitted signal by AP *l*.

We can rewrite the receiver signal in compact form as

$$y_k^{\mathrm{dl}} = \sum_{i=1}^{K} \begin{bmatrix} \mathbf{h}_{k1} \\ \vdots \\ \mathbf{h}_{kL} \end{bmatrix}^{\mathrm{H}} \begin{bmatrix} \mathbf{c}_{i1} \mathbf{P}_{i1} \\ \vdots \\ \mathbf{c}_{iL} \mathbf{P}_{iL} \end{bmatrix} \varsigma_i + n_k = \sum_{i=1}^{K} \mathbf{h}_k^{\mathrm{H}} \mathbf{c}_i \mathbf{P}_i \varsigma_i + n_k \tag{3. 7}$$

Where $\mathbf{h}_k = [\mathbf{h}_{k1}^{\mathrm{T}} \quad \ldots \mathbf{h}_{kL}^{\mathrm{T}}]^{\mathrm{T}} \in \mathbb{C}^{LN}$ is the collective channel from all APs to user k, the block-diagonal matrix $\mathbf{c}_i = \mathrm{diagonal}(\mathbf{c}_{i1}, \ldots, \mathbf{c}_{iL})$ selects the transmitting APs for UE i, and $\mathbf{P}_i = \left[\mathbf{P}_{i1}^{\mathrm{T}} \ldots \mathbf{P}_{iL}^{\mathrm{T}}\right]^{\mathrm{T}} \in \mathbb{C}^{LN}$ denoted the assigned collective precoding vector for UE i.

3.3.3.2.1 Spectral efficiency of centralized implementation

Now a feasible expression for spectral efficiency that is applicable to all precoding techniques will be presented. The received signal for UE *k* in equation (3.7) can be decomposed into three parts and reformulated as follows (Björnson & Sanguinetti, 2020):

$$y_k^{\mathrm{dl}} = \underbrace{\mathbf{h}_k^{\mathrm{H}}\mathbf{c}_k\mathbf{P}_k\varsigma_k}_{\text{Desired signal}} + \underbrace{\sum_{\substack{i=1 \\ i\neq k}}^{K} \mathbf{h}_k^{\mathrm{H}}\mathbf{c}_i\mathbf{P}_i\varsigma_i}_{\text{Inter-user interference}} + \underbrace{n_k}_{\text{Noise}} \tag{3. 8}$$

The goal of the UE is to retrieve information from the initial component despite the existence of interference from other users and noise, denoted by the subsequent two parts. The product of the desired signal ς_k and the expression $\mathbf{h}_k^{\mathrm{H}}\mathbf{c}_k\mathbf{P}_k$ is known as the effective downlink channel, which signifies that the precoding technique efficiently transforms the multi-antenna channel $\mathbf{h}_k$ into a unit-antenna channel represented by $\mathbf{h}_k^{\mathrm{H}}\mathbf{c}_k\mathbf{P}_k$.

An achievable downlink spectral efficiency of UE *k* with centralized operation is (Bjornson & Sanguinetti, 2020), (Björnson & Sanguinetti, 2020)

$$\mathrm{SE}_k^{(\mathrm{dl,c})} = \frac{\tau_d}{\tau_c}\log_2\left(1 + \mathrm{SINR}_k^{(\mathrm{dl,c})}\right) \text{ bit/s/Hz} \tag{3. 9}$$

where $\mathrm{SINR}_k^{(\mathrm{dl},c)}$ is the effective SINR

$$\mathrm{SINR}_k^{(\mathrm{dl},c)} = \frac{\left|\mathbb{E}\{\mathbf{h}_k^{\mathrm{H}}\mathbf{c}_k\mathbf{P}_k\}\right|^2}{\sum_{i=1}^{K}\mathbb{E}\left\{\left|\mathbf{h}_k^{\mathrm{H}}\mathbf{c}_i\mathbf{P}_i\right|^2\right\} - \left|\mathbb{E}\{\mathbf{h}_k^{\mathrm{H}}\mathbf{c}_k\mathbf{P}_k\}\right|^2 + \sigma_{\mathrm{dl}}^2} \tag{3. 10}$$

The portion of every coherence block allocated for downlink signal transmission is indicated by the pre-log factor τ_d/τ_c. With the selection of the DUCC and any precoding vector $\mathbf{P}_k$, the spectral efficiency expression in (3.9) is valid.

- **Centralized transmit precoding**

The precoding vector designated for UE *k* in a centralized configuration is denoted as

$$\mathbf{P}_k = \sqrt{\rho_k}\frac{\overline{\mathbf{P}}_k}{\sqrt{\mathbb{E}\left\{\left\|\overline{\mathbf{P}}_k\right\|^2\right\}}} \tag{3. 11}$$

The assigned sum power transmitted from all serving APs to UE *k* is denoted by $\rho_k \geq 0$, and the vector $\overline{\mathbf{P}}_k \in \mathbb{C}^{LN}$, which is arbitrarily scaled, indicates the direction of the precoding vector. It is important to note that the normalization described in equation (3. 11) ensures that

$$\mathbb{E}\{\|\mathbf{P}_k\|^2\} = \rho_k \tag{3. 12}$$

3.3.3.2.2 MMSE precoding

The downlink MMSE precoding vector obtained from (3. 11) can be given as (Bjornson & Sanguinetti, 2020), (Björnson & Sanguinetti, 2020)

$$\overline{\mathbf{P}}_k^{\text{MMSE}} = p_k \left(\sum_{i=1}^{K} p_i \mathbf{c}_k \left(\hat{\mathbf{h}}_i \hat{\mathbf{h}}_i^{\text{H}} + \mathbf{R}_i \right) \mathbf{c}_k + \sigma_{\text{dl}}^2 \mathbf{I}_{LN} \right)^{-1} \mathbf{c}_k \hat{\mathbf{h}}_k \tag{3. 13}$$

where $\mathbf{R}_i$ is the entire estimation error correlation matrix corresponding to all UEs in the coverage area.

3.3.3.2.3 PMMSE precoding

Given a distributed network of UEs operating in a cell-free massive MIMO network, it is rational to assume that the interference affecting a particular UE (labeled as UE *k*) is largely constructed by a small group of neighboring UEs positioned in close proximity to UE k. This observation enables us to scale down the optimal MMSE precoding complexity. Consequently, only those UEs linked to the same set of APs as user k are incorporated in the inverse matrix in equation (3.13).

Using $\mathcal{S}_k$, it is possible to derive an alternative partial MMSE (PMMSE) precoding method from equation (3. 11) as mentioned in (Nayebi et al., 2016), (Björnson & Sanguinetti, 2020).

$$\overline{\mathbf{P}}_k^{\text{PMMSE}} = p_k \left(\sum_{i \in \mathcal{S}_k} p_i \mathbf{c}_k \hat{\mathbf{h}}_i \hat{\mathbf{h}}_i^{\text{H}} \mathbf{c}_k + \mathbf{R}_{\mathcal{S}_k} + \sigma_{\text{dl}}^2 \mathbf{I}_{LN} \right)^{-1} \mathbf{c}_k \hat{\mathbf{h}}_k \tag{3. 14}$$

where $\mathbf{R}_{\mathcal{S}_k}$ is the entire estimation error correlation matrix corresponding to those users in the set $\mathcal{S}_k$, which is comprised of all the UEs served by the same APs as UE k. Since it has the same structure as MMSE precoding, this precoding technique is anticipated to perform similarly, with the exception that it ignores those users that are solely in the service of other

APs, thereby minimizing the computational cost. All the UEs that fall under the effect of the APs that service user k ought to be incorporated in $\mathcal{S}_k$ if the DUCC is properly built.

3.3.3.2.4 PRZF precoding

It would be helpful to see whether more complexity reduction is possible without significantly degrading performance. An alternative approach is derived from the simplification of PMMSE, which involves disregarding the estimation error correlation matrix $\mathbf{R}_{\mathcal{S}_k}$ in equation (3. 14). Partial Regularized Zero Forcing (PRZF) precoding can be obtained from equation (3. 11) as follows (Björnson & Sanguinetti, 2020)

$$\overline{\mathbf{P}}_k^{\mathrm{PRZF}} = \left[\mathbf{c}_k \hat{\mathbf{h}}_{\mathcal{S}_k} \left(\hat{\mathbf{h}}_{\mathcal{S}_k}^{\mathrm{H}} \mathbf{c}_k \hat{\mathbf{h}}_{\mathcal{S}_k} + \sigma_{\mathrm{dl}}^2 p_{\mathcal{S}_k}^{-1}\right)^{-1}\right]_{:,1} \tag{3. 15}$$

To obtain $\hat{\mathbf{h}}_{\mathcal{S}_k} \in \mathbb{C}^{LN \times |\mathcal{S}_k|}$, all the estimated channel vectors $\hat{\mathbf{h}}_i$ are stacked with indices $i \in \mathcal{S}_k$ and place them in a column-wise manner. The first column of $\hat{\mathbf{h}}_{\mathcal{S}_k}$ is $\hat{\mathbf{h}}_k$. Additionally, $p_{\mathcal{S}_k} \in \mathbb{R}^{|\mathcal{S}_k| \times |\mathcal{S}_k|}$ is a diagonal matrix consisting of transmit powers p_i for $i \in \mathcal{S}_k$, which are arranged in the same pattern as the columns of $\hat{\mathbf{h}}_{\mathcal{S}_k}$.

3.3.3.3 Downlink distributed implementation

To achieve downlink communication in a distributed system, it is feasible to utilize a method where most of the processing is performed locally at every AP. In this approach, the CPU is responsible for encoding the downlink signals $\{\varsigma_i : i = 1, \ldots, K\}$ and transmitting them to the serving APs. Subsequently, each AP performs the remaining signal processing independently. It should be noted that the CPU is a virtual unit, and the encoding function can be executed from any location within the network without requiring a physical centralized unit. The distributed operation has a notable advantage in that new APs can be added without necessitating an upgrade to the computational ability of the CPU. This is feasible since every AP has its own local processor that can perform baseband processing tasks. In the distributed implementation (Björnson & Sanguinetti, 2020), each AP l independently constructs its transmitted signal as

$$\mathbf{x}_l = \sum_{i=1}^{K} \mathbf{c}_{il} \mathbf{P}_{il} \varsigma_i \tag{3. 16}$$

as previously mentioned in (3.2).

3.3.3.3.1 Spectral efficiency of the distributed implementation

The signal that UE *k* receives can be expressed as

$$\begin{aligned} y_k^{\mathrm{dl}} &= \sum_{l=1}^{L} \mathbf{h}_{kl}^{\mathrm{H}} \mathbf{x}_l + n_k \\ &= \underbrace{\left(\sum_{l=1}^{L} \mathbf{h}_{kl}^{\mathrm{H}} \mathbf{c}_{kl} \mathbf{P}_{kl} \right) \varsigma_k}_{\text{Desired signal}} + \underbrace{\sum_{\substack{i=1 \\ i \neq k}}^{K} \left(\sum_{l=1}^{L} \mathbf{h}_{kl}^{\mathrm{H}} \mathbf{c}_{il} \mathbf{P}_{il} \right) \varsigma_i}_{\text{Inter-user interference}} + \underbrace{n_k}_{\text{Noise}} \end{aligned} \tag{3. 17}$$

The scenario of centralized downlink implementation in (3. 5) is the same as the one described here, except for the precoding selection process. In this case, each AP must perform precoding selection locally using the channel estimates available to them. The UE has access to the same information for signal detection in both cases.

Therefore, the SE of UE k achieved by the decentralized operation is

$$\mathrm{SE}_k^{(\mathrm{dl,d})} = \frac{\tau_d}{\tau_c} \log_2 \left(1 + \mathrm{SINR}_k^{(\mathrm{dl,d})} \right) \text{ bit/s/Hz} \tag{3. 18}$$

with the effective SINR given by

$$\mathrm{SINR}_k^{(\mathrm{dl,d})} = \frac{\left| \sum_{l=1}^{L} \mathbb{E}\{ \mathbf{h}_{kl}^{\mathrm{H}} \mathbf{c}_{kl} \mathbf{P}_{kl} \} \right|^2}{\sum_{i=1}^{K} \mathbb{E}\left\{ \left| \sum_{l=1}^{L} \mathbf{h}_{kl}^{\mathrm{H}} \mathbf{c}_{il} \mathbf{P}_{il} \right|^2 \right\} - \left| \sum_{l=1}^{L} \mathbb{E}\{ \mathbf{h}_{kl}^{\mathrm{H}} \mathbf{c}_{kl} \mathbf{P}_{kl} \} \right|^2 + \sigma_{dl}^2} \tag{3. 19}$$

The interpretation of the spectral efficiency of UE k and its SINR is the same as in the centralized scenario.

- **Local transmit precoding**

To transmit downlink data to a specific UE *k*, only a specific group of APs are involved. Therefore, it is sufficient to select the effective precoding vectors $\mathbf{c}_{kl}\mathbf{P}_{kl}$ only for APs in the set $\mathcal{M}_k$. The precoding vector used by an AP *l* serving UE k can be represented as:

$$\mathbf{P}_{kl} = \sqrt{\rho_{kl}} \frac{\bar{\mathbf{P}}_{kl}}{\sqrt{\mathbb{E}\left\{ \| \bar{\mathbf{P}}_{kl} \|^2 \right\}}} \tag{3. 20}$$

Here, $p_{kl} \geq 0$ represents the power assigned by AP l to user k for transmission. Moreover, the vector $\overline{\mathbf{P}}_{kl} \in \mathbb{C}^N$ is adjusted in scale to indicate the direction of the precoding vector. It is worth mentioning that the normalization present in equation (3.20) ensures that:

$$\mathbb{E}\left\{\|\overline{\mathbf{P}}_{kl}\|^2\right\} = \rho_{kl} \tag{3. 21}$$

3.3.3.3.2 LMMSE precoding

The downlink LMMSE precoding described in (Björnson & Sanguinetti, 2020) can be derived by utilizing equation (3. 20) as

$$\overline{\mathbf{P}}_k^{\mathrm{LMMSE}} = p_k \left(\sum_{i=1}^{K} p_i \left(\hat{\mathbf{h}}_{il} \hat{\mathbf{h}}_{il}^{\mathrm{H}} + \mathbf{R}_{il} \right) + \sigma_{\mathrm{dl}}^2 \mathbf{I}_N \right)^{-1} \mathbf{c}_{kl} \hat{\mathbf{h}}_{kl} \tag{3. 22}$$

Since the LMMSE precoding in (3. 22) includes an entire set of all UEs in the network, it is not a scalable approach. The following two scalable options are examined.

3.3.3.3.3 LPMMSE precoding

A scalable approximation of LMMSE precoding (Björnson & Sanguinetti, 2020) can be obtained by considering only the UEs supported by the AP. This can be called LPMMSE precoding and obtained from (3. 20) using

$$\overline{\mathbf{P}}_k^{\mathrm{LPMMSE}} = p_k \left(\sum_{i \in c_l} p_i \left(\hat{\mathbf{h}}_{il} \hat{\mathbf{h}}_{il}^{\mathrm{H}} + \mathbf{P}_{il} \right) + \sigma_{\mathrm{dl}}^2 \mathbf{I}_N \right)^{-1} \mathbf{c}_{kl} \hat{\mathbf{h}}_{kl} \tag{3. 23}$$

3.3.3.3.4 MR precoding

From (Nayebi et al., 2016) and (Ngo et al., 2017) the scalable form of MR precoding, which is obtained from (3. 20) can be expressed as

$$\overline{\mathbf{P}}_{kl}^{\mathrm{MR}} = \mathbf{c}_{kl} \hat{\mathbf{h}}_{kl} \tag{3. 24}$$

The aim of this scheme is to enhance the received power proportion of the intended UE from AP l, which constitutes the numerator of the effective SINR. Nevertheless, the MR precoding technique disregards the interference produced by the access point, especially among the UEs it serves.

3.3.4 Proposed method

The primary goal of this thesis is to design an efficient precoding technique based on the existing precoding algorithm.

Our proposed method involves replacing the initial predator position in the marine predator algorithm with the precoding vector mentioned in equation (3.15). In the MPA, minimizing the objective function, which is typically a cost function, is crucial. For our approach, the objective function is the interference signal $\sum_{\substack{i=1 \\ i\neq k}}^{K} \mathbf{h}_k^{\mathrm{H}} \mathbf{c}_i \mathbf{P}_i \varsigma_i$ which is referred to in the second term of equation (3.8). Our primary goal is to generate a new precoding vector based on $\overline{\mathbf{P}}_k^{\mathrm{PRZF}}$ and MPA, which can minimize these interference signals to maximize the SINR signal in equation (3.10), resulting in a higher SE in equation (3.9).

According to the theory of survival of the fittest, it is believed that the most skilled foragers in nature are the top predators. As a result, the most adept solution is selected as the top predator ($\overline{\mathbf{P}}_k^{\mathrm{PRZF}}$ in our case) to form a matrix known as the Elite. This matrix consists of arrays that facilitate the search and detection of prey by utilizing information on their positions (Ramezani et al., 2021).

$$\text{Elite} = \begin{bmatrix} X_{1,1}^{l} & X_{1,2}^{l} & \cdots & X_{1,d}^{l} \\ X_{2,1}^{l} & X_{2,2}^{l} & \cdots & X_{2,d}^{l} \\ \vdots & \vdots & \vdots & \vdots \\ \vdots & \vdots & \vdots & \vdots \\ \vdots & \vdots & \vdots & \vdots \\ X_{n,1}^{l} & X_{n,2}^{l} & \cdots & X_{n,d}^{l} \end{bmatrix}_{n\times d} \tag{3. 25}$$

The Elite matrix is constructed by replicating the top predator (i.e. $\overline{\mathbf{P}}_k^{\mathrm{PRZF}}$) vector $\overrightarrow{X^l}$ n times, where n represents the number of search agents and d represents the number of dimensions. It should be noted that both the predator and the prey are regarded as search agents since while the predator is searching for its prey, the prey is also searching for its food. At the end of each iteration, if a better predator is found, it will replace the current top predator in the Elite matrix, which will then be updated accordingly.

A matrix called Prey, which has the same dimensions as the Elite matrix, is also utilized. The predators update their positions based on this matrix. Simply put, the initial Prey is created during the initialization process, and the fittest one (predator) is used to construct the

Elite matrix. From (Ramezani et al., 2021), (Jangir et al., 2023) the Prey matrix is represented as follows:

$$\text{Prey} = \begin{bmatrix} X_{1,1} & X_{1,2} & \cdots & X_{1,d} \\ X_{2,1} & X_{2,2} & \cdots & X_{2,d} \\ X_{3,1} & X_{3,2} & \cdots & X_{3,d} \\ \vdots & \vdots & \vdots & \vdots \\ \vdots & \vdots & \vdots & \vdots \\ X_{n,1} & X_{n,2} & \cdots & X_{n,d} \end{bmatrix}_{n \times d} \tag{3. 26}$$

In equation (3.27), $X_{i,j}$ presents the j-th dimension of i-th prey. It is important to note that the entire optimization process is primarily and directly linked to these two matrices.

The optimization process of MPA is categorized into three principal stages, each of which takes into account various velocity ratios and simulates the complete life cycle of a predator and its prey. These phases are established according to the principles that govern the natural movements of predators and prey while replicating their movements in the marine. The three phases are described in different literature (Ramezani et al., 2021), (Jangir et al., 2023), (Faramarzi et al., 2020), (Al-Betar et al., 2023) as follows:

Phase 1: The first phase of MPA optimization deals with scenarios where the predator is moving at a higher velocity than its prey, resulting in a high-velocity ratio. This typically occurs during the initial iterations of the optimization process when exploration is crucial. In cases where the velocity ratio is equal to or greater than 10 (v ≥ 10), the optimal strategy for the predator is to remain stationary. The mathematical model of this rule is applied as follows:

$$\begin{aligned} &\text{While } Iteration < \frac{1}{3} Max\_Iteration \\ &\overrightarrow{stepsize_i} = \vec{R}_B \otimes \left(\overrightarrow{Elite_i} - \vec{R}_B \otimes \overrightarrow{Prey_i}\right) \qquad i = 1, \ldots . n \\ &\overrightarrow{Prey_i} = \overrightarrow{Prey_i} + P.\vec{R} \otimes \overrightarrow{stepsize_i} \end{aligned} \tag{3. 28}$$

The mathematical model applied in the first phase of MPA optimization involves a vector, $\vec{R}_B$, which consists of random numbers that follow a Normal distribution and represent Brownian motion. The symbol ⊗ represents entry-wise multiplication. By multiplying $\vec{R}_B$with prey, the movement of the prey is simulated. P=0.5 is a constant value, and R is a vector of uniform random numbers ranging from 0 to 1. This scenario occurs

during the first third of the iterations when the exploration ability is high, resulting in a high step size or velocity of movement. "*Iteration*" represents the current iteration, while "*Max_Iteration*" represents the maximum number of iterations.

Phase 2: During the intermediate phase of optimization, when both predator and prey are moving at the same speed or in unit velocity ratio, it appears as though both are seeking out their target. This phase involves a balance between exploration and exploitation, with half of the population designated for each. In this phase, the prey is responsible for exploitation while the predator focuses on exploration. According to the rule, when the prey moves using Lévy, the most effective strategy for the predator in unit velocity ratio is Brownian motion. Therefore, this research assumes that the prey uses Lévy motion while the predator uses Brownian motion.

$$While\ \frac{1}{3}\ Max\_Iteration < Iteration\ < \frac{2}{3}\ Max\_Iteration$$

For the first half of the population

$$\begin{aligned} \overrightarrow{stepsize_i} &= \vec{R}_L \otimes \left(\overrightarrow{Elite_i} - \vec{R}_L \otimes \overrightarrow{Prey_i}\right) \qquad i = 1, \ldots . \frac{n}{2} \\ \overrightarrow{Prey_i} &= \overrightarrow{Prey_i} + P.\vec{R}\ \otimes\ \overrightarrow{stepsize_i} \end{aligned} \tag{3. 29}$$

The vector $\vec{R}_L$ consists of random numbers that follow the Lévy distribution and are used to represent the Lévy movement of the prey. When $\vec{R}_L$ is multiplied by the Prey, it simulates the prey's movement using the Lévy distribution. Additionally, adding the step size to the prey's position simulates the prey's overall movement. As Lévy distributions often involve small steps, this movement aids in the exploitation phase. For the second half of the population, this study assumes:

$$\begin{aligned} \overrightarrow{stepsize_i} &= \vec{R}_B \otimes \left(\vec{R}_B \otimes \overrightarrow{Elite_i} - \overrightarrow{Prey_i}\right) \qquad i = \frac{n}{2}, \ldots . n \\ \overrightarrow{Prey_i} &= \overrightarrow{Elite_i} + P.\mathrm{CF} \otimes\ \overrightarrow{stepsize_i} \end{aligned} \tag{3. 30}$$

The parameter CF (convergence factor), which is calculated as $CF = (1 - \frac{Iteration}{Max\_Iteration})^{(2\frac{Iteration}{Max\_Iteration})}$, is used to adjust the step size of the predator's movement adaptively. By multiplying the vector $\vec{R}_B$ with Elite, the predator's movement is simulated

using Brownian motion. As a result, the prey updates its position based on the movement of the predators in a Brownian manner.

Phase 3: In cases where the predator is moving faster than the prey or in a low-velocity ratio, which typically occurs in the final phase of the optimization process, there is a higher focus on exploitation. In a low-velocity ratio scenario where the predator is ten times faster than the prey (v = 0.1), the most effective strategy for the predator is to use Lévy motion. This phase can be presented as:

$$While\ \ Iteration > \frac{2}{3}\ Max\_Iteration$$

$$\begin{aligned} \overrightarrow{stepsize_i} &= \vec{R}_L \otimes \left(\vec{R}_L \otimes \overrightarrow{Elite_i} - \overrightarrow{Prey_i}\right) \qquad i = 1, \ldots . n \\ \overrightarrow{Prey_i} &= \overrightarrow{Elite_i} + P.\mathrm{CF} \otimes \overrightarrow{stepsize_i} \end{aligned} \tag{3. 31}$$

The movement of the predator using the Lévy strategy is simulated by multiplying the vector $\vec{R}_L$ with Elite, while the addition of the step size to the Elite's position simulates the predator's movement, aiding in the update of the prey's position.

Marine predators can change their behavior due to various environmental factors, such as the formation of eddies or the influence of Fish Aggregating Devices (FADs). FADs are regarded as local peaks, and their effect is similar to getting trapped in these locations during a search. To avoid being stuck in local peaks during simulations, it is important to consider longer jumps. Therefore, the FADs effect is expressed mathematically as:

$$\overrightarrow{Prey_i} = \begin{cases} \overrightarrow{Prey_i} + CF\left[\vec{X}_{min} + \vec{R} \otimes \left(\vec{X}_{max} - \vec{X}_{min}\right)\right] \otimes \vec{U} & if\ r \le FADs \\ \overrightarrow{Prey_i} + \left[FADs(1-r) + r\right]\left(\overrightarrow{Prey_{r1}} - \overrightarrow{Prey_{r2}}\right) & if\ r > FADs \end{cases} \tag{3. 32}$$

The probability of FADs' effect on the optimization process is represented by FADs = 0.2. The vector $\vec{U}$ is a binary vector consisting of arrays containing either zero or one. To construct this vector, a random vector is generated from the range [0, 1], and if an array in the vector is less than 0.2, it is changed to zero, whereas if it is greater than 0.2, it is changed to one. The uniform random number r is chosen from the range [0, 1]. The vectors $\vec{X}_{min}$ and $\vec{X}_{max}$ include the lower and upper bounds of the dimensions, respectively. The subscripts r1 and r2 represent random indexes of the prey matrix.

The working principle of the proposed precoding technique can be described in the form of block diagram and flow chart as follows.

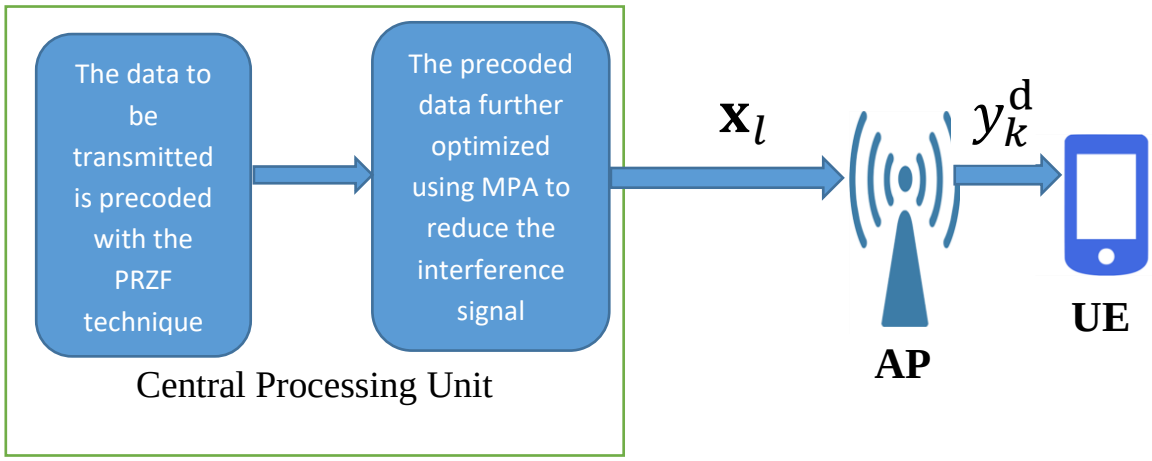

Figure 3.2: Block diagram of proposed precoder based on PRZF and MPA techniques

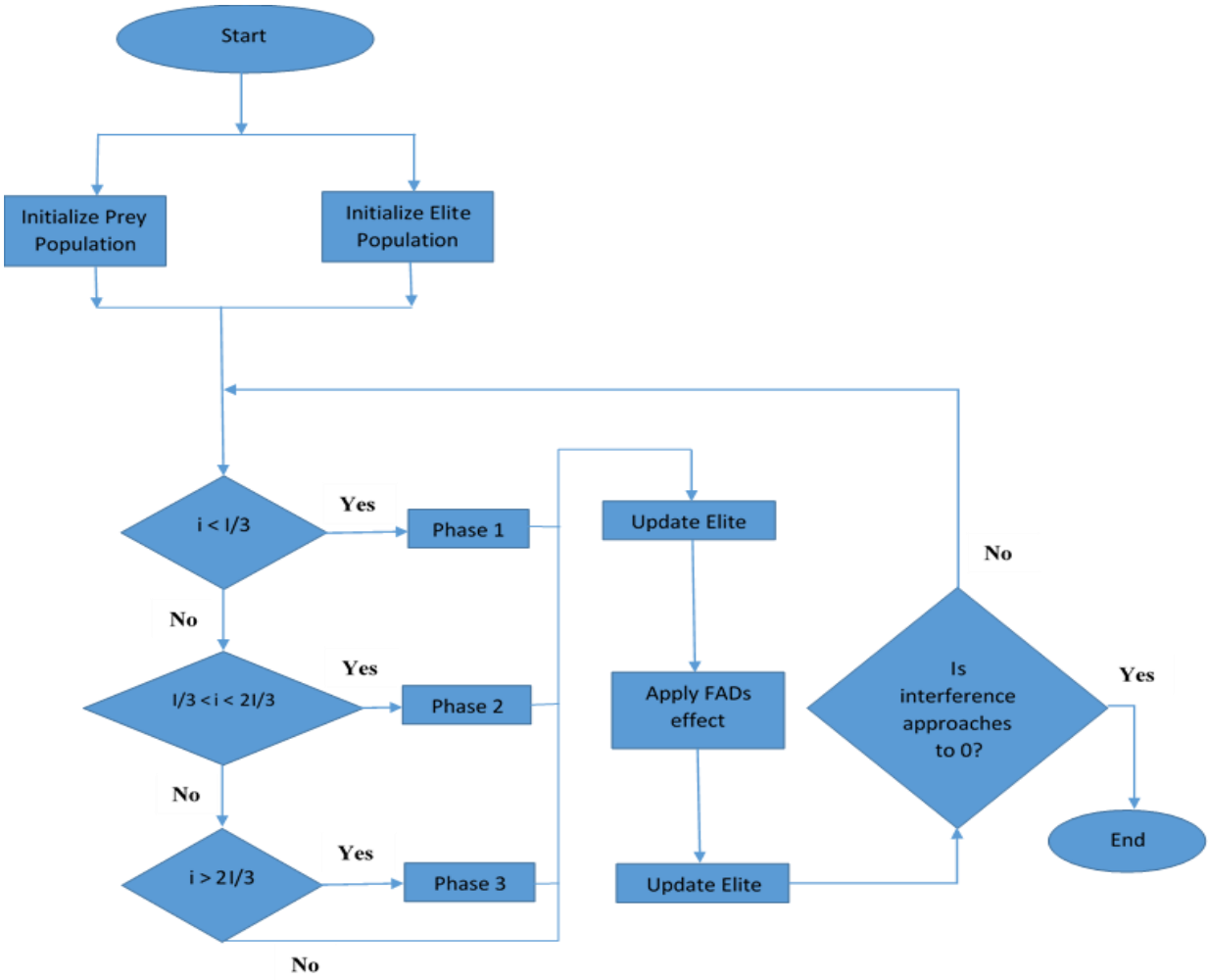

Figure 3.3: Flowchart of the proposed precoder based on PRZF with MPA optimization technique

Algorithm 1: Pseudo-code of the proposed precoding scheme based on PRZF with MPA is stated as follows

Setup initial prey (search agent) populations

Construct the Elite matrix using the PRZF precoder

While termination condition are not fulfilled

Calculate the fitness

If Iteration < Max_Iteration/3

Update prey populations based on Equation (3. 33)

Else if Max_Iteration/3 < Iteration < 2*Max_Iteration/3

For the initial 50% of the population

Update prey populations based on Equation (3. 28)

For the remaining 50% of the population

Update prey populations based on Equation (3. 29)

Else if Iteration > 2*Max_Iteration/3

Update prey populations based on Equation (3. 30)

End (if)

Update Elite matrix and perform memory saving

Apply FADs effect and update Elite matrix based on Equation (3. 31)

End **while**

3.3.5 Number of complex multiplications

The computational complexity of the precoding algorithms affected by several factors, such as the number of transmit antennas, the number of users, and the number of receive antennas. As the number of antennas and users increases, the computational complexity of the precoding algorithms also increases. Since the proposed precoding algorithm is a hybrid of PRZF and MPA algorithms, the computational complexity of this precoding algorithm can be obtained by summing up the computational complexity of PRZF and MPA algorithms. Thus the computational complexity of PRZF is given as $\frac{|\mathcal{S}_k|^2+|\mathcal{S}_k|}{2}N|\mathcal{M}_k| + |\mathcal{S}_k|^2 + |\mathcal{S}_k|N|\mathcal{M}_k| + \frac{|\mathcal{S}_k|^3-|\mathcal{S}_k|}{3}$ in (Björnson & Sanguinetti, 2020) and the computational complexity of the MPA algorithm can be given as $O(t(dn + Cof * n))$ where t is iteration, d is problem dimension, n is a number of agents, Cof is the cost of the objective function. Therefore, the computational complexity of the proposed algorithm can be given as $\frac{|\mathcal{S}_k|^2+|\mathcal{S}_k|}{2}N|\mathcal{M}_k| + |\mathcal{S}_k|^2 + |\mathcal{S}_k|N|\mathcal{M}_k| + \frac{|\mathcal{S}_k|^3-|\mathcal{S}_k|}{3} + t(dn + Cof * n)$. Table 3.1 shows the computational complexity of different existing precoding techniques which are discussed in (Björnson & Sanguinetti, 2020), (Bjornson & Sanguinetti, 2020).

Table 3.1: Computational complexity of different precoding schemes

Scheme	Precoding vector computational complexity
MMSE	$\frac{(N\lvert\mathcal{M}_k\rvert)^2 + N\lvert\mathcal{M}_k\rvert}{2}K + (N\lvert\mathcal{M}_k\rvert)^2 + \frac{(N\lvert\mathcal{M}_k\rvert)^3 - N\lvert\mathcal{M}_k\rvert}{3}$
PMMSE	$\frac{(N\lvert\mathcal{M}_k\rvert)^2 + N\lvert\mathcal{M}_k\rvert}{2}\lvert\mathcal{S}_k\rvert + (N\lvert\mathcal{M}_k\rvert)^2 + \frac{(N\lvert\mathcal{M}_k\rvert)^3 - N\lvert\mathcal{M}_k\rvert}{3}$
PRZF	$\frac{\lvert\mathcal{S}_k\rvert^2 + \lvert\mathcal{S}_k\rvert}{2}N\lvert\mathcal{M}_k\rvert + \lvert\mathcal{S}_k\rvert^2 + \lvert\mathcal{S}_k\rvert N\lvert\mathcal{M}_k\rvert + \frac{\lvert\mathcal{S}_k\rvert^3 - \lvert\mathcal{S}_k\rvert}{3}$
LMMSE	$\frac{N^2 + N}{2}K\lvert\mathcal{M}_k\rvert + N^2\lvert\mathcal{M}_k\rvert + \frac{N^3 - N}{3}\lvert\mathcal{M}_k\rvert$
LPMMSE	$\frac{N^2 + N}{2}\sum_{l\in\mathcal{M}_k}\lvert c_l\rvert + \left(\frac{N^3 - N}{3} + N^2\right)\lvert\mathcal{M}_k\rvert$

CHAPTER FOUR

4. RESULT AND DISCUSSION

To demonstrate the effectiveness of user-centric cell-free massive MIMO in realistic scenarios, we will introduce a network configuration that will serve as an ongoing illustration in this thesis. The primary parameters are presented in Table 4.1. The coverage area totals 1 km × 1 km or 2 km × 2 km, while the number of antennas is M = LN = 500, M=1500, M=2500. The number of APs is either L = 1500, L=500 or L = 100, and the number of antennas per each AP is N = 1, N = 3, or N=5. To imitate a large network deployment having no edges, we use a wrap-around topology where all APs and users receive interference from every directions. It is assumed that the APs are randomly and uniformly deployed over the network coverage area. The communication undergoes within a 20 MHz bandwidth, with a sum noise power of -94 dBm for both APs and UEs, which includes thermal noise and a 7dB noise figure in the receiver hardware. The maximum power transmitted from each AP in the downlink is 100 mW. A coherence block of τ_c = 200 samples, consistent with a 100 KHz coherence bandwidth and, a two milisecond coherence time was used, which is suitable for sub-6 GHz bands with high mobility and significant channel dispersion, allowing for outdoor propagation and user mobility conditions.

Table 4.1: Parameters used for the simulation (Björnson & Sanguinetti, 2020)

No.	Parameters	Value or Type
1	Network area	1 km^2 or 2 km^2
2	Network layout	Random deployment
3	The number of APs used	100, 500 or 1500
4	The number of antennas assigned to each AP	1, 3 or 5
5	Total number of antennas	500, 1500 or 2500
6	Bandwidth	20 MHz
7	Noise power of receiver	σ_{dl}^2 = -94 dBm
8	Highest transmit power in the downlink	100 mW
9	The number of samples in each coherence block.	τ_c =200
10	Gain at 1 km distance	Y= -140.6 dB
11	Exponent in the pathloss model	α =3.67

12	Height separation between UE and AP	10 m
13	Standard deviation of shadow fading	$\sigma_{sf} = 4$
14	Channel	Rayleigh fading
15	Number of search agents	25
16	Number of iteration	10
17	Dimension	20

4.1 Performance Comparison of the Proposed Precoding Technique and Existing Precoders

To assess and compare the performance of the proposed precoder with other existing precoding techniques, different parameters are taken into account, including average spectral efficiency, sum spectral efficiency, and cumulative distribution function. These parameters provide valuable insights into the efficiency and effectiveness of different precoding methods, allowing for a comprehensive performance evaluation and comparison.

4.1.1 Performance comparisons of the proposed precoder with other precoders based on average spectral efficiency

Within this section, our focus is to quantify the downlink average spectral efficiency attained by both centralized and decentralized implementations of user-centric cell-free massive MIMO. We will employ the various precoding techniques outlined in Chapter Three, including the proposed method, along with other existing precoding techniques. Through these comparisons, we aim to gain insights into the performance differences among these approaches and evaluate the effectiveness of the proposed scheme.

Simulation results presented in this thesis aimed to evaluate the performance of the proposed algorithm against recently developed cell-free massive MIMO precoders. Spectral efficiency was used to measure performance, with varying numbers of UE and antennas per AP.

To generate these simulation results, MATLAB software is utilized. MATLAB provides a powerful environment for conducting simulations, enabling the implementation of algorithms and the analysis of system performance. Through MATLAB, the simulations can be executed, and the resulting average spectral efficiency values can be obtained, allowing for a comprehensive comparison between the proposed algorithm and other existing cell-free Massive MIMO precoders in downlink transmission.

Figure 4.1 shows the average spectral efficiency per UE for the chosen setup, which includes L=500 APs with a single antenna per each AP in a 1 km^2 area. The comparison is made between centralized operation using the proposed method, PMMSE and PRZF precoding, and distributed operation using LPMMSE or LMR precoding. As we can see from the graph, the proposed algorithm outperformed all the existing algorithms (i.e. PMMSE, PRZF, LPMMSE, and LMR) at all UE values. The proposed algorithm achieved an average spectral efficiency of 9.89066 bit/s/Hz when the number of UEs in the coverage area is K=20, whereas the PMMSE and PRZF algorithms achieved an average spectral efficiency of 9.39817 bit/s/Hz and 9.3713 bit/s/Hz respectively at the same number of UEs K=20. The precoding algorithms in the distributed scheme, which are LPMMSE and LMR showed a poor performance by achieving an average spectral efficiency of 5.03777 bit/s/Hz and 2.78105 bit/s/Hz for the same number of UEs K=20. From this, we can see that the centralized schemes exhibit better performance compared to the distributed schemes. When the number of UEs available in the network area becomes K=100, while PMMSE and PRZF algorithms achieved an average spectral efficiency of 5.39495 bit/s/Hz and 5.11485 bit/s/Hz, the proposed method achieved an average spectral efficiency of 5.5186 bit/s/Hz. LP-MMSE and LMR achieved an average spectral efficiency of 2.54254 bit/s/Hz and 1.63945 bit/s/Hz for UEs K=100, which is poor performance compared to the centralized precoding schemes.

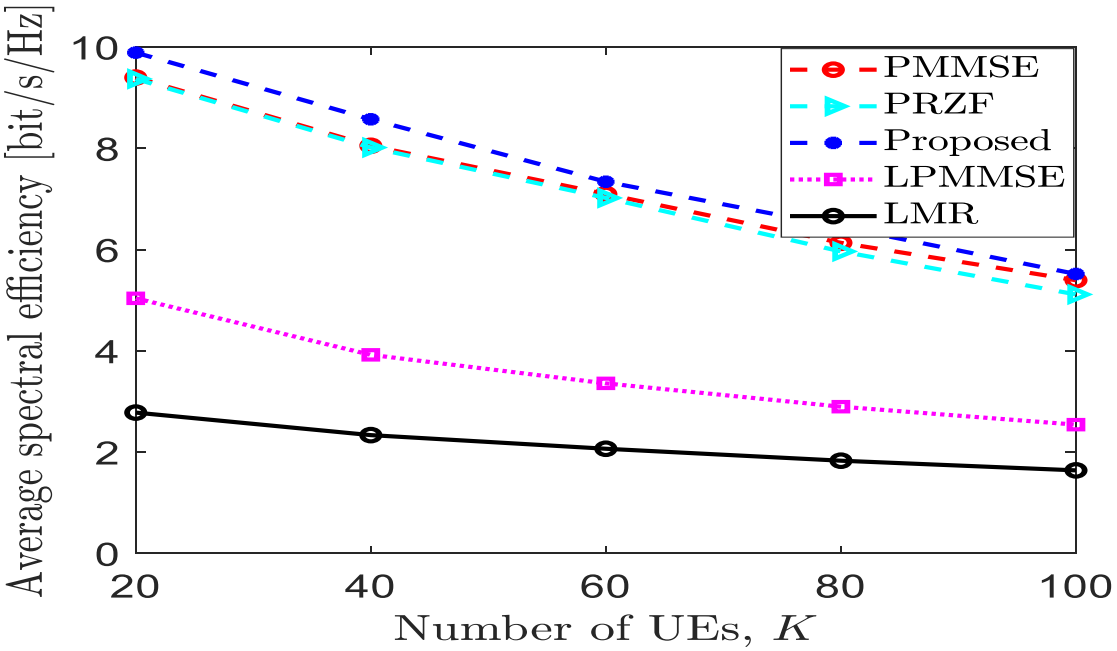

Figure 4.1: Average downlink spectral efficiency per UE as a function of the number of UEs for both centralized and distributed operations. We use L = 500 and N = 1 deployed in a 1 km^2 area.

Table 4.2 illustrates the performance comparison between the centralized proposed precoder and other centralized and distributed precoding methods for different numbers of users which ranges up to a maximum of K=100, and the number of APs is L=500 which are equipped with a single antenna in a 1km^2 area. As can be seen from the table, the proposed precoding technique outperforms the other methods. The table below depicts the tabular form representation of Figure 4.1 by considering some number of UEs.

Table 4.2: Average downlink spectral efficiency per UE comparison of the proposed method with other centralized and distributed precoding schemes at L = 500 and N = 1 deployed in a 1 km^2 area.

Avg. SE / UE	PMMSE	PRZF	PROPOSED	LPMMSE	LMR
20	9.39817	9.3713	9.89066	5.03777	2.78105
40	8.05082	8.0162	8.57396	3.92152	2.33585
60	7.09721	7.02086	7.34046	3.3581	2.0665
80	6.13384	5.96418	6.44906	2.8974	1.83058
100	5.39495	5.11485	5.5186	2.54254	1.63945

Figure 4.2 shows the average spectral efficiency per user equipment for the selected setup, which contains L=500 APs with N=3 antennas per AP in a 1 km2 area. In this setup, the proposed algorithm achieved an average spectral efficiency of 12.1254 bits/second/hertz when there were K=20 UEs in the network. In comparison, the PMMSE and PRZF algorithms achieved average spectral efficiencies of 11.089 bits/s/Hz and 11.0598 bits/s/Hz respectively with K=20 UEs. The precoding algorithms in the distributed scheme, which are LPMMSE and LMR, showed poor performance with average spectral efficiencies of 8.5097 bits/s/Hz and 3.51978 bits/s/Hz respectively for K=20 UEs.

This shows that the centralized precoding schemes perform better than the distributed schemes. When there were K=100 UEs in the network area, PMMSE and PRZF achieved average spectral efficiencies of 8.07463 bits/s/Hz and 7.85168 bits/s/Hz respectively. In comparison, the proposed method achieved an average spectral efficiency of 8.86136 bits/s/Hz. LPMMSE and LMR achieved average spectral efficiencies of only 5.24892 bits/s/Hz and 2.38236 bits/s/Hz respectively with K=100 UEs, showing poor performance relative to the centralized precoding techniques. The average spectral efficiency per UE in

this setup is higher than in Figure 4.1. This result shows that the average spectral efficiency per user equipment increases with a greater number of transmitting antennas in the network.

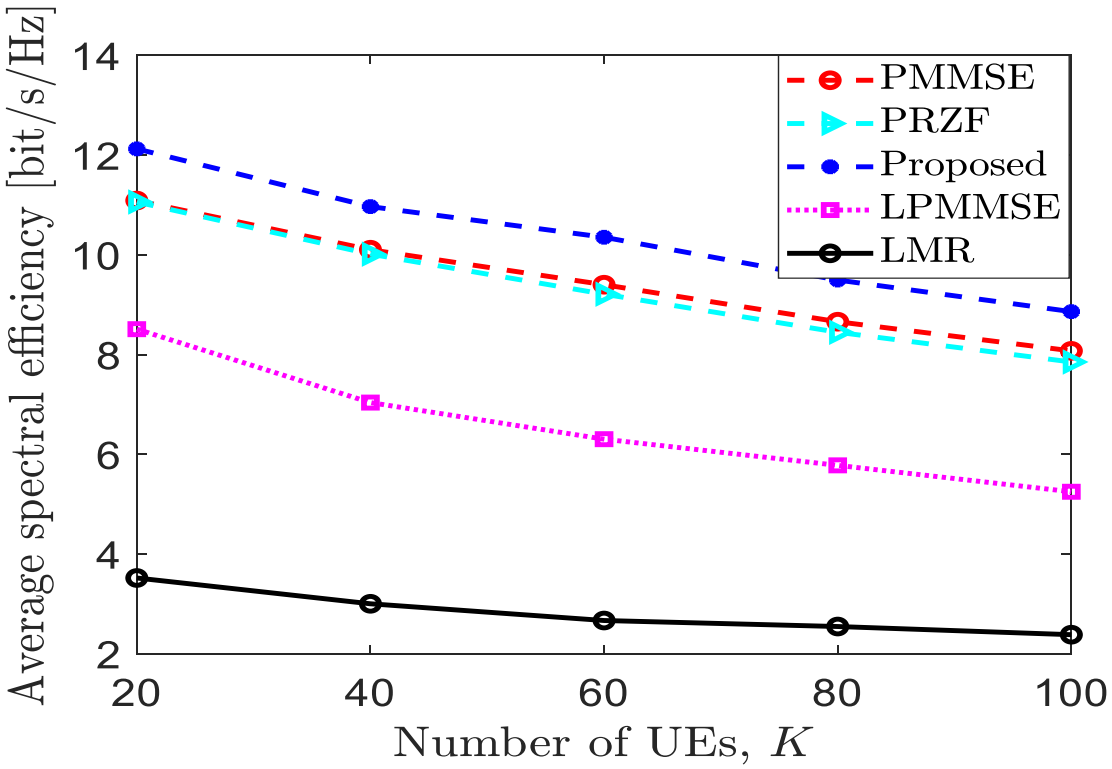

Figure 4.2: Average downlink spectral efficiency per UE as a function of the number of UEs for both centralized and distributed operations. We consider L = 500 and N = 3 implemented in the 1 km^2 network area.

Table 4.3 compares the performance of different distributed and centralized precoding methods, including the proposed precoder, for a maximum of 100 users, 500 access points, and three antennas per each AP. The table shows that the proposed precoder outperforms the other precoding techniques. Additionally, the table represents the information in Figure 4.2 in a tabular form for a selected number of UEs.

Table 4.3: Average downlink spectral efficiency per UE comparison of the proposed method with other centralized and distributed precoding schemes at L = 500 and N = 3 implemented in a 1 km^2 area.

Avg. SE / UE	PMMSE	PRZF	PROPOSED	LPMMSE	LMR
20	11.0891	11.0598	12.1254	8.5097	3.51978
40	10.103	10.0144	10.9676	7.03738	3.00225
60	9.40108	9.21163	10.3532	6.30347	2.66678
80	8.65904	8.44782	9.49478	5.77843	2.54621
100	8.07463	7.85168	8.86136	5.24892	2.38236

Figure 4.3 illustrates the average spectral efficiency per user equipment for the setup containing L=500 APs each having N=5 antennas within a 1 km^2 area. For 20 UEs, K=20, the proposed algorithm achieved an average spectral efficiency of 13.24 bit/s/Hz, while the PMMSE and PRZF algorithms achieved 11.9 bit/s/Hz and 11.91 bit/s/Hz, respectively. The distributed precoding schemes, LPMMSE and LMR, performed poorly with 9.948 bit/s/Hz and 3.814 bit/s/Hz, respectively.

This shows that centralized schemes outperform distributed schemes. For 100 UEs (K=100), the proposed method achieved 10.07 bit/s/Hz, while PMMSE and PRZF achieved 8.926 bit/s/Hz and 8.685 bit/s/Hz, respectively. LPMMSE and LMR achieved 6.363 bit/s/Hz and 2.841 bit/s/Hz, indicating the significantly poorer performance of the distributed precoding schemes compared to the centralized schemes. The average spectral efficiency per user in this setup is higher than in Figures 4.1 and 4.2, showing that average spectral efficiency per user increases with more transmit antennas in the network.

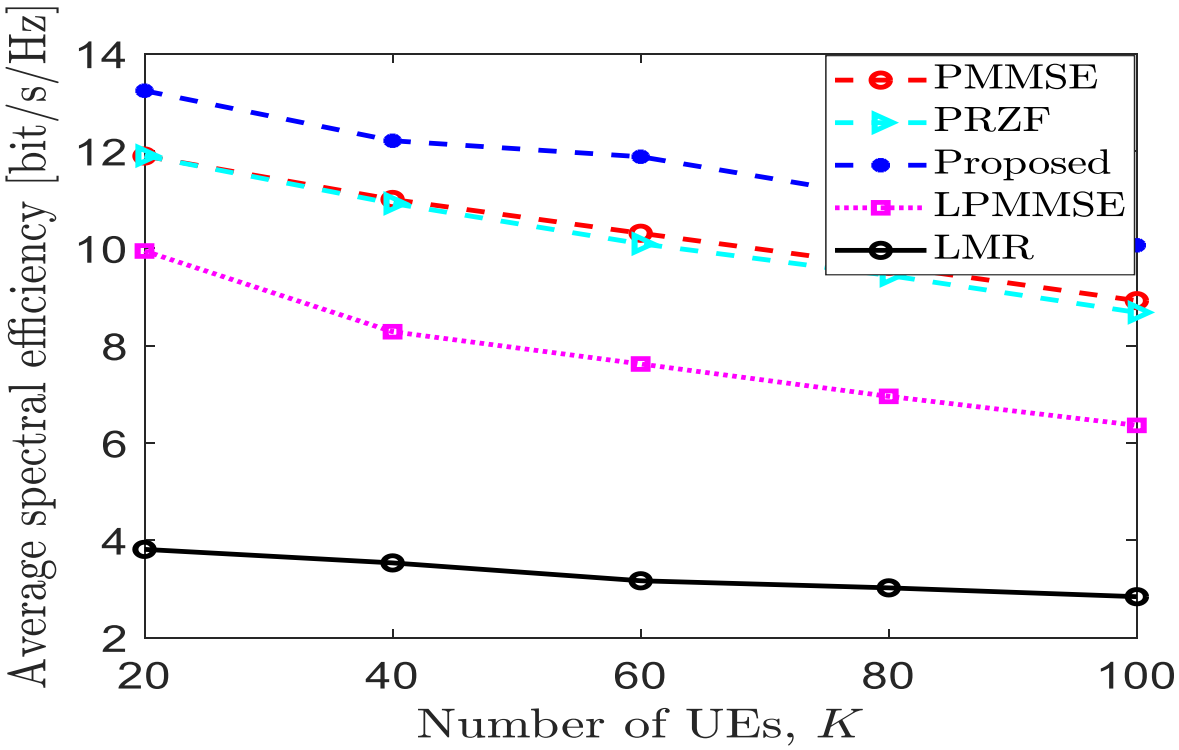

Figure 4.3: Average downlink spectral efficiency per UE as a function of the number of UEs for both centralized and distributed operations. We use L = 500 and N = 5 implemented in a 1 km^2 network area.

Table 4.4 compares the performance of different distributed and centralized precoding methods, including the proposed precoder, for a maximum of 100 users, 500 APs, and five antennas per AP in a 1km² area. The table shows that the proposed precoder outperforms the other precoding techniques. Additionally, the table represents the information in Figure 4.3 in a tabular form for a selected number of UEs.

Table 4.4: Average downlink spectral efficiency per UE comparison of the proposed method with other centralized and distributed precoding schemes at L = 500 and N = 5 in 1 km^2 area.

Avg. SE / UE	PMMSE	PRZF	PROPOSED	LPMMSE	LMR
20	11.9	11.91	13.24	9.948	3.814
40	11.01	10.93	12.21	8.288	3.536
60	10.31	10.1	11.89	7.625	3.168
80	9.634	9.445	11.04	6.96	3.023
100	8.926	8.685	10.07	6.363	2.841

Figure 4.4 shows the average spectral efficiency per user equipment for the selected setup, which contains L=1500 APs having N=1 antennas per AP in a 1 km^2 area. In this setup, the proposed algorithm achieved an average spectral efficiency of 13.34 bits/second/hertz when there were K=20 UEs in the network. In comparison, the PMMSE and PRZF algorithms achieved average spectral efficiencies of 11.76 bits/s/Hz and 11.77 bits/s/Hz respectively with K=20 UEs. The precoding algorithms in the distributed scheme, which are LPMMSE and LMR, showed poor performance with average spectral efficiencies of 6.262 bits/s/Hz and 3.751 bits/s/Hz respectively for K=20 UEs. This shows that the centralized schemes outperform the distributed schemes. When there were K=100 UEs in the network area, PMMSE and PRZF achieved average spectral efficiencies of 8.259 bits/s/Hz and 8.187 bits/s/Hz respectively. In comparison, the proposed method achieved an average spectral efficiency of 9.481 bits/s/Hz. LPMMSE and LMR achieved average spectral efficiencies of only 4.065 bits/s/Hz and 2.673 bits/s/Hz respectively with K=100 UEs, showing poor performance relative to the centralized precoding techniques. The average spectral efficiency per user equipment in this setup is higher than in Figure 4.2. This indicates that the average spectral efficiency per user equipment increases when each AP is equipped with a single antenna in such a way that there is an equal number of total antennas in the network coverage area as in the setup for Figure 4.2.

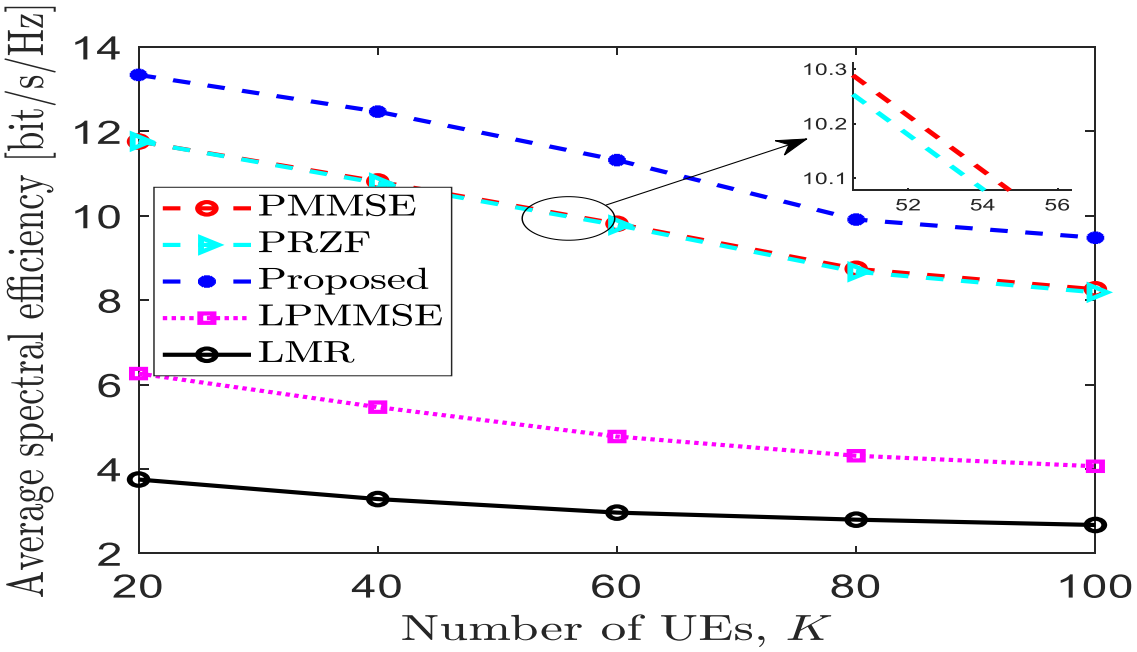

Figure 4.4: Average downlink spectral efficiency per UE as a function of the number of UEs for both centralized and distributed operations. We use L = 1500 and N = 1 implemented in the 1 km^2 network area.

Table 4.5 compares the performance of different centralized and precoding methods, including the proposed precoder, for a maximum of 100 users, 1500 access points, and a single antenna per AP. The table shows that the proposed precoder outperforms the other precoding techniques. Additionally, the table represents the information in Figure 4.4 in a tabular form for a selected number of UEs.

Table 4.5: Average downlink spectral efficiency per UE comparison of the proposed method with other centralized and distributed precoding schemes at L = 1500 and N = 1 implemented in a 1 km^2 area.

Avg. SE / UE	PMMSE	PRZF	PROPOSED	LPMMSE	LMR
20	11.76	11.77	13.34	6.262	3.751
40	10.82	10.78	12.47	5.466	3.287
60	9.813	9.781	11.32	4.77	2.966
80	8.745	8.673	9.913	4.314	2.799
100	8.259	8.187	9.481	4.065	2.673

In the chosen setup, which consists of L=500 APs with one antenna per AP covering a 2 km^2 area, Figure 4.5 displays the average spectral efficiency per user equipment. The proposed method achieved an average spectral efficiency of 7.13941 bit/s/Hz for 20 UEs, while PMMSE and PRZF achieved 6.676 bit/s/Hz and 6.65619 bit/s/Hz, respectively, for the same number of UEs.

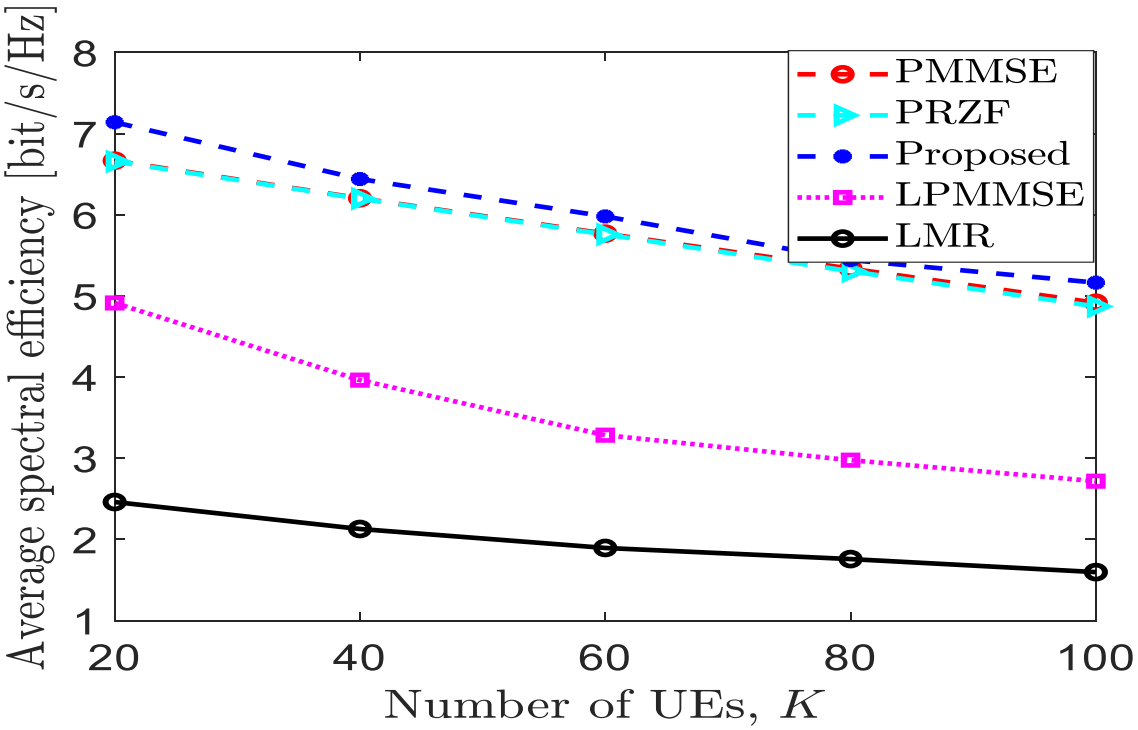

Figure 4.5: Average downlink spectral efficiency per UE as a function of the number of UEs for both centralized and distributed operations. We consider L = 500 and N = 1 deployed in a 2 km^2 area.

However, the distributed precoding algorithms (LPMMSE and LMR) exhibited poor performance, with average spectral efficiencies of 4.91302 bit/s/Hz and 2.46093 bit/s/Hz for 20 UEs. These results indicate that centralized schemes perform better than distributed schemes. When the number of UEs increased to 100, the proposed algorithm achieved an average spectral efficiency of 5.16333 bit/s/Hz, while PMMSE and PRZF achieved 4.91567 bit/s/Hz and 4.87063 bit/s/Hz, respectively. LPMMSE and LMR achieved much lower average spectral efficiencies of 2.7174 bit/s/Hz and 1.59719 bit/s/Hz, respectively, for 100 UEs. Notably, the average spectral efficiency per user equipment in this setup was lower than that in Figure 4.1, which had the same number of APs and antennas per AP. This suggests that as the deployment area of the network expands while the number of transmitting antennas stays constant, the average spectral efficiency per user equipment decreases.

Table 4.6 displays a comparison of the performance of different distributed and centralized precoding methods, including the proposed precoder, for a maximum of 100 users, 500 APs, and one antenna per AP in a 2 km² area. The table shows that the proposed precoder

outperforms the other precoding techniques. Additionally, the table provides a tabular representation of Figure 4.5 for a selected number of UEs.

Table 4.6: Average downlink spectral efficiency per UE comparison of the proposed method with other centralized and distributed precoding schemes at L = 500 and N = 1 in a 2 km^2 area.

Avg. SE / UE	PMMSE	PRZF	PROPOSED	LPMMSE	LMR
20	6.676	6.65619	7.13941	4.91302	2.46093
40	6.20299	6.1979	6.43993	3.96236	2.12854
60	5.76725	5.75714	5.97944	3.28433	1.89482
80	5.33576	5.30397	5.44173	2.97633	1.75779
100	4.91567	4.87063	5.16333	2.7174	1.59719

4.1.2 Performance comparisons of the proposed precoder with other precoders based on sum spectral efficiency

The sum spectral efficiency is the total sum spectral efficiency within the coverage area. The following simulation results are presented to evaluate the sum spectral efficiency performance of the proposed and other currently available precoding techniques. The simulation results in this study analyze the performance of the proposed precoder in downlink data transmission, comparing it to recently introduced scalable cell-free massive MIMO precoders, based on the number of UE. The performance is evaluated by measuring sum spectral efficiency against the number of user equipment, with variations in the number of APs, antennas per access point, and coverage area.

Figure 4.6 depicts the sum spectral efficiency for a setup consisting of L=500 APs with one antenna per AP distributed over a 1km^2 area. The comparison is between distributed operation using LPMMSE or LMR precoding and centralized operation using the proposed method, PMMSE, and PRZF precoding. The proposed algorithm outperformed all existing algorithms (i.e., PMMSE, PRZF, LPMMSE, and LMR) at all UE values, achieving a sum spectral efficiency of 197.813 bit/s/Hz for 20 UEs. In contrast, PMMSE and PRZF achieved a sum spectral efficiency of 187.963 bit/s/Hz and 187.426 bit/s/Hz, respectively, for the same number of UEs.

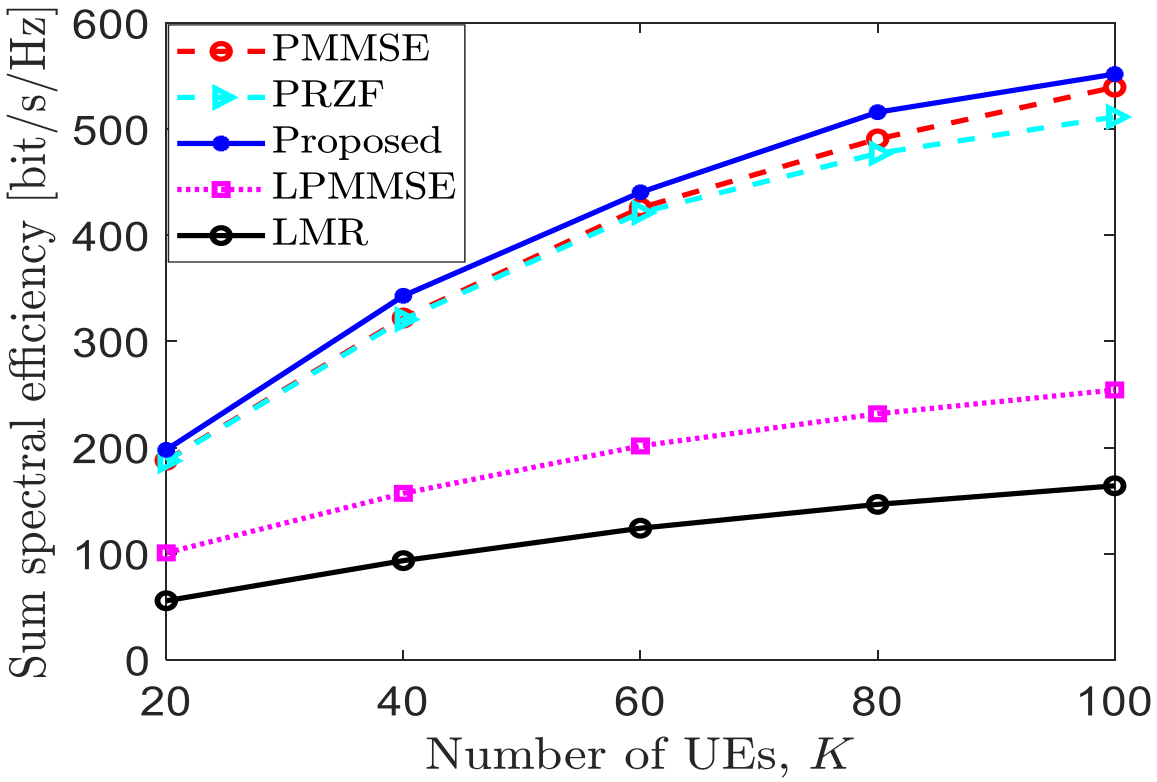

Figure 4.6: Sum downlink spectral efficiency as a function of the number of UEs for both centralized and distributed operations. We consider L = 500 and N = 1 deployed in a 1 km^2 area.

The precoding algorithms in the distributed scheme (LPMMSE and LMR) exhibited poor performance, achieving a sum spectral efficiency of 100.755 bit/s/Hz and 55.6209 bit/s/Hz for 20 UEs. These results suggest that centralized schemes perform better than distributed schemes. When the number of UEs increased to 100, the proposed algorithm achieved a sum spectral efficiency of 551.86 bit/s/Hz, while PMMSE and PRZF achieved 539.495 bit/s/Hz and 511.485 bit/s/Hz, respectively. LPMMSE and LMR achieved much lower sum spectral efficiencies of 254.254 bit/s/Hz and 163.945 bit/s/Hz, respectively, for 100 UEs, indicating poor performance compared to centralized precoding schemes.

Table 4.7 indicates the performance comparison between the centralized proposed precoder and other centralized and distributed precoding methods for a different number of users which ranges up to a maximum of K=100 and the number of APs L=500 and N=1 antennas per each AP in 1 km^2 area. It is evident from the table that the proposed precoder outperforms the other precoding techniques. The table below depicts the tabular form representation of Figure 4.6 by considering some number of UEs.

Table 4.7: Sum downlink spectral efficiency comparison of the proposed method with other centralized and distributed precoding schemes at L = 500 and N = 1 in 1 km^2 area.

Sum SE / UE	PMMSE	PRZF	PROPOSED	LPMMSE	LMR
20	187.963	187.426	197.813	100.755	55.6209
40	322.033	320.648	342.958	156.861	93.4339
60	425.833	421.252	440.428	201.486	123.99
80	490.707	477.135	515.925	231.792	146.443
100	539.495	511.485	551.86	254.254	163.945

Figure 4.7 depicts the total spectral efficiency in the selected configuration, which involves 500 APs with 3 antennas per AP, covering a 1km^2 area. In this particular setup, the proposed algorithm attained a sum spectral efficiency of 242.508 bit/s/Hz when there were 20 UEs in the network (K=20). In comparison, the PMMSE and PRZF algorithms achieved sum spectral efficiencies of 221.783 bit/s/Hz and 221.195 bit/s/Hz respectively for the same number of UEs (K=20). The LPMMSE and LMR precoding algorithms in the distributed scheme displayed inferior performance, reaching sum spectral efficiencies of 170.194 bit/s/Hz and 70.3956 bit/s/Hz respectively for K=20 UEs. These results indicate that centralized schemes outperform distributed schemes.

When the number of UEs in the network increased to 100 (K=100), the proposed method achieved a sum spectral efficiency of 886.136 bit/s/Hz, while the PMMSE and PRZF algorithms attained 807.463 bit/s/Hz and 785.168 bit/s/Hz respectively. On the other hand, the LPMMSE and LMR algorithms yielded lower sum spectral efficiencies of 524.892 bit/s/Hz and 238.236 bit/s/Hz for K=100 UEs, showcasing poorer performance compared to the centralized precoding schemes. Notably, the sum spectral efficiency in this configuration exceeded that shown in Figure 4.6, suggesting an increase in overall spectral efficiency as the number of transmit antennas in the network rises.

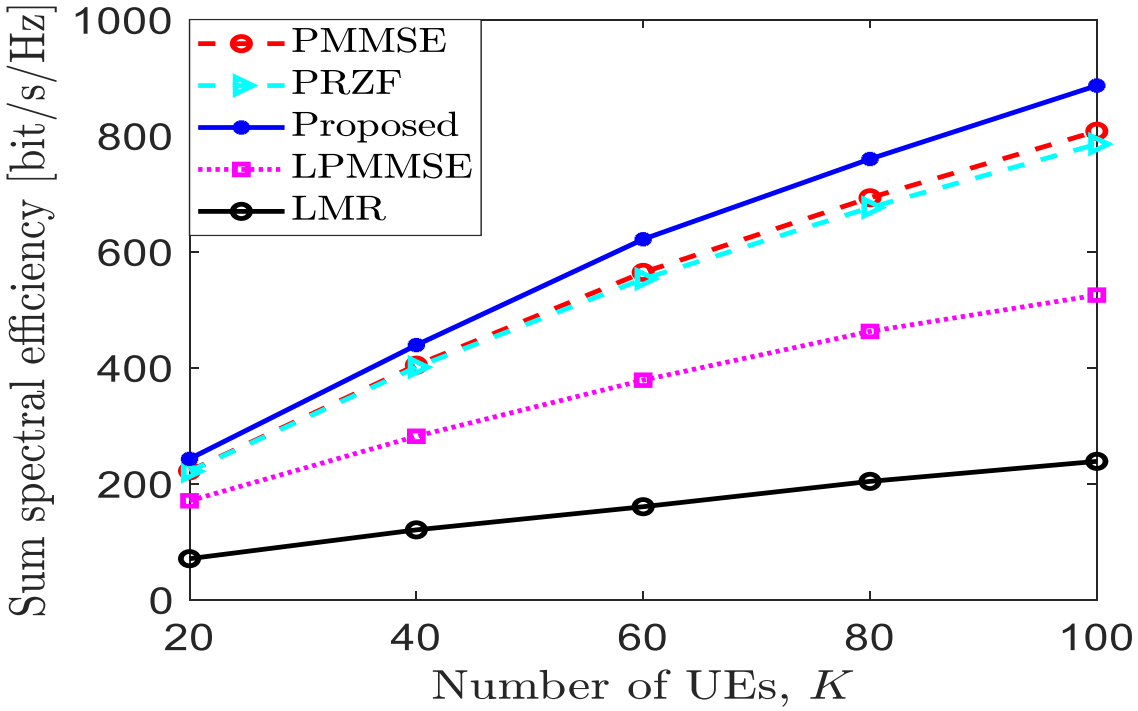

Figure 4.7: Sum downlink spectral efficiency as a function of the number of UEs for both centralized and distributed operations. We consider L = 500 and N = 3 deployed in a 1 km^2 area.

Table 4.8 indicates the performance comparison between the centralized proposed precoder and other centralized and distributed precoding methods for a different number of users which ranges up to a maximum of K=100 and number of APs L=500 and N=3 antennas per each AP in 1km^2 area. The table clearly shows that the proposed precoding technique performs better than the other precoding methods.The table below depicts the tabular form representation of Figure 4.7 by considering some number of UEs.

Table 4.8: Sum downlink spectral efficiency comparison of the proposed method with other centralized and distributed precoding schemes at L = 500 and N = 3 in 1 km^2 area.

Sum SE / UE	PMMSE	PRZF	PROPOSED	LPMMSE	LMR
20	221.783	221.195	242.508	170.194	70.3956
40	404.12	400.574	438.705	281.495	120.09
60	564.065	552.698	621.192	378.208	160.007
80	692.723	675.825	759.582	462.274	203.697
100	807.463	785.168	886.136	524.892	238.236

Figure 4.8 presents the total spectral efficiency in the selected configuration, which involves 500 APs with 5 antennas per AP, covering a 1km² area. In this setup, the PMMSE and PRZF algorithms achieved sum spectral efficiencies of 238 bit/s/Hz and 238.1 bit/s/Hz respectively when there were 20 UEs in the network (K=20). In comparison, the proposed algorithm achieved a sum spectral efficiency of 264.9 bit/s/Hz for the same number of UEs (K=20). The LPMMSE and LMR precoding algorithms in the distributed scheme displayed inferior performance, reaching sum spectral efficiencies of 199 bit/s/Hz and 76.27 bit/s/Hz respectively for K=20 UEs. These results indicate that centralized schemes outperform distributed schemes.

When the number of users in the network increased to 100 (K=100), the proposed method achieved a sum spectral efficiency of 1007 bit/s/Hz, while the PMMSE and PRZF algorithms attained 892.6 bit/s/Hz and 868.5 bit/s/Hz respectively. On the other hand, the LPMMSE and LMR algorithms yielded lower sum spectral efficiencies of 636.3 bit/s/Hz and 284.1 bit/s/Hz for K=100 UEs, showcasing poorer performance compared to the centralized precoding schemes. Notably, the sum spectral efficiency in this configuration exceeded that shown in Figure 4.7, suggesting an increase in overall spectral efficiency as the number of transmit antennas in the network rises.

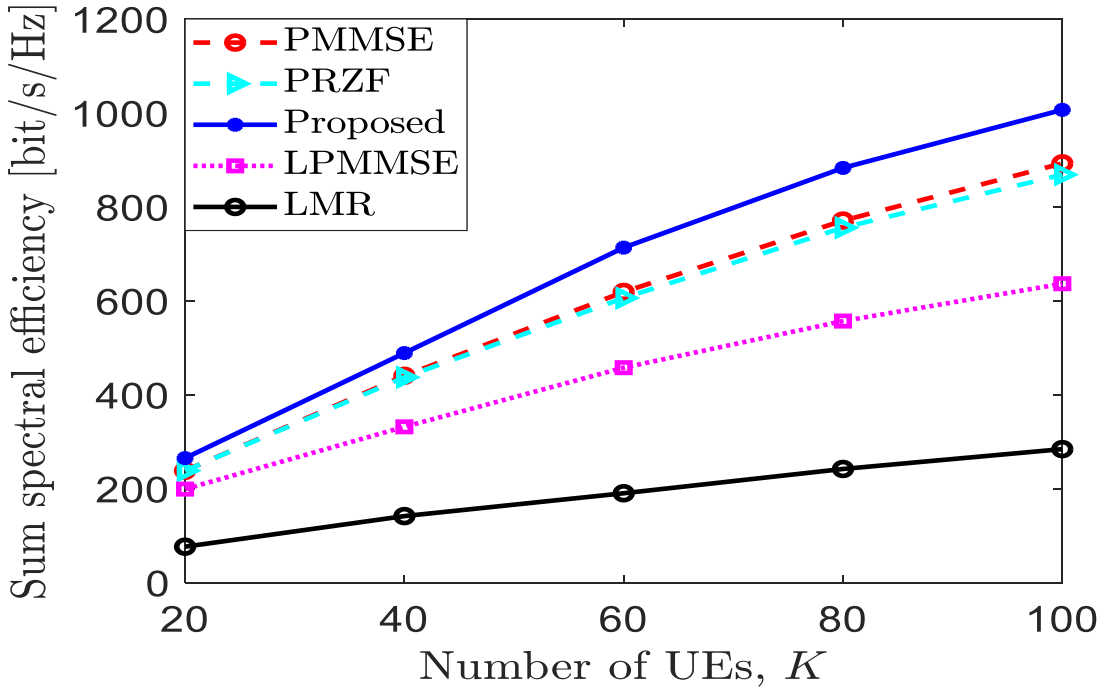

Figure 4.8: Sum downlink spectral efficiency comparison of the proposed method with other centralized and distributed precoding schemes at L = 500 and N = 5 in a 1 km^2 area.

Table 4.9 provides a tabular representation of the results presented in Figure 4.8 for a selected number of users, allowing for an easy comparison of the achieved sum spectral efficiencies across the different precoding methods. These results highlight the superior performance of the proposed precoding method in a cell-free massive MIMO system with an extensive number of antennas and APs.

Table 4.9: Sum downlink spectral efficiency comparison of the proposed method with other centralized and distributed precoding schemes at L = 500 and N = 5 in a 1 km^2 area.

Sum SE / UE	PMMSE	PRZF	PROPOSED	LPMMSE	LMR
20	238	238.1	264.9	199	76.27
40	440.3	437	488.6	331.5	141.4
60	618.8	605.8	713.1	457.5	190.1
80	770.7	755.6	882.9	556.8	241.8
100	892.6	868.5	1007	636.3	284.1

Figure 4.9 depicts the total spectral efficiency in the selected configuration, which involves 1500 APs with a single antenna per AP, covering a 1km² area. In this particular setup, the proposed algorithm attained a sum spectral efficiency of 266.8 bit/s/Hz when there were 20 UEs in the network (K=20). In comparison, the PMMSE and PRZF algorithms achieved sum spectral efficiencies of 235.2 bit/s/Hz and 235.3 bit/s/Hz respectively for the same number of UEs (K=20). The LPMMSE and LMR precoding algorithms in the distributed scheme displayed inferior performance, reaching sum spectral efficiencies of 125.2 bit/s/Hz and 75.01 bit/s/Hz respectively for K=20 UEs. These results indicate that centralized schemes outperform distributed schemes.

When the number of users in the network increased to 100 (K=100), the proposed method achieved a sum spectral efficiency of 948.1 bit/s/Hz, while the PMMSE and PRZF algorithms attained 825.9 bit/s/Hz and 818.7 bit/s/Hz respectively. On the other hand, the LPMMSE and LMR algorithms yielded lower sum spectral efficiencies of 406.5 bit/s/Hz and 267.3 bit/s/Hz for K=100 UEs, showcasing poorer performance compared to the centralized precoding schemes. Notably, the sum spectral efficiency in this configuration exceeded that shown in Figure 4.7, suggesting an increase in overall spectral efficiency as the antennas are deployed in a distributed manner rather than deploying multi-antenna APs.

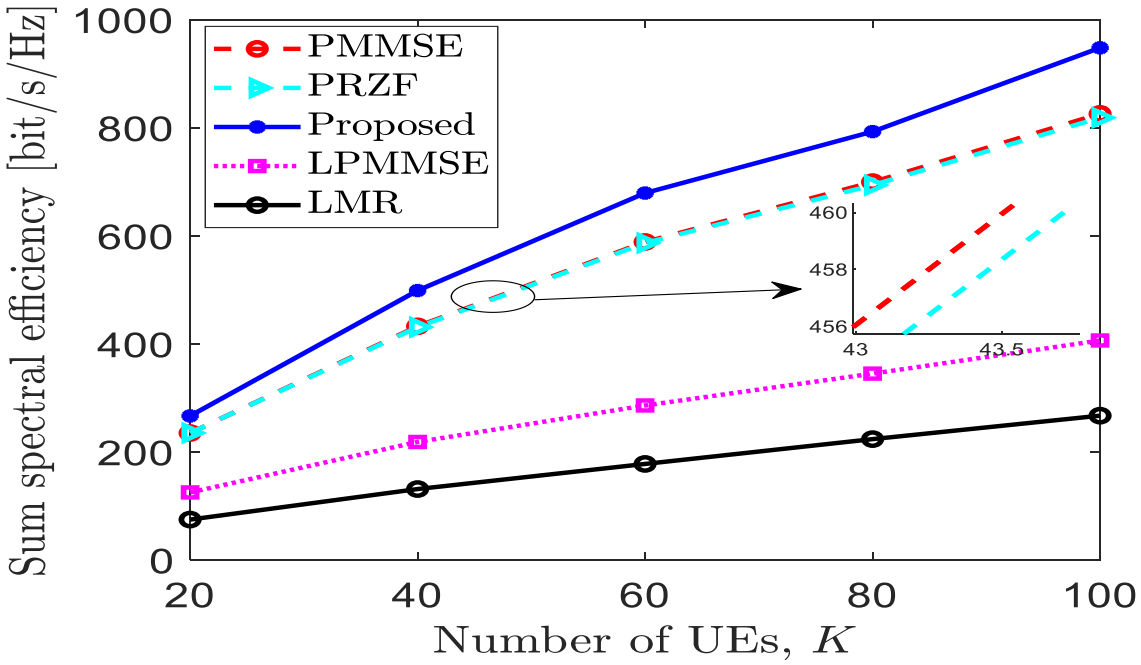

Figure 4.9: Sum downlink spectral efficiency as a function of the number of UEs for both centralized and distributed operations. We consider L = 1500 and N = 1 deployed in a 1 km^2 area.

Table 4.10 shows the performance comparison between the centralized proposed precoder and other centralized and distributed precoding methods for a different number of users which ranges up to a maximum of K=100 and the number of APs L=1500 and N=1 antennas per each AP in 1km^2 area. As we observed from the table the performance of the proposed precoder is better than that of the other precoding techniques. The table below depicts the tabular form representation of Figure 4.9 by considering some UEs.

Table 4.10: Sum downlink spectral efficiency comparison of the proposed method with other centralized and distributed precoding schemes at L = 1500 and N = 1 in 1 km^2 area.

Sum SE / UE	PMMSE	PRZF	PROPOSED	LPMMSE	LMR
20	235.2	235.3	266.8	125.2	75.01
40	432.6	431.1	498.8	218.7	131.5
60	588.8	586.8	679.3	286.2	178
80	699.6	693.9	793	345.1	223.9
100	825.9	818.7	948.1	406.5	267.3

Figure 4.10 illustrates the total spectral efficiency in the chosen configuration, which consists of 500 APs with 1 antenna per AP, covering a 2 km² area. In this setup, the PMMSE and PRZF algorithms achieved sum spectral efficiencies of 133.321 bit/s/Hz and 133.124 bit/s/Hz respectively when there were 20 UEs in the network (K=20). In comparison, the proposed algorithm achieved a sum spectral efficiency of 142.788 bit/s/Hz for the same number of UEs (K=20). The LPMMSE and LMR precoding algorithms in the distributed scheme displayed inferior performance, reaching sum spectral efficiencies of 98.2604 bit/s/Hz and 49.2185 bit/s/Hz respectively for K=20 UEs. These results indicate that centralized schemes outperform distributed schemes.

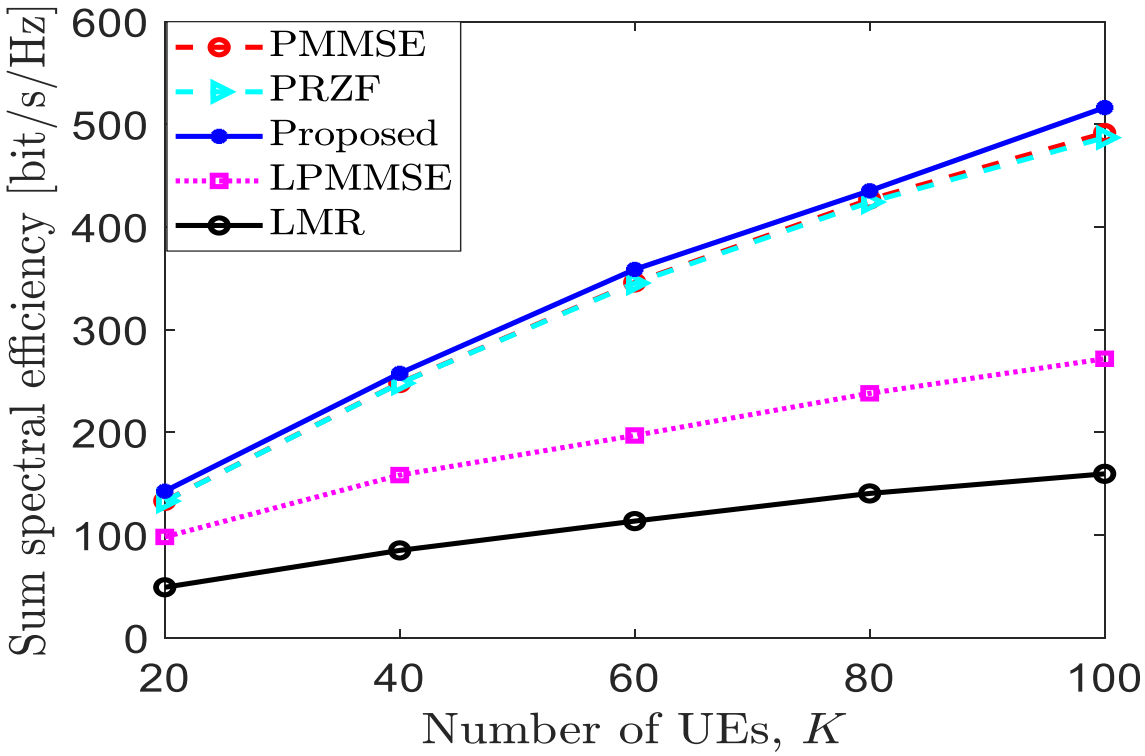

Figure 4.10: Sum downlink spectral efficiency as a function of the number of UEs for both centralized and distributed operations. We consider L = 500 and N = 1 deployed in a 2 km^2 area.

When the number of users in the network increased to 100 (K=100), the proposed method achieved a sum spectral efficiency of 516.333 bit/s/Hz, while the PMMSE and PRZF algorithms attained 491.567 bit/s/Hz and 487.063 bit/s/Hz respectively. On the other hand, the LPMMSE and LMR algorithms yielded lower sum spectral efficiencies of 271.74 bit/s/Hz and 159.719 bit/s/Hz for K=100 UEs, showcasing poorer performance compared to

the centralized precoding schemes. Importantly, the sum spectral efficiency in this configuration was lower than that shown in Figure 4.6, which had the same number of APs and antennas per AP as this setup. This demonstrates that the sum spectral efficiency decreases when the deployment area of the network increases while the number of transmit antennas remains constant.

Table 4.11 provides a performance comparison among the centralized proposed precoder, other centralized precoding methods, and distributed precoding methods. The evaluation considers varying numbers of users, up to a maximum of K=100, having L=500 APs and N=1 antenna per each AP in a 2 km² area. Notably, the results in the table demonstrate that the proposed precoder achieves better performance than the other precoding techniques. The table below presents a tabular representation of Figure 4.10, focusing on a specific number of UEs. Upon examining the results in the table, it becomes apparent that the performance of this particular setup is lower compared to the setup discussed in Table 4.7. This can be attributed to the fact that the APs in this setup are more dispersed compared to the setup in Table 4.7.

Table 4.11: Sum downlink spectral efficiency comparison of the proposed method with other centralized and distributed precoding schemes at L = 500 and N = 1 in a 2 km^2 area.

Sum SE / UE	PMMSE	PRZF	PROPOSED	LPMMSE	LMR
20	133.321	133.124	142.788	98.2604	49.2185
40	248.12	247.916	257.597	158.494	85.1416
60	346.035	345.428	358.766	197.06	113.689
80	426.861	424.318	435.339	238.107	140.623
100	491.567	487.063	516.333	271.74	159.719

4.1.3 Performance comparisons of the proposed precoder with other precoders based on cumulative distribution function

In wireless communication, the cumulative distribution function (CDF) versus spectral efficiency is a common way to visualize the performance of a communication system. Spectral efficiency is a measure of how efficiently a wireless system uses its available spectrum and is typically expressed in bit/s/Hz. The CDF, on the other hand, is a statistical function that describes the probability of a random variable (in this case, the spectral

efficiency) falling below a certain value. When plotting the CDF versus spectral efficiency, the x-axis represents the spectral efficiency, while the y-axis represents the probability of achieving that spectral efficiency or better. This allows us to see the distribution of spectral efficiency values across the wireless network, and how likely it is to achieve a certain level of spectral efficiency. In general, a higher spectral efficiency indicates better performance in terms of the system's ability to transmit more data over the available frequency spectrum.

Comparing the CDFs for centralized and distributed implementations of user-centric cell-free massive MIMO can help in understanding the impact of different system configurations on the performance of the network. By analyzing the CDFs, one can identify the range of SE values that can be achieved and the probability of achieving those values with different precoding techniques. This data can be utilized to optimize the system parameters and enhance the overall performance of the network.

According to Figure 4.11, using MMSE precoding with all APs results in decreased spectral efficiency compared to schemes limiting the number of UE served by each AP. It is more efficient to select the best APs for power allocation, rather than transmitting from all APs. The performance difference between MMSE, PMMSE, and PRZF is minimal. While MMSE (All) and MMSE (DCC) are not scalable, PMMSE and PRZF are scalable and provide almost the same spectral efficiency. The proposed scalable precoding scheme in centralized operation achieves the highest spectral efficiency among all existing precoders.

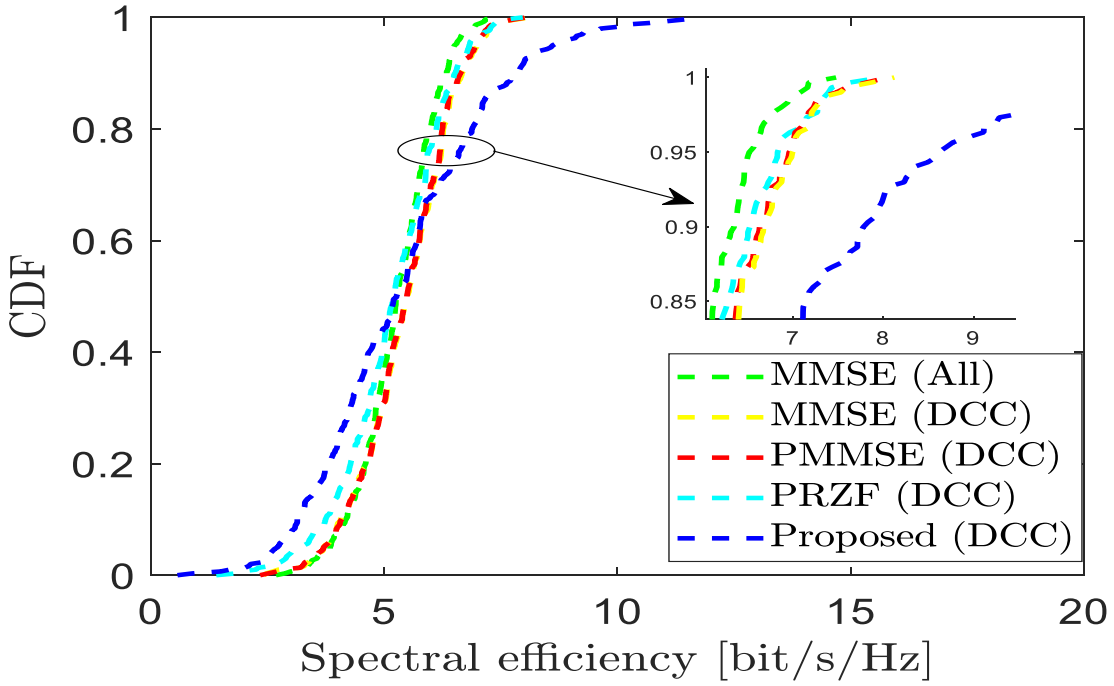

Figure 4.11: CDF of the downlink spectral efficiency per user in centralized operation for comparison of different precoding schemes when L=500, N=1, and K=100.

Table 4.12 presents a comprehensive comparison of the SE per UE for different precoding techniques and shows the statistical values of the CDF for each technique, which are also presented in Figure 4.11. This allows us to evaluate the performance of each technique over different ranges of SE per UE. The table reveals that the proposed precoding scheme achieves the highest SE per UE, indicating that it is effective in maximizing the spectral efficiency of the system. Overall, the table provides valuable insights into the performance of different precoding techniques and highlights the effectiveness of the proposed scheme.

Table 4.12: CDF of SE per UE of different precoding techniques in centralized operation with L=500, N=1, and K=100.

SE per UE / UE	MMSE (All)	MMSE (DCC)	PMMSE (DCC)	PRZF (DCC)	PROPOSED
0.2	4.575	4.612	4.59	4.257	3.745
0.4	5.081	5.198	5.187	4.963	4.694
0.6	5.53	5.769	5.761	5.541	5.7
0.8	5.952	6.272	6.249	6.124	6.945
1	7.475	7.58	7.59	7.974	11.48

Figure 4.12 indicates that the proposed centralized precoding technique all the schemes in distributed operation. It is surprising that using the LMMSE precoding scheme with all APs provodes much smaller spectral efficiency relative to the DCC operation with LMMSE and its scalable form LPMMSE.

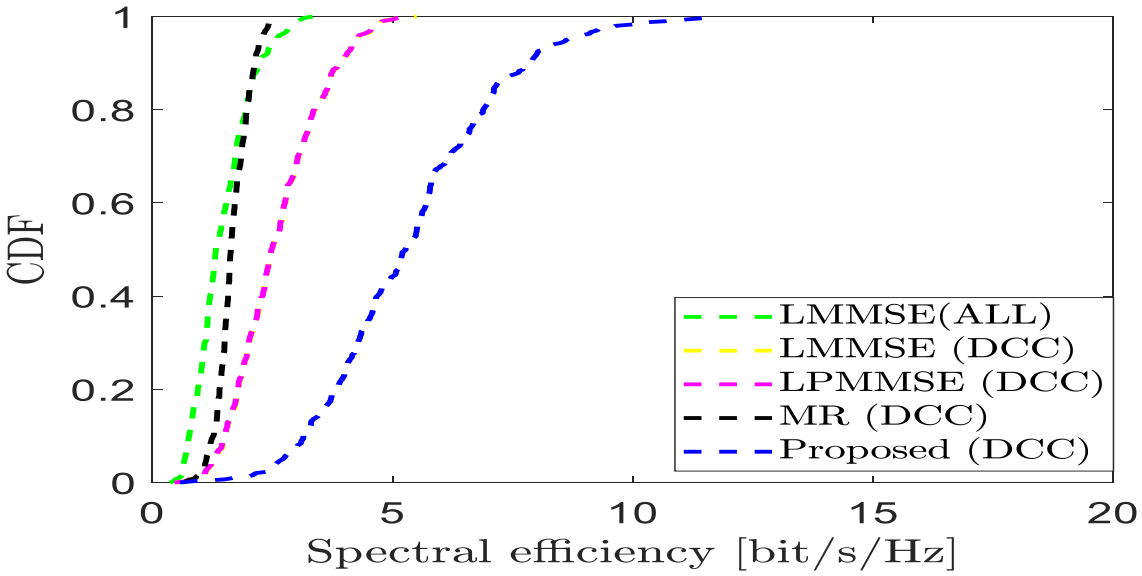

Figure 4.12: CDF of the downlink spectral efficiency per user in the distributed operation compared with the proposed centralized scheme with L=500, N=1, and K=100.

This unpredicted finding can be attributed to the power allocation scheme assumed in the all-APs approach. Sending data to all UEs is not an efficient approach since the channel gain of most UEs to a specific AP is relatively low. This is similar to shouting and only being audible to the nearest UEs, which leads to extra interference with nearby UEs. The AP then assigns power to faraway UEs, depriving nearby UEs of the power that could have been utilized to serve them. This suboptimal power allocation can be improved with the DCC, which allocates power only to UEs allocated to an AP with favorable channel conditions. It is interesting to note that the DCC implementation of LMMSE and its scalable form performed almost identically.

Table 4.13 presents a thorough comparison of the SE per UE for various precoding techniques in both distributed and centralized implementations. It displays the statistical values of the CDF for each technique depicted in Figure 4.12. This enables us to assess the performance of each technique across different SE per UE ranges. Upon reviewing the table, it becomes evident that the proposed precoding method achieves the highest SE per UE. This indicates that the suggested technique effectively maximizes the system's spectral efficiency.

In summary, the table offers valuable insights into the performance of diverse precoding techniques, highlighting the efficacy of the proposed approach.

Table 4.13: CDF of SE per UE of different precoding techniques in distributed operation compared with the proposed method in centralized operation with L=500, N=1, and K=100.

SE per UE / CDF	LMMSE (All)	LMMSE (DCC)	LPMMSE (DCC)	MR (DCC)	PROPOSED
0.2	0.9537	1.9537	1.9537	1.406	3.745
0.4	1.238	2.307	2.307	1.58	4.694
0.6	1.542	2.737	2.737	1.712	5.7
0.8	1.977	3.49	3.49	1.977	6.945
1	3.337	5.479	5.479	2.602	11.48

Figure 4.13 depicts a visual representation of various comparison criteria among different precoding techniques. The figure encompasses comparisons between precoding methods in terms of centralized and distributed operations, as well as scalable and unscalable precoders. It also includes a comparison between the proposed centralized scalable precoding technique and all existing schemes. The results indicate that the centralized operation yields higher spectral efficiency compared to the distributed operation. Furthermore, the scalable precoders exhibit similar performance to the unscalable optimum precoders. Significantly, the proposed precoder surpasses the performance of all existing precoding schemes.

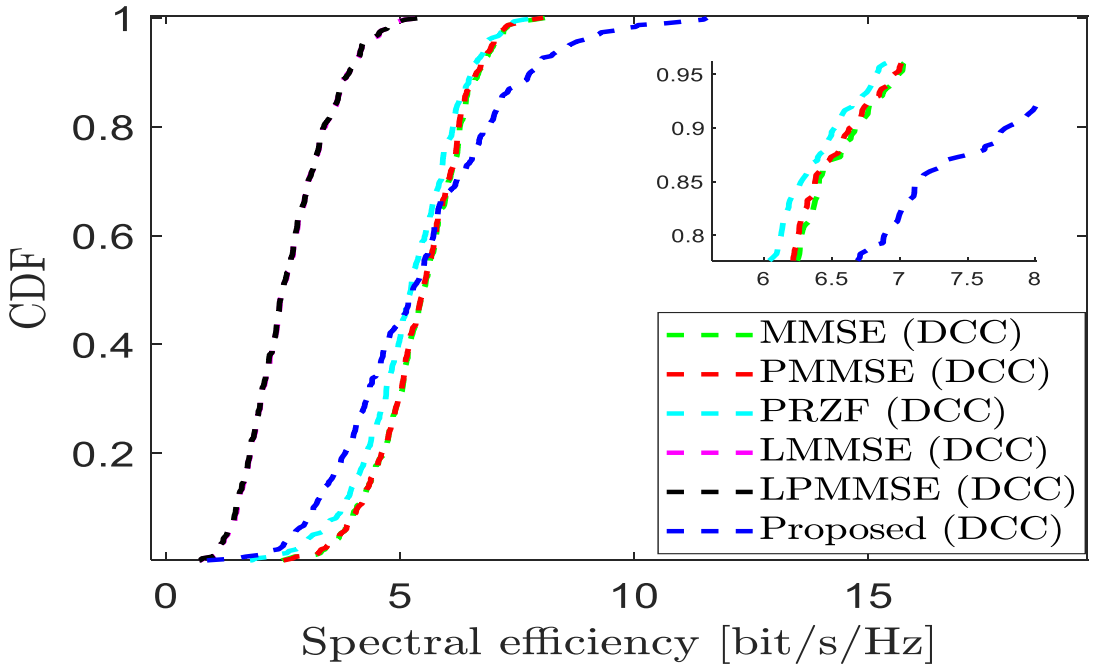

Figure 4.13: CDF of the downlink spectral efficiency per user for different precoders both in the distributed and centralized operation with L=500, N=1, and K=100.

The main finding in Figure 4.14 is that the proposed scalable precoding technique in centralized operation achieved the highest spectral efficiency compared to all existing precoders. The setup in this case contains L=500, N=3 and K=100. MMSE precoding, when utilized with all APs, results in smaller spectral efficiency in comparison to schemes that employ the DCC framework to restrict the number of UE served by each AP. Transmitting from all APs in the downlink operation is not an efficient approach. Instead, choosing the best APs proves to be more effective in achieving power allocation that mitigates interference. The performance difference between MMSE, PMMSE, and PRZF precoding techniques is minimal. MMSE (All), which employs MMSE precoding to serve all UEs using all APs, and MMSE (DCC) are not scalable schemes. However, the fully scalable PMMSE and PRZF precoding schemes yield almost similar SE values with the optimum unscalable precoders.

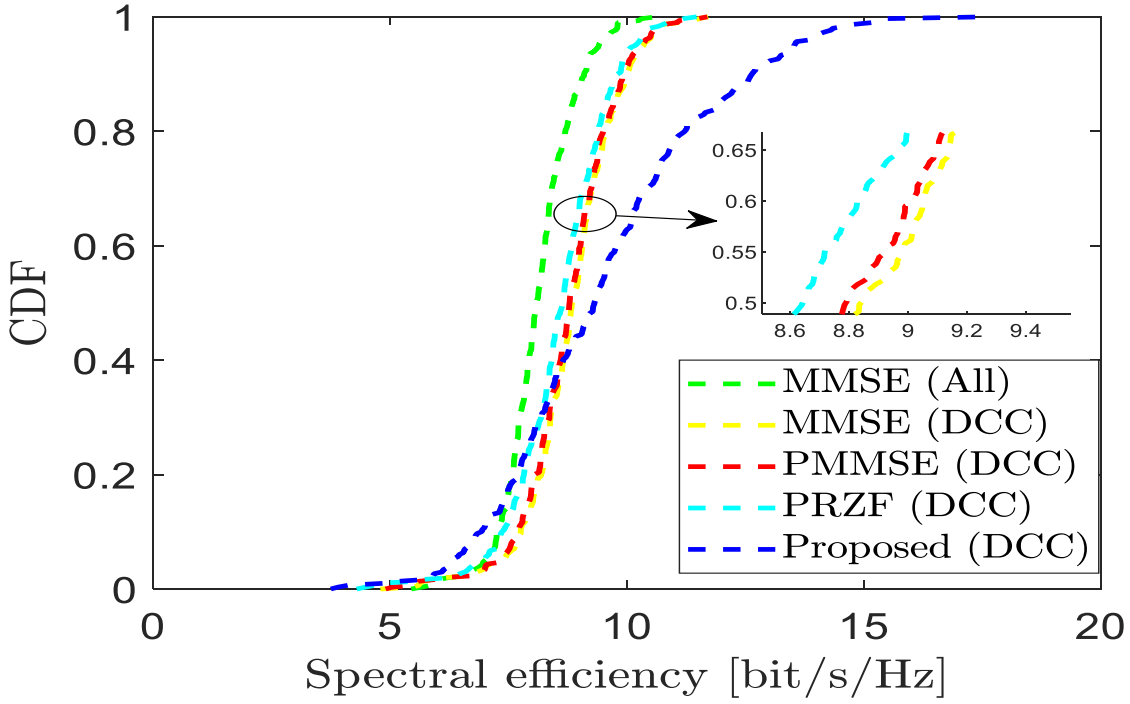

Figure 4.14: CDF of the downlink spectral efficiency per user in centralized operation for comparison of different precoding schemes when L=500, N=3, and K=100.

Table 4.14 presents a statistical representation of the results shown in Figure 4.14 for selected CDF values. It provides a quantitative analysis of the performance of different precoding techniques, including the proposed method and existing approaches. The table allows for a closer examination of the achieved SE values and their relation with the CDF. Upon reviewing the table, it becomes evident that the proposed technique performs better than the existing precoding schemes, particularly when the CDF approaches its upper tail. This indicates that the proposed method excels in maximizing SE, especially in scenarios where higher SE values are desired. By providing statistical values for specific CDF points, Table 4.14 offers a detailed insight into the performance comparison of different precoding techniques. It reaffirms the effectiveness of the proposed method in achieving higher SE, particularly in extreme cases represented by the upper tail of the CDF. These findings validate the superiority of the proposed method and its potential for enhancing system performance.

Table 4.14: CDF of SE per UE of different precoding techniques in centralized operation with L=500, N=3, and K=100.

SE per UE / CDF	MMSE (All)	MMSE (DCC)	PMMSE (DCC)	PRZF (DCC)	PROPOSED
0.2	7.58518	8.20974	8.0628	7.82667	7.70678
0.4	7.93566	8.7034	8.6124	8.42131	8.73206
0.6	8.27023	9.05494	9.02225	8.82705	9.79705
0.8	8.70195	9.5477	9.51237	9.39617	11.2458
1	10.6227	11.6961	11.6961	11.4702	17.6055

In Figure 4.15, it is evident that the proposed centralized precoding technique exhibits superior performance compared to all other techniques in the distributed operation. However, an unexpected finding arises when comparing the LMMSE precoding scheme that utilizes all APs with the DCC implementation of LMMSE and its scalable version LPMMSE. Surprisingly, the LMMSE precoding scheme with all APs yields sufficiently lower spectral efficiency relative to the DCC operation with LMMSE and its scalable counterpart. This surprising finding can be attributed to the assumed power allocation scheme. In general, the majority of UEs have very low channel gains to a specific AP. In this scenario, broadcasting to all users is inefficient, similar to shouting and only being audible to the nearest UEs. As a result, the AP utilizes power that could have been directed towards nearby UEs, but instead assigns it to distant UEs. This allocation of power to distant UEs leads to additional interference for nearby UEs, compromising their performance. On the other hand, the DCC implementation offers a superior heuristic power allocation method that allocates power solely to UEs assigned to an AP with favorable channel conditions. This approach avoids wasting power on UEs with weak channel gains and focuses on serving UEs with better reception quality. As a result, the DCC implementation mitigates interference and improves overall system performance. Interestingly, it is observed that the DCC implementation of LMMSE precoding and its scalable version (LPMMSE) perform almost identically. This implies that the scalability feature of LPMMSE does not significantly impact its performance compared to the non-scalable DCC implementation of LMMSE.

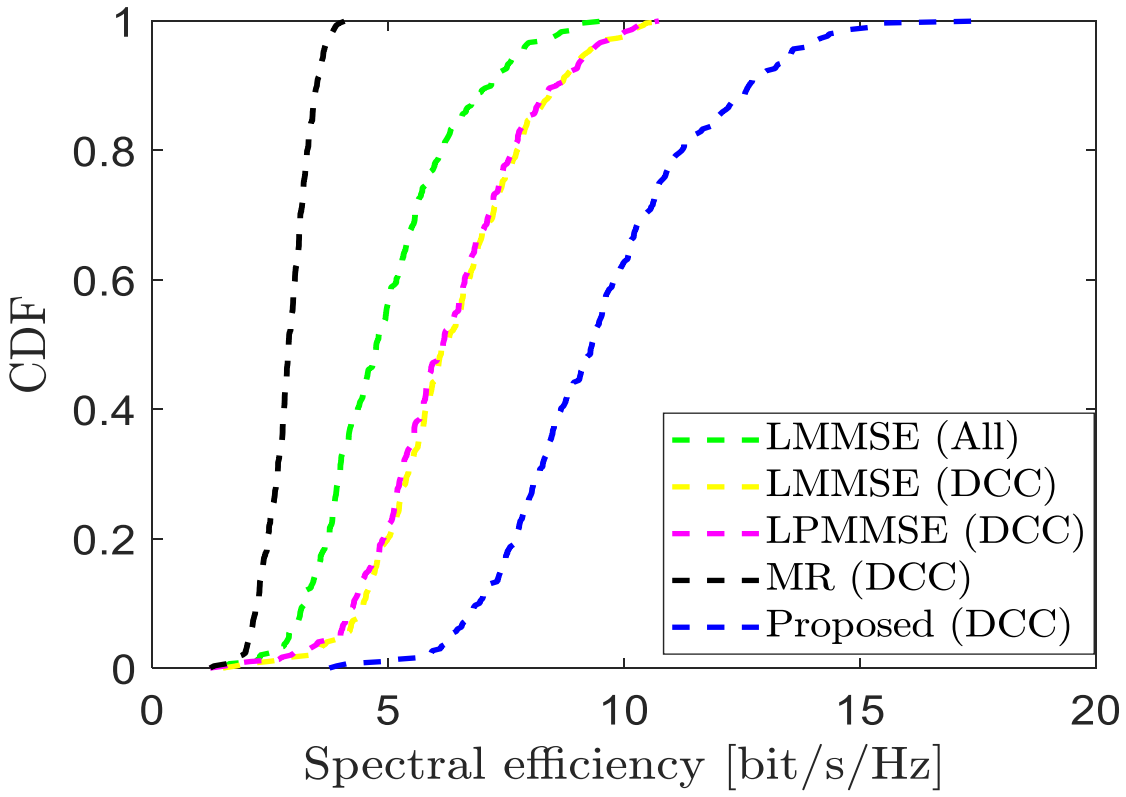

Figure 4.15: CDF of the downlink spectral efficiency per user in the distributed operation compared with the proposed centralized scheme with L=500, N=3, and K=100.

Table 4.15 offers a comprehensive comparison of the SE per UE for various precoding techniques in both distributed and proposed centralized operations. It presents statistical values of the CDF for each technique, as depicted in Figure 4.15. This enables us to assess the performance of each technique across different ranges of SE per UE. Upon analyzing the table, it becomes apparent that the proposed precoding scheme achieves the highest SE per UE among all the techniques considered. This indicates that the proposed precoding scheme is effective in maximizing the total spectral efficiency of the network system. The superior performance of the proposed scheme suggests that it provides significant improvements compared to other precoding techniques.

Table 4.15: CDF of SE per UE of different precoding techniques in distributed operation compared with the proposed method in centralized operation with L=500, N=3, and K=100.

SE per UE / CDF	LMMSE (All)	LMMSE (DCC)	LPMMSE (DCC)	MR (DCC)	PROPOSED
0.2	3.74319	4.98702	4.90292	2.4486	7.70678
0.4	4.37973	5.82819	5.7024	2.79098	8.73205
0.6	5.17122	6.70906	6.61664	3.01967	9.79705
0.8	6.17135	7.89298	7.65966	3.29302	11.2664
1	9.56389	10.8965	10.7309	3.96518	17.6055

Figure 4.16 provides a graphical representation that illustrates various comparison criteria between different precoding techniques. The figure encompasses several aspects of the comparisons, including centralized versus distributed operations, scalable versus unscalable precoders, and a comparison between the proposed centralized scalable precoding technique and existing schemes. The results depicted in the figure highlight that the centralized operation achieves higher spectral efficiency compared to the distributed operation. This implies that a centralized approach to precoding leads to improved spectral efficiency performance in the system. Furthermore, the figure indicates that the scalable precoders perform similarly to the unscalable optimum precoders. This suggests that scalable precoding techniques offer comparable performance while providing the advantage of flexibility and adaptability to changing system conditions or requirements. Importantly, the proposed precoding scheme outperforms all existing precoding schemes. This signifies that the proposed scheme exhibits superior performance in based on spectral efficiency or other desirable metrics compared to the previously established techniques

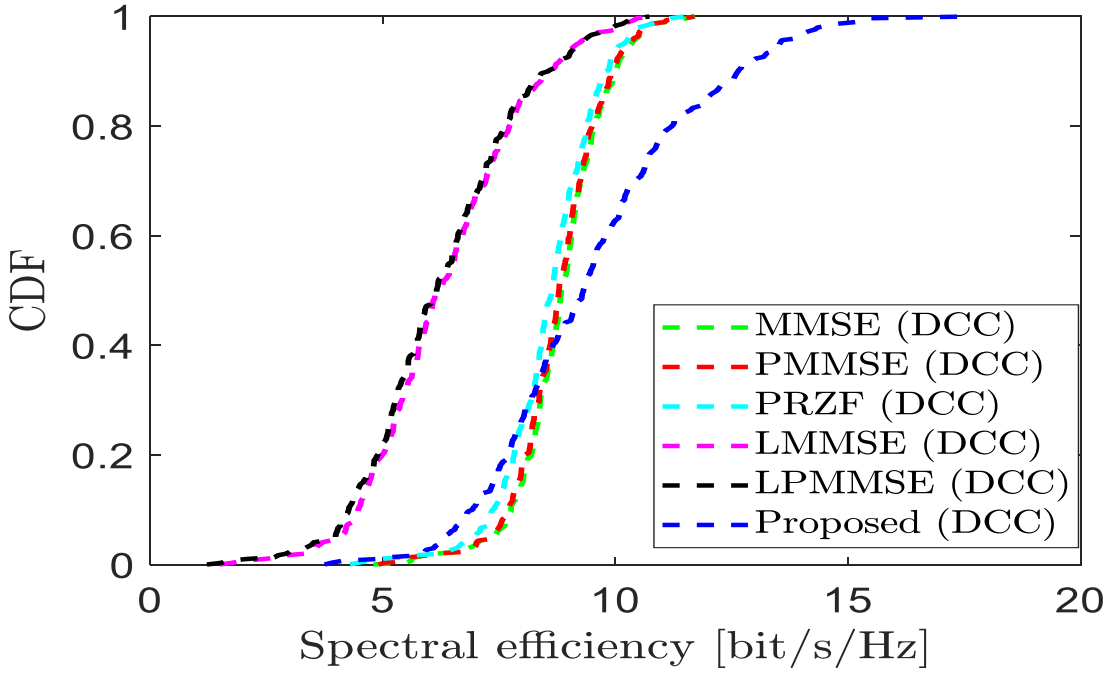

Figure 4.16: CDF of the downlink spectral efficiency per user for different precoders both in the distributed and centralized operation with L=500, N=3, and K=100.

4.1.3 Summary of spectral efficiency performance comparison

According to the simulation results presented above, the proposed precoder outperforms the existing precoders in terms of spectral efficiency. Specifically, when L=500, N=1, and K=20, the proposed precoder achieved an average downlink SE of 9.89066, which is higher than the average downlink SE of 9.39817 achieved by the PMMSE precoder. This represents a percentage performance improvement of the proposed precoder from the PMMSE precoder which is given by $\frac{9.890662-9.39817}{9.890662} \text{x } 100\% = 4.98\%$. Similarly, when L=500, N=5, and K=100, the proposed precoder achieved an average downlink SE of 10.07, which is higher than the Average downlink SE of 8.685 achieved by the PRZF precoder. This represents a percentage performance improvement of 13.75%. The results of the simulations show that the proposed precoder outperformed both the PMMSE and LPMMSE precoders in terms of sum downlink SE. Specifically, for a network area of 1 km square with L=500, N=5, and K=100 users, the proposed precoder achieved an optimal sum downlink SE of 1007, while the PMMSE precoder only achieved a sum downlink SE of 892.6. This represents a percentage performance improvement of 11.36%. Similarly, for a network area of 1 km square with L=1500, N=1, and K=100 users, the proposed precoder achieved an optimal sum downlink SE of 948.1, while the LPMMSE precoder only achieved a sum downlink SE of

406.5. This represents a percentage performance improvement of 57.12%. These improvements are attributed to the use of the MPA algorithm for interference suppression.

4.1.4 Performance comparisons of the proposed precoder with other precoders based on number of multiplications

Figure 4.17 shows the average number of complex multiplications needed to execute different centralized precoding schemes, which are based on the data presented in Table 3.1. The DCC method involves computing the matrix inverse individually for each user, which results in in a higher number of complex multiplications for 20 users relative to MMSE precoding, where all users are served by all APs. Conversely, with an increase in the number of users, the computational complexity of DCC reduces, but it rises when all users served by all APs. Therefore, a well-designed DCC can efficiently reduce the computational complexity of a large number of UEs. The results suggest that scalable techniques can be implemented with minimal spectral efficiency loss, leading to a significant reduction in complexity, as demonstrated in figures below.

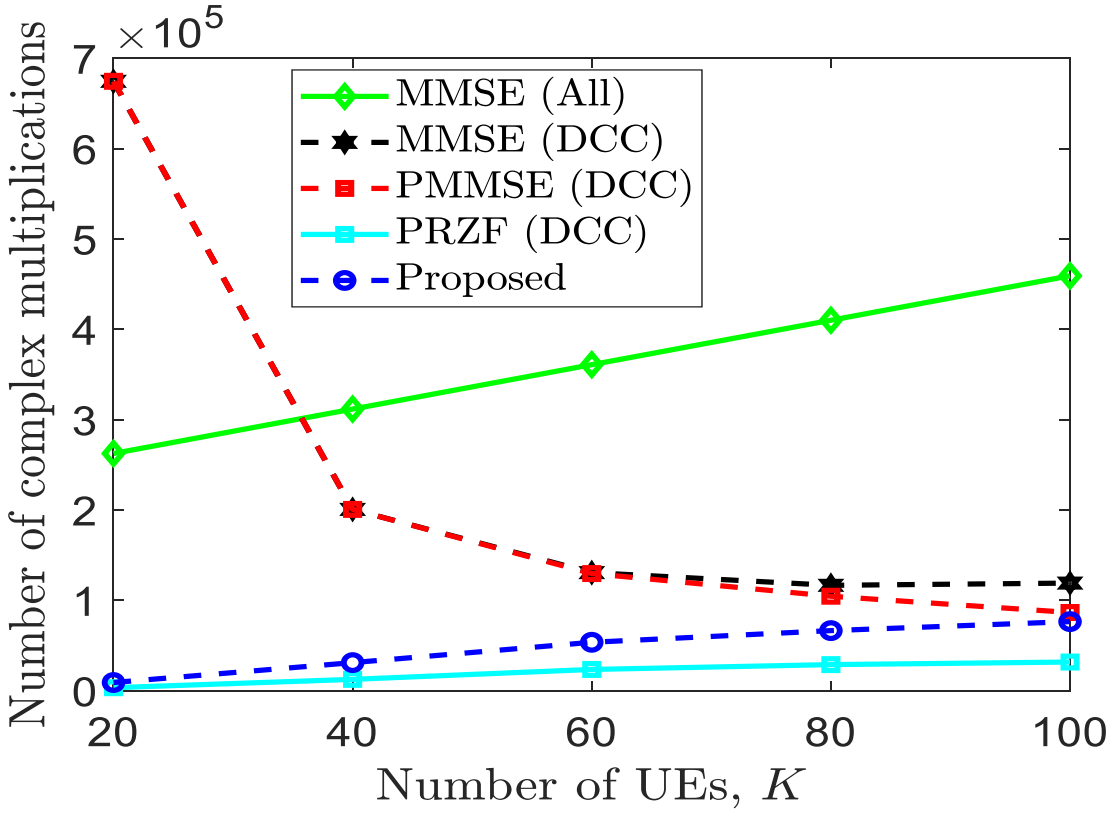

Figure 4.17: Number of complex multiplications versus the number of user equipment graphs for different precoders in the centralized operation of cell-free massive MIMO. We consider L=100 and N=4.

Table 4.16 presents the numerical values of various precoding schemes utilized in centralized operations. These values correspond to the results depicted in Figure 4.17.

Table 4.16: The numerical outcomes of complex multiplication counts for different precoders in the centralized implementation, with respect to the number of UEs.

UEs	Number of complex multiplications				
	MMSE(All)	MMSE(DCC)	PMMSE(DCC)	PRZF(DCC)	PROPOSED
20	262492	674453	674453	324246	8983
40	311652	200595	200595	12486	31007
60	360812	130621	129584	234469	53516
80	409972	116576	104498	28801	66433
100	459132	119029	865003	31656	76406

Based on the data presented in Figure 4.18, it is noticeable that the scalable precoding LPMMSE and MR techniques do not exhibit an increase in the average number of complex multiplications as K increases. Conversely, the unscalable LMMSE schemes experience a rise in total complexity as K grows. As a result, it becomes evident that scalability plays a crucial role in distributed operations as well. It is worth mentioning that the vertical scale in the distributed implementation is significantly smaller than in the centralized implementation due to the less computationally complex nature of the distributed schemes.

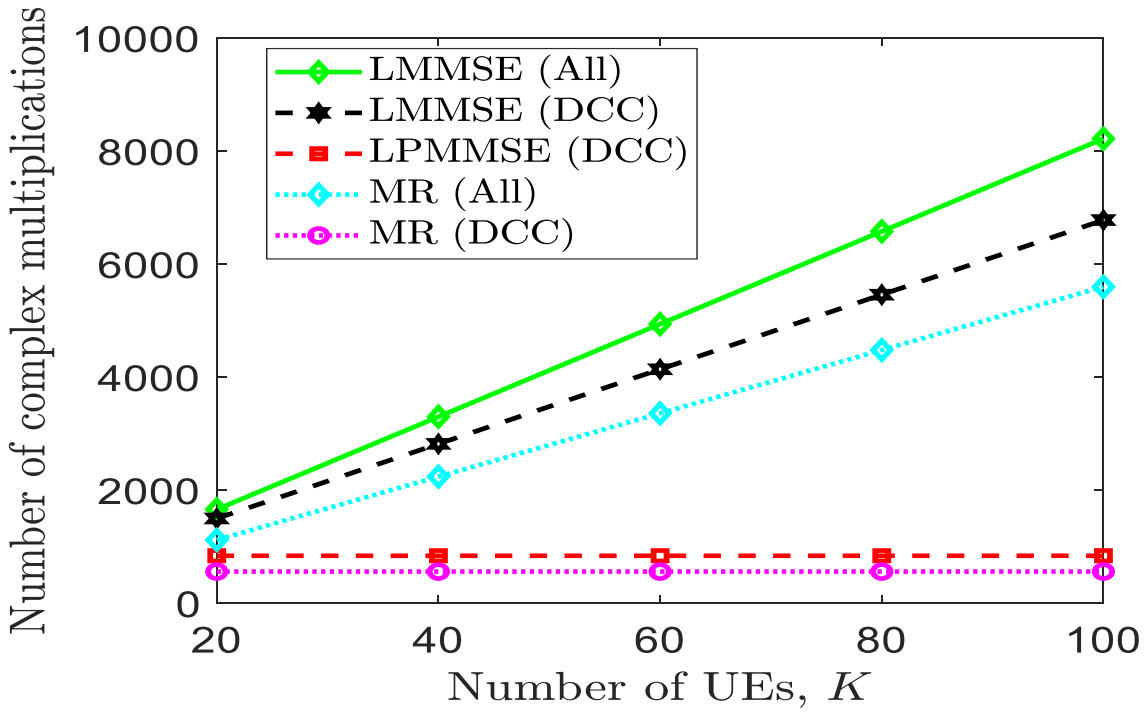

Figure 4.18: Number of complex multiplications versus the number of user equipment graphs for different precoders in the distributed operation of cell-free massive MIMO. We consider L=100 and N=4.

Table 4.17 displays the numerical values of different precoding schemes used in distributed operations, which correspond to the results shown in Figure 4.18. The numerical values in Table 4.17 are considerably lower than those in Table 4.16, indicating that distributed operation results in less computational complexity, while centralized operation has a higher computational complexity.

Table 4.17: The numerical outcomes of various precoders' complex multiplication counts in the distributed implementation, relative to the number of UEs.

UEs	Number of complex multiplications				
	LMMSE(All)	LMMSE(DCC)	LPMMSE(DCC)	MR(All)	MR(DCC)
20	1660	1500	840	1120	560
40	3300	2820	840	2240	560
60	4940	4140	840	3360	560
80	6580	5460	840	4480	560
100	8220	6780	840	5600	560

In Figure 4.19, various centralized precoding schemes are compared in terms of the average number of complex multiplications required to compute them, using the data from Table 3.1. The proposed scheme requires 91890 multiplications for 100 UEs, while Figure 4.17 shows that the same number of UEs requires 76406 multiplications. This suggests that the number of complex multiplications increases as the number of transmitting antennas increases.

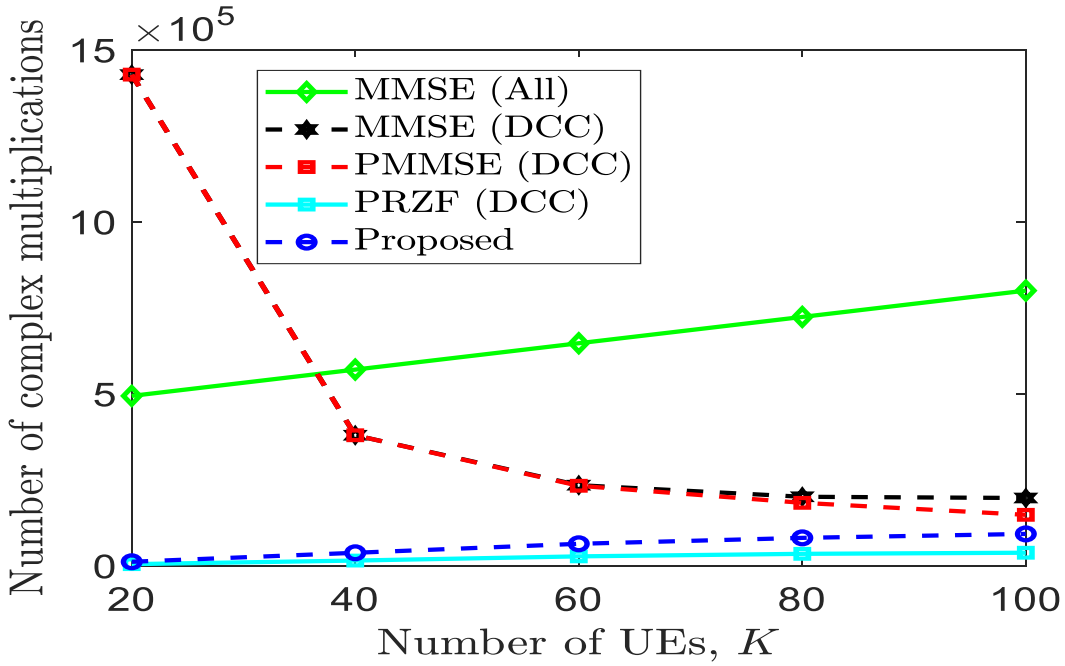

Figure 4.19: Number of complex multiplications versus the number of user equipment graphs for different precoders in the centralized operation of cell-free massive MIMO. We consider L=100 and N=5.

According to Figure 4.20, the scalable precoding LPMMSE and MR techniques do not experience an increase in the average number of complex multiplications as K increases. This is illustrated by the fact that the LPMMSE scheme requires 1191 multiplications for any number of UEs, whereas in Figure 4.18, the same number of UEs only requires 840 multiplications. As a result, it seems that the number of complex multiplications rises with an increase in the number of transmitting antennas.

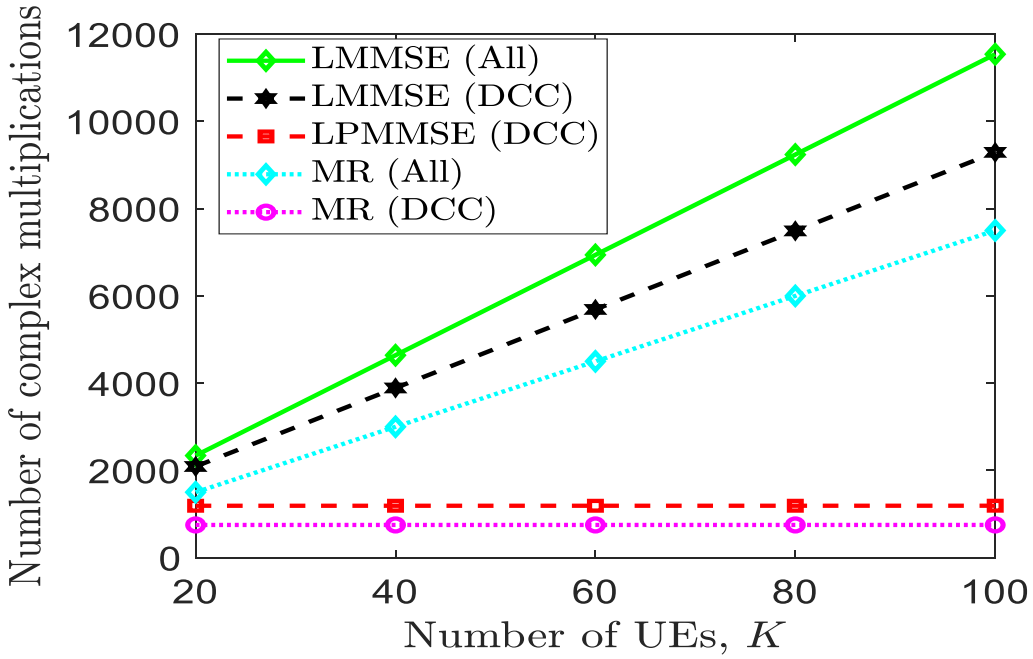

Figure 4.20: Number of complex multiplications versus the number of user equipment graphs for different precoders in the distributed operation of cell-free massive MIMO. We consider L=100 and N=5.

4.1.5 Computational time

Computational time refers to the duration it takes for a computer or system to complete a given task or calculation. The amount of computational time needed for a specific task or algorithm depends on several factors, including the size of the input data, the complexity of the algorithm, the processing power of the hardware, and the efficiency of the software implementation.

To evaluate the spectral efficiency of a system with L=500 APs, N=1 antenna per AP, and a maximum of 100 UEs, we conducted simulations using both existing precoding techniques and the proposed technique. We ran 1000 different channel realizations on a Core i-7 HP laptop with 4 GB RAM and a 128 GB solid-state drive.

Our results show that the simulation of existing precoding techniques took 42 hours and 32 minutes, while the simulation of the proposed technique took 43 hours and 44 minutes. The proposed algorithm required only a slightly longer computational time, indicating that it offers acceptable performance relative to its computational cost.

5. CONCLUSION AND RECOMMENDATION

5.1 Conclusion

The downlink portion of a cell-free massive MIMO system can be executed using distributed or centralized operation. In centralized implementation, the CPU processes signals which are going to be transmitted and selects precoding vectors, while the APs focus solely on the physical transmission. This centralized approach enables coherent reception of signals transmitted from multiple APs at desired UE while simultaneously suppressing interference at undesired UEs.

In contrast, with the distributed operation, every AP receives a downlink signal from the CPU and independently constructs the signal to be transmitted using a local precoding scheme based on its own channel estimates. Although the signals which are transmitted from the serving APs can still be seamlessly received at the intended UE, the capability to suppress interference is diminished in comparison to centralized implementation. The interference suppression ability of an AP is restricted by the fact that it can only reduce the interference it creates itself, which is in turn limited by the number of antennas available on the AP.

Furthermore, the information provided has indicated that the centralized precoding schemes have outperformed the distributed precoding schemes. The proposed precoding method in the context of the thesis has been designed to be scalable and centralized, and it has exhibited higher performance compared to all existing precoding schemes discussed. Specifically, the proposed precoder has outperformed the existing PRZF precoder by 13.75% and LPMMSE precoder by 36.8% in terms of both the average and sum spectral efficiency for 100 users and 500 APs each equipped with five antennas. This improvement can be attributed to the MPA algorithm, which has assisted in suppressing the interference signal in the PRZF precoder. In addition, deploying a large number of APs each with a single antenna can result in higher spectral efficiency compared to deploying the same total number of antennas in the coverage area with each AP equipped with multiple antennas.

In summary, the choice between centralized and distributed operation in the downlink of a cell-free network has had implications for interference suppression. Centralized precoding schemes have demonstrated superior performance compared to the distributed precoding schemes, and the proposed centralized precoding method in the thesis has outperformed

existing schemes due to the incorporation of the MPA algorithm for interference suppression in the PRZF precoder.

5.2 Recommendation

Cell-free massive MIMO network is a new technology that has yet to be widely implemented. To facilitate its implementation, extensive research is needed. The proposed precoding scheme in this thesis has only been evaluated at the simulation level, and it is recommended to test this algorithm in a practical network for further validation. Additionally, future work will involve developing machine learning and deep learning-based signal processing algorithms to improve the efficiency and performance of cell-free massive MIMO. Technical challenges such as channel estimation, power allocation, and user association need to be addressed to bring this technology to practical implementation. Overall, practical testing of the proposed precoding scheme and the development of machine learning and deep learning-based algorithms are crucial steps toward making cell-free massive MIMO a reality.

Research Fund Acknowledgement

This research project is funded by Adama Science and Technology University under the grant number ASTU/SM-R/739/23, Adama, Ethiopia

Reference

Akyildiz, I. F., Kak, A., & Nie, S. (2020). 6G and Beyond: The Future of Wireless Communications Systems. *IEEE Access*, *8*, 133995–134030. https://doi.org/10.1109/ACCESS.2020.3010896

Alammari, A. A., Sharique, M., & Moinuddin, A. A. (2022). User-Centric Cell-Free and Co-Located Cellular Large Scale MU-MIMO Systems: A Comparative Performance Study With Spatial Channel Correlation in Dense Urban Scenario. *IEEE Access*, *10*, 48792–48809. https://doi.org/10.1109/ACCESS.2022.3172290

Al-Betar, M. A., Awadallah, M. A., Makhadmeh, S. N., Alyasseri, Z. A. A., Al-Naymat, G., & Mirjalili, S. (2023). Marine Predators Algorithm: A Review. *Archives of Computational Methods in Engineering*. https://doi.org/10.1007/s11831-023-09912

Albreem, M., Juntti, M., & Shahabuddin, S. (2019). Massive MIMO Detection Techniques: A Survey. In *IEEE Communications Surveys & Tutorials: Vol. PP* (p. 1). https://doi.org/10.1109/COMST.2019.2935810

Alonzo, M., Buzzi, S., Zappone, A., & D'Elia, C. (2019). Energy-Efficient Power Control in Cell-Free and User-Centric Massive MIMO at Millimeter Wave. *IEEE Transactions on Green Communications and Networking*, *3*(3), 651–663. https://doi.org/10.1109/TGCN.2019.2908228

Alzubaidi, O. T. H., Hindia, M. N., Dimyati, K., Noordin, K. A., Wahab, A. N. A., Qamar, F., & Hassan, R. (2022a). Interference Challenges and Management in B5G Network Design: A Comprehensive Review. *Electronics*, *11*(18), Article 18. https://doi.org/10.3390/electronics11182842

Alzubaidi, O. T. H., Hindia, M. N., Dimyati, K., Noordin, K. A., Wahab, A. N. A., Qamar, F., & Hassan, R. (2022b). Interference Challenges and Management in B5G Network

Design: A Comprehensive Review. *Electronics*, *11*(18), Article 18. https://doi.org/10.3390/electronics11182842

Björnson, E., Hoydis, J., & Sanguinetti, L. (2017). Massive MIMO Networks: Spectral, Energy, and Hardware Efficiency. *Foundations and Trends® in Signal Processing*, *11*, 154–655. https://doi.org/10.1561/2000000093

Bjornson, E., & Sanguinetti, L. (2019). A New Look at Cell-Free Massive MIMO: Making It Practical With Dynamic Cooperation. *2019 IEEE 30th Annual International Symposium on Personal, Indoor and Mobile Radio Communications (PIMRC)*, 1–6. https://doi.org/10.1109/PIMRC.2019.8904101

Bjornson, E., & Sanguinetti, L. (2020). Making Cell-Free Massive MIMO Competitive With MMSE Processing and Centralized Implementation. *IEEE Transactions on Wireless Communications*, *19*(1), 77–90. https://doi.org/10.1109/TWC.2019.2941478

Björnson, E., & Sanguinetti, L. (2020). Scalable Cell-Free Massive MIMO Systems. *IEEE Transactions on Communications*, *68*(7), 4247–4261. https://doi.org/10.1109/TCOMM.2020.2987311

Buzzi, S., & D'Andrea, C. (2017). Cell-Free Massive MIMO: User-Centric Approach. *IEEE Wireless Communications Letters*, *6*(6), 706–709. https://doi.org/10.1109/LWC.2017.2734893

Castanheira, D., & Gameiro, A. (2010). Distributed antenna system capacity scaling [Coordinated and Distributed MIMO]. *IEEE Wireless Communications*, *17*(3), 68–75. https://doi.org/10.1109/MWC.2010.5490981

Choi, W., & Andrews, J. (2007). Downlink performance and capacity of distributed antenna systems in a multicell environment. *IEEE Transactions on Wireless Communications*, *6*(1), 69–73. https://doi.org/10.1109/TWC.2007.05207

Datta, S., Amudala, D. N., Sharma, E., Budhiraja, R., & Panwar, S. S. (2022). Full-Duplex Cell-Free Massive MIMO Systems: Analysis and Decentralized Optimization. *IEEE Open Journal of the Communications Society*, *3*, 31–50. https://doi.org/10.1109/OJCOMS.2021.3135153

Deepa, V., Haridass, M., Selvamuthu, D., & Kalita, P. (2023). Analysis of energy efficiency of small cell base station in 4G/5G networks. *Telecommunication Systems*, *82*(3), 381–401. https://doi.org/10.1007/s11235-022-00987-y

Du, L., Li, L., Ngo, H. Q., Mai, T. C., & Matthaiou, M. (2021). Cell-Free Massive MIMO: Joint Maximum-Ratio and Zero-Forcing Precoder With Power Control. *IEEE Transactions on Communications*, *69*(6), 3741–3756. https://doi.org/10.1109/TCOMM.2021.3059300

Elhoushy, S., Ibrahim, M., & Hamouda, W. (2022). Cell-Free Massive MIMO: A Survey. *IEEE Communications Surveys & Tutorials*, *24*(1), 492–523. https://doi.org/10.1109/COMST.2021.3123267

Faramarzi, A., Heidarinejad, M., Mirjalili, S., & Gandomi, A. (2020). Marine Predators Algorithm: A Nature-inspired Metaheuristic. *Expert Systems with Applications*, *152*, 113377. https://doi.org/10.1016/j.eswa.2020.113377

Garg, J., Gupta, K., & Ghosh, P. K. (2013). Performance analysis of MIMO wireless communications over fading channels-A Review. *International Journal of Advanced Research in Electrical, Electronics and Instrumentation Engineering*, *2*(4), 1272–1302.

He, H., Yu, X., Zhang, J., Song, S., & Letaief, K. B. (2021). Cell-Free Massive MIMO for 6G Wireless Communication Networks. *Journal of Communications and Information Networks*, *6*(4), 321–335. https://doi.org/10.23919/JCIN.2021.9663100

He, S., Wang, T., & Wang, S. (2020). Mobility-driven user-centric AP clustering in mobile edge computing-based ultra-dense networks. *Digital Communications and Networks*, *6*(2), 210–216. https://doi.org/10.1016/j.dcan.2019.08.003

Hu, B., Wang, Y., Wang, C., & Wang, L. (2017). A user-centric clustering method for mobility management in ultra-dense networks. *2017 9th International Conference on Wireless Communications and Signal Processing (WCSP)*, 1–5. https://doi.org/10.1109/WCSP.2017.8170946

Interdonato, G., Björnson, E., Quoc Ngo, H., Frenger, P., & Larsson, E. G. (2019). Ubiquitous cell-free Massive MIMO communications. *EURASIP Journal on Wireless Communications and Networking*, *2019*(1), 197. https://doi.org/10.1186/s13638-019-1507-0

Interdonato, G., Karlsson, M., Bjornson, E., & Larsson, E. G. (2018). Downlink Spectral Efficiency of Cell-Free Massive MIMO with Full-Pilot Zero-Forcing. *2018 IEEE Global Conference on Signal and Information Processing (GlobalSIP)*, 1003–1007. https://doi.org/10.1109/GlobalSIP.2018.8646666

Interdonato, G., Karlsson, M., Björnson, E., & Larsson, E. G. (2020). Local Partial Zero-Forcing Precoding for Cell-Free Massive MIMO. *IEEE Transactions on Wireless Communications*, *19*(7), 4758–4774. https://doi.org/10.1109/TWC.2020.2987027

Interdonato, G., Ngo, H. Q., & Larsson, E. G. (2021). Enhanced Normalized Conjugate Beamforming for Cell-Free Massive MIMO. *IEEE Transactions on Communications*, *69*(5), 2863–2877. https://doi.org/10.1109/TCOMM.2021.3055522

Irram, F., Ali, M., Maqbool, Z., Qamar, F., & Rodrigues, J. J. (2020). Coordinated Multi-Point Transmission in 5G and Beyond Heterogeneous Networks. *2020 IEEE 23rd*

International Multitopic Conference (INMIC), 1–6. https://doi.org/10.1109/INMIC50486.2020.9318091

Jangir, P., Buch, H., Mirjalili, S., & Manoharan, P. (2023). MOMPA: Multi-objective marine predator algorithm for solving multi-objective optimization problems. *Evolutionary Intelligence*, *16*(1), 169–195. https://doi.org/10.1007/s12065-021-00649-z

Jia, Y., Xu, P., & Guo, X. (2022). MIMO system capacity based on different numbers of antennas. *Results in Engineering*, *15*, 100577. https://doi.org/10.1016/j.rineng.2022.100577

Jin, S.-N., Yue, D.-W., & Nguyen, H. H. (2021). Spectral Efficiency of a Frequency-Selective Cell-Free Massive MIMO System With Phase Noise. *IEEE Wireless Communications Letters*, *10*(3), 483–487. https://doi.org/10.1109/LWC.2020.3035364

Kaluuba, L. L., Taban-Wani, G., & Waigumbulizi, D. (2006). The Fading Channel Problem and Its Impact on Wireless Communication Systems in Uganda. In J. A. Mwakali & G. Taban-Wani (Eds.), *Proceedings from the International Conference on Advances in Engineering and Technology* (pp. 621–634). Elsevier Science Ltd. https://doi.org/10.1016/B978-008045312-5/50068-6

Katoch, S., Chauhan, S. S., & Kumar, V. (2021). A review on genetic algorithm: Past, present, and future. *Multimedia Tools and Applications*, *80*(5), 8091–8126. https://doi.org/10.1007/s11042-020-10139-6

kaur, J., Khanna, M., & Gaba, G. S. (2017). Performance Analysis of Rayleigh and Rician Fading Channel Model. *International Journal of Multimedia and Ubiquitous Engineering*, *12*(8), 37–42. https://doi.org/10.14257/ijmue.2017.12.8.04

Kim, M., Choi, I.-K., Hong, S.-E., & Na, J.-H. (2022). Joint Centralized and Distributed Precoding in Scalable Cell-Free Massive MIMO Systems. *2022 13th International*

Conference on Information and Communication Technology Convergence (ICTC), 1254–1257. https://doi.org/10.1109/ICTC55196.2022.9952405

Kinoshita, K., Utano, T., Onoe, S., & Nagata, K. (2018). *History of Mobile Communications with a Look Back at NTT DOCOMO R&D and Outlook for the Future*.

Koziel, S., & Yang, X.-S. (Eds.). (2011). *Computational Optimization, Methods and Algorithms* (Vol. 356). Springer Berlin Heidelberg. https://doi.org/10.1007/978-3-642-20859-1

Kumar, N. N., & Chandana, P. (2021). *MASSIVE MIMO USING MRC TECHNIQUE MAKING CELL - FREE*. *11*(02).

Kuo, C.-C. J., Tsai, S.-H., Tadjpour, L., & Chang, Y.-H. (2008). Precoding Techniques for MIMO Channels. In C.-C. J. Kuo, S.-H. Tsai, L. Tadjpour, & Y.-H. Chang (Eds.), *Precoding Techniques for Digital Communication Systems* (pp. 67–113). Springer US. https://doi.org/10.1007/978-0-387-71769-2_4

Larsson, E. G., Edfors, O., Tufvesson, F., & Marzetta, T. L. (2014). Massive MIMO for Next Generation Wireless Systems. *IEEE Communications Magazine*, *52*(2), 186–195. https://doi.org/10.1109/MCOM.2014.6736761

Li, Y., Tian, Y., & Yang, C. (2015). Energy-Efficient Coordinated Beamforming Under Minimal Data Rate Constraint of Each User. *IEEE Transactions on Vehicular Technology*, *64*(6), 2387–2397. https://doi.org/10.1109/TVT.2014.2343255

Marzetta, T. L. (2010). Noncooperative cellular wireless with unlimited numbers of base station antennas. *IEEE Transactions on Wireless Communications*, *9*(11), 3590–3600.

Mendoza, C. F., Schwarz, S., & Rupp, M. (2020). Cluster Formation in Scalable Cell-free Massive MIMO Networks. *2020 16th International Conference on Wireless and*

Mobile Computing, Networking and Communications (WiMob), 62–67. https://doi.org/10.1109/WiMob50308.2020.9253391

Nayebi, E., Ashikhmin, A., Marzetta, T. L., & Rao, B. D. (2016). Performance of cell-free massive MIMO systems with MMSE and LSFD receivers. *2016 50th Asilomar Conference on Signals, Systems and Computers*, 203–207. https://doi.org/10.1109/ACSSC.2016.7869024

Nayebi, E., Ashikhmin, A., Marzetta, T. L., Yang, H., & Rao, B. D. (2017). Precoding and Power Optimization in Cell-Free Massive MIMO Systems. *IEEE Transactions on Wireless Communications*, *16*(7), 4445–4459. https://doi.org/10.1109/TWC.2017.2698449

Ngo, H. Q., Ashikhmin, A., Yang, H., Larsson, E. G., & Marzetta, T. L. (2015). Cell-Free Massive MIMO: Uniformly great service for everyone. *2015 IEEE 16th International Workshop on Signal Processing Advances in Wireless Communications (SPAWC)*, 201–205. https://doi.org/10.1109/SPAWC.2015.7227028

Ngo, H. Q., Ashikhmin, A., Yang, H., Larsson, E. G., & Marzetta, T. L. (2017). Cell-Free Massive MIMO Versus Small Cells. *IEEE Transactions on Wireless Communications*, *16*(3), 1834–1850. https://doi.org/10.1109/TWC.2017.2655515

Onwubolu, G. C., & Babu, B. V. (2004). *New Optimization Techniques in Engineering* (Vol. 141). Springer. https://doi.org/10.1007/978-3-540-39930-8

Pandi, N., & Nargund, M. (2018). Mobile Communication - Past, Present and Future: A Review. *The Scientific Bulletin of Electrical Engineering Faculty*, *18*(2), 12–29. https://doi.org/10.1515/sbeef-2017-0028

Pathak, S., & Katiyar, H. (2016). Performance Analysis of Wireless link in Rician Fading Channel. *International Journal of Advanced Research in Computer and Communication Engineering*, *5*(4), 101–105.

Qiao, Y., Qiao, X., Luo, R., Dai, Z., & Yang, L. (2022). Joint Precoding Scheme with Enhanced Spectral Efficiency for Cell-Free Massive MIMO Downlink. *2022 IEEE 8th International Conference on Computer and Communications (ICCC)*, 950–955. https://doi.org/10.1109/ICCC56324.2022.10065761

Qiu, J., Xu, K., Shen, Z., Xie, W., Zhang, D., & Li, X. (2019). Downlink Performance Analysis of Cell-Free Massive MIMO over Spatially Correlated Rayleigh Channels. *2019 IEEE 19th International Conference on Communication Technology (ICCT)*, 122–127. https://doi.org/10.1109/ICCT46805.2019.8947237

Ramezani, M., Bahmanyar, D., & Razmjooy, N. (2021). A New Improved Model of Marine Predator Algorithm for Optimization Problems. *Arabian Journal for Science and Engineering*, *46*(9), 8803–8826. https://doi.org/10.1007/s13369-021-05688-3

Rezaei, K., & Rezaei, H. (2022). An improved firefly algorithm for numerical optimization problems and it's application in constrained optimization. *Engineering with Computers*, *38*(4), 3793–3813. https://doi.org/10.1007/s00366-021-01412-9

Solaija, M. S. J., Salman, H., Kihero, A. B., Saglam, M. I., & Arslan, H. (2021). Generalized Coordinated Multipoint Framework for 5G and Beyond. *IEEE Access*, *9*, 72499–72515. https://doi.org/10.1109/ACCESS.2021.3079190

Talatahari, S. (2013). *Metaheuristic Applications in Structures and Infrastructures: 17. Optimum Performance-Based Seismic Design of Frames Using Metaheuristic Optimization Algorithms*. Elsevier Science.

Tan, L., Zhang, Z., & Wang, D. (2022). Performance of Multiuser Downlink Cell-Free Massive MIMO Systems With Hard Deadlines. *IEEE Access*, *10*, 62910–62919. https://doi.org/10.1109/ACCESS.2022.3176946

Vadda, L., Rao, G., & Bidikar, B. (2016). Fast Fading Mobile Channel Modeling for Wireless Communication. *Procedia Computer Science*, *85*, 777–781. https://doi.org/10.1016/j.procs.2016.05.265

Viswanathan, H., & Weldon, M. (2014). The Past, Present, and Future of Mobile Communications. *Bell Labs Technical Journal*, *19*, 8–21. https://doi.org/10.15325/BLTJ.2014.2335491

Wang, D., Qiu, A., Zhou, Q., Partani, S., & Schotten, H. D. (2023). *The Effect of Variable Factors on the Handover Performance for Ultra Dense Network* (arXiv:2301.08053). arXiv. http://arxiv.org/abs/2301.08053

Wiame, C., Oestges, C., & Vandendorpe, L. (2023). *Joint data rate and EMF exposure analysis in user-centric cell-free massive MIMO networks* (arXiv:2301.11127). arXiv. http://arxiv.org/abs/2301.11127

Xiaohu, Y., Wang, C.-X., Huang, J., Gao, X., Zhang, Z., Wang, M., Huang, Y., Zhang, C., Jiang, Y., Wang, J., Zhu, M., Sheng, B., Wang, D., Pan, Z., Zhu, P., Yang, Y., Liu, Z., Ding, Z., Tao, X., & Liang, Y.-C. (2021). Towards 6G wireless communication networks: Vision, enabling technologies, and new paradigm shifts. *Science China Information Sciences*, *64*. https://doi.org/10.1007/s11432-020-2955-6

Yang, H., & Marzetta, T. L. (2014). A Macro Cellular Wireless Network with Uniformly High User Throughputs. *2014 IEEE 80th Vehicular Technology Conference (VTC2014-Fall)*, 1–5. https://doi.org/10.1109/VTCFall.2014.6965818

Yang, X.-S., Koziel, S., & Leifsson, L. (2013). Computational Optimization, Modelling and Simulation: Recent Trends and Challenges. *Procedia Computer Science*, *18*, 855–860. https://doi.org/10.1016/j.procs.2013.05.250

Yao, Y., Tian, Z., Chen, Z., Wang, M., & Jia, Y. (2022). Joint association and beamforming optimization in reconfigurable intelligent surface-enhanced user-centric networks. *Intelligent and Converged Networks*, *3*(4), 340–350. https://doi.org/10.23919/ICN.2022.0027

Zhang, H., & Sun, G. (2002). Feature selection using Tabu search method. *Pattern Recognition*, *35*, 701–711. https://doi.org/10.1016/S0031-3203(01)00046-2

Zhang, J., Chen, R., Andrews, J., Ghosh, A., & Heath, R. (2009). Networked MIMO with Clustered Linear Precoding. *Wireless Communications, IEEE Transactions On*, *8*, 1910–1921. https://doi.org/10.1109/TWC.2009.080180

Zhang, J., Chen, S., Lin, Y., Zheng, J., ai, bo, & Hanzo, L. (2019). Cell-free massive MIMO: A new next-generation paradigm. *IEEE Access*, *PP*, 1–1. https://doi.org/10.1109/ACCESS.2019.2930208

Zhang, Z., Wang, N., Zhang, J., & Mu, X. (2018). Dynamic User-Centric Clustering for Uplink Cooperation in Multi-Cell Wireless Networks. *IEEE Access*, *6*, 8526–8538. https://doi.org/10.1109/ACCESS.2018.2792222

Zhou, S., Zhao, M., Xu, X., Wang, J., & Yao, Y. (2003). Distributed wireless communication system: A new architecture for future public wireless access. *Communications Magazine, IEEE*, *41*, 108–113. https://doi.org/10.1109/MCOM.2003.1186553